COMPUTERISED

SYNTHESIS, CHARACTERIZATION AND CATALYTIC PROPERTIES OF MICROPOROUS TITANOSILICATE MOLECULAR SIEVES

A THESIS
SUBMITTED TO THE
UNIVERSITY OF POONA
FOR THE DEGREE OF
DOCTOR OF PHILOSOPHY
(IN CHEMISTRY)

BY

TAPAN KUMAR DAS

CATALYSIS DIVISION
NATIONAL CHEMICAL LABORATORY
PUNE - 411 008, INDIA.

(FEBRUARY 1997)

COMPUTERISLD

TH-1080

DEDICATED

TO

MY BELOVED PARENTS

CERTIFICATE

Certified that the work incorporated in the thesis **"Synthesis, Characterization and Catalytic Properties of Microporous Titanosilicate Molecular Sieves"** submitted by **Mr. Tapan Kumar Das**, for the degree of Doctor of Philosophy, was carried out by the candidate under my supervision in the Catalysis Division, National Chemical Laboratory, Pune, India. Materials obtained from other sources have been duly acknowledged in the thesis.

S. Sivasanker 26/2/97

[Dr. S. SIVASANKER]

(Research Guide)

ACKNOWLEDGMENTS

I express my profound gratitude to my research guide, Dr. S. Sivasanker, Deputy Director, National Chemical Laboratory, Pune, for his invaluable guidance, numerous discussions and constructive suggestions through out the course of this investigation.

I am indebted to Dr. A.V. Ramaswamy, Head, Catalysis Division, NCL, for providing me all facilities required for my work.

I am grateful to Dr.(Mrs.) A.J. Chandwadkar for her useful suggestions and guidance in carrying out the research work.

I owe my special thanks to Dr. R. Vetrivel and Dr. S. Ganapathy for carrying out much of the computer modeling and NMR studies due to which the presentation of this work has improved very much.

The help and cooperation extended by Drs. B.S. Rao, H.S. Soni, A.A. Belhekar, S.G. Hegde, N. Jacob, V. Ramaswamy and all the other scientific and non scientific staffs in the Catalysis Division, NCL, in completing my research work successfully are duly acknowledged.

I take the opportunity to thank my friends, Tomal, Sourav, Soumen, Sanjoy, Sukhen, Sanjib, Karuna, Krishanu, Tania, Tilu, Nepu, Nihar, Sipra, Amitava, Jayanta, Subir, Tushar, Debasis, Rajib, Raghavan, Anil, Eric, Chloe, Tapas, Venkatathri, Maloy, Nikhil and Binod who constantly provided me an encouraging companionship.

Finally, my thanks are due to Dr. P. Ratnasamy, Director, NCL, for allowing me to carry out the research at NCL and to submit the work in the form of a thesis for the award of the Ph.D. degree and to the Council of Scientific and Industrial Research (CSIR), New Delhi, India, for providing me a research fellowship.

Tapan Kumar Das.

[TAPAN KUMAR DAS]

CONTENTS

1. GENERAL INTRODUCTION

1.1 ZEOLITES 1

1.1.1 Chemical Composition 1

1.1.2 Structure and Classification of Zeolites 2

1.1.3 Zeolite synthesis 3

1.1.4 Role of Organic Templates in Zeolite Synthesis 5

1.2 MODIFICATION OF ZEOLITES 5

1.2.1 Isomorphous Substitution 6

1.2.2 Cation Exchange 7

1.3 ACIDITY AND BASICITY IN ZEOLITES 7

1.4 PHYSICO-CHEMICAL CHARACTERIZATION 8

1.4.1 X-ray Diffraction 8

1.4.2 Infrared Spectroscopy 9

1.4.3 Nuclear Magnetic Resonance 10

1.4.4 Sorption and Diffusion in Zeolites 11

1.5 ZEOLITES IN CATALYSIS 13

1.6 TITANOSILICATE MOLECULAR SIEVES 14

1.7 STRUCTURE OF ETS-10 17

1.8 SCOPE OF THE THESIS 24

1.9 REFERENCES 26

2. SYNTHESIS AND MODIFICATION OF ETS-10

2.1 PART-I : SYNTHESIS OF ETS-10 34

2.1.1 INTRODUCTION 34

2.1.2 EXPERIMENTAL 35

2.1.2.1 Synthesis using $TiCl_3$ 37

2.1.2.1(i) Synthesis in the Absence of Templates 37

A. Synthesis of ETS-4(seed) 37
B. Synthesis of ETS-10 using seeds of ETS-4 37
C. Synthesis of ETS-10 without using seeds of ETS-4 39

2.1.2.1(ii) Synthesis of the Presence of Templates 40

A. Synthesis of ETS-10 using choline chloride 40
B. Synthesis of ETS-10 using hexaethyl diquat-5 41

2.1.2.2 Synthesis using $TICl_4$ 42

2.1.3 RESUTS AND DISCUSSION 43

2.1.3.1 Kinetic Studies of Synthesis using $TiCl_3$ 43

2.1.3.1(i) Kinetics of Crystallization in the Absence of Templates 43

A. Influence of temperature on crystallization 43
B. Influence of water content of the gel 45
C. Influence of seed concentration 51
D. Influence of titanium content of the gel 51

2.1.3.1(ii) Kinetics of Crystallization in the Presence of Templates 51

A. Influence of temperature on crystallization 52
B. Influence of water content of the gel 56
C. Influence of template concentration 56
D. Influence of titanium content of the gel 59

2.1.3.2 Kinetics of Crystallization during Synthesis using $TiCl_4$ 62

A. Influence of temperature on crystallization 62
B. Influence of water content of the gel 62

2.2 PART-II MODIFICATION OF ETS-10 66

2.2.1 INTRODUCTION 66

2.2.2 PREPARATION OF MODIFIED ETS -10 66

2.2.2.1 Isomorphous Substitution 66
2.2.2.2 Cation Exchange 67
2.2.2.3 Impregnation with Platinum 68

2.3 REFERENCES 69

3. PHUSICO-CHEMICAL CHARACTERIZATION

3.1 INTRODUCTION 72

3.2 EXPERIMENTAL 72

3.2.1 Chemical Analysis 72
3.2.2 X-ray Diffraction 73
3.2.3 Infrared Spectroscopy 73
3.2.4 UV-Visible Spectroscopy 74
3.2.5 Thermal Analysis 74
3.2.6 Solid State MAS NMR Spectroscopy 75
3.2.7 Molecular Modeling 76
3.2.8 Scanning Electron Microscopy 76
3.2.9 Temperature Programmed Desorption of NH_3 76
3.2.10 Pt-dispersion Measurement by H_2 Chemisorption 79

3.3 RESULTS AND DISCUSSION 79

3.3.1 Chemical Analysis 79
3.3.2 X-ray Diffraction 81
3.3.3 Infrared Spectroscopy 86
3.3.4 UV-Visible Spectroscopy 89
3.3.5 Thermal Analysis 93
3.3.6 Solid State MAS NMR Spectroscopy 97

3.3.6.1 ^{29}Si MAS NMR Spectra of ETS-10(E) 97
3.3.6.2 ^{27}Al, ^{29}Si MAS NMR of ETAS-10 102
3.3.7 Molecular Modeling Studies 105
3.3.8 Scanning Electron Microscopy 111
3.3.9 NH_3-TDP Measurements 113

3.3.10 Pt- dispersion by H_2 Chemisorption 116

3.4 REFERENCES 118

4. SORPTION PROPERITIES OF ETS-10

4.1 INTRODUCTION 120

4.2 EXPERIMENTAL 121

4.2.1 Surface area Measurements 121
4.2.2 Adsorption Measurements 121
4.2.3 Adsorption Isotherms 122

4.3 RESUTLS AND DISCUSSION 122

4.3.1 Surface area Measurements 122
4.3.2 Adsorption of Probe Moleules 124
4.3.3 Adsorption Isotherms 124
4.3.4 Application of Isotherm Equations 130

4.3.1.1 Langmuir Isotherm Equation 130
4.3.1.2 Dubinin Isotherm Equation 130
4.3.1.3 Chemical affinity and the Selectivity of the Sorbate phase 135
4.3.1.4 Isosteric Heats (Q_{st}) of Sorption 140

4.4 REFERENCES 144

5. CATALYTIC PROPERTIES OF ETS-10

5.1 INTRODUCTION 146

5.2 EXPERIMENTAL 147

5.2.1 Preparation of Catalysts 147
5.2.2 Catalytic Reactions 147

5.3 ISOMERIZATION OF m-XYLENE AND 1,3,5 TRIMETHYLBENZENE 148

5.3.1 Isomerization of m-Xylene 146
5.3.2 Isomerization of 1,3,5-Trimethylbenzene 150

5.4 DEHYDRATION OF n-BYTANOL 152

5.5 HYDROISOMERIZATION OF n-HEZANE 154

5.5.1 Introduction 154
5.5.2 Influence of Pt-content 154
5.5.3 Influence of Temperature 158
5.5.4 Influence of Space velocity 158
5.5.5 Influence of H2/n-hexane (mole) Ratio 161

5.6 AROMATIZATION OF n-HEXANE 163

5.6.1 Introduction 163
5.6.2 Effect of nature of Exchanged Metal ion the Aromatization of N-Hexane 163
5.6.3 Studies on Pt-Cs-ETS-10 170
5.6.3.1 Influence of Pt-content 172
5.6.3.2 Influence of Duration of Run 172
5.6.3.3 Influence of Temperature 172
5.6.3.4 Influence of Space velocity 175
5.6.3.5 Comparison with Pt-Al2O3 175

5.6 REFERENCES 179

6. SUMMARY AND CONCLUSIONS

6.1 SYNTHESIS AND KINETIS OF CRYSTALLIZATION 182

6.1.1 Synthesis in Absence of Templates 182
6.1.2 Synthesis in Presence of Templates 182

6.2 CHARACTERIZATION 183

6.3 SORPTION PROPERTIES 184

6.4 CATALYTIC PROPERTIES OF ETS-10 185

6.4.1 Isomerization of m-Xylene and 1,3,5-Trimethylbenzene 185
6.4.2 n-Butanol Dehydration 185
6.4.3 Hydroisomerization of n-hexabe 185
6.4.4 Aromatization n-hexane 185

TH-1080

CHAPTER I

GENERAL INTRODUCTION

1.1 ZEOLITES

In 1756, a Swedish mineralogist, Cronstedt *[1]* observed that the mineral stilbite liberated steam, when heated. This result led him to coin the term zeolite, which is derived from the two Greek words "zeo" to boil and "lithos" stone. Until now, more than 40 natural and 160 synthetic zeolites have been identified with different structures. Zeolites are interesting materials because their pores are uniform in the size range of small molecules (3-13Å). Zeolites can be included under the broader distinction of "molecular sieves". The major applications of zeolites are as cation exchangers in detergent formulations, as adsorbents in drying and separation processes and as catalysts in petroleum and petrochemical industries.

1.1.1 Chemical Composition

Zeolites *[2,3]* are crystalline, microporous aluminosilicates containing a rigid three-dimensional framework of $[SiO_4]^{4-}$ and $[AlO_4]^{5-}$ tetrahedra linked by corner sharing of oxygen ions in such a way that two $[AlO_4]^{5-}$ units are not adjacent *[4]*. The tetrahedral $[AlO_4]^{5-}$ units impart a negative charge (1 unit per Al^{3+}) to the lattice which is counter-balanced by non-framework cations. These cations are easily exchanged giving the zeolites their characteristic ion-exchange properties. More importantly, the cations can be replaced by protons to yield catalytically active solid acids.

Through the 1980s, a variety of novel microporous framework structures were synthesized based on aluminophosphate systems *[5]*. In their pure form, the aluminophosphates are termed as $AlPO_4$s and consist of alternating tetrahedral $[AlO_4]^{5-}$ and $[PO_4]^{3-}$ groups linked through corner sharing of the O-ions. Overall, the frameworks have no net charge and consequently possess no ion-exchange properties and little catalytic potential. Framework substitutions are, however, possible to produce silicoaluminophosphates (SAPOs)

[6] and metal substituted aluminophosphates (MeAPOs) possessing ion-exchange properties *[7]*. In all these materials, the framework metal atoms are ostensibly in tetrahedral coordination although under certain circumstances (*e.g.*, various hydration conditions) the coordination might change to five- or six-fold.

There are, however, some microporous materials where the crystalline framework is made up of ions in different coordinations. ETS-10, the principal material discussed in this thesis, is a titanosilicate composed of tetrahedral $[SiO_4]^{4-}$ and octahedral $[TiO_6]^{8-}$ units. Its crystallographic unit cell can be expressed as :

$$M_{2x/n}[\,(TiO_3)_x\,(SiO_2)_y]\,zH_2O$$

where "M" represents the exchangeable charge balancing cations, generally from the groups I or II of the periodic table or rare-earth elements or organic cations and "n" represents the valency of the cation. The ratio of y/x is constant (*e.g.*, in ETS-10, y/x = 5 and represents the ratio of Si to Ti present in the unit cell). The z represents the number of water molecules, which are reversibly adsorbed in the pores.

1.1.2 Structure and Classification of Zeolites

The primary building unit of the zeolite structure is the individual tetrahedral TO_4 unit, where T is either Si or Al. A secondary building unit (SBU) consists of selected geometric groupings of these tetrahedra. These secondary building units which are 4, 6 and 8-membered rings, 4-1, 5-1 and 4-4-1 branched rings *[3]* can be used to describe most of the known zeolite structures. For the broader classification of microporous materials which includes titanosilicates, additional types of building units are required; these will be discussed in section 1.7, later in the Chapter.

The classification of zeolites can be made on the basis of their morphological characteristics *[2,8-10]*, crystal structure *[2,11]*, chemical composition *[2,12]*, effective pore

diameter *[2,13]* and natural occurrence *[2]*. The classification of zeolites according to their chemical composition has been made on the basis of their silica-to-alumina ratio (SAR) into the following groups *[12]*: (a) low silica zeolites; SAR = 1-1.5 (A, X, sodalite *etc.*), (b) medium silica zeolites; SAR = 1.5-10 (Y, L, mordenite *etc.*), (c) high silica zeolites; SAR = 10 - several thousands (ZSM-5, ZSM-11, EU-1 *etc.*) and (d) Al-free, pure silica zeolites (silicalite-1, silicalite-2, silicious polymorph of MCM-41 *etc.*).

Zeolites are also classified according to their pore openings *[13,14]*. Zeolites containing 8, 10 and 12-membered ring pore opening are referred to as small (pore diameter = 3-4Å), medium (pore diameter = 5-6Å) and large pore (pore diameter ≥ 7Å), respectively. Zeolites can also be classified according to the dimension of the pores, *i.e.*, one-dimensional (1D), two-dimensional (2D) and three-dimensional (3D). Some common natural and synthetic zeolites and other microporous materials are listed in Table 1.1.

1.1.3 Zeolite Synthesis

A conventional synthesis procedure designed for aluminosilicates involves the hydrothermal crystallization of a basic alkali metal aluminosilicate gel (at a certain temperature) under autogeneous pressure *[8]*. Using a fluoride as the mineralizing agent, a method has been developed where the crystallization takes place in neutral to acidic medium *[19]*. In recent years, procedures for the synthesis of metallosilicates containing an element other than Al, such as B-silicate, Fe-silicate, Ti-silicate, V-silicate and Sn-silicate have been investigated *[20-30]*. When metallosilicates are synthesized from gels containing metal ions, these may occupy one or more or all of the following locations in the crystalline solid.

- lattice framework positions
- surface defect sites
- cation exchange sites

Table 1.1 : Classification of some typical microporous and mesoporous materials based on their pore geometry *[9,15-18]*.

Molecular Sieve Type	Ring Size[a] of Channels	Pore Size of Largest Channel[b](Å)	Dimensionality of Channel System
Small Pore			
Linde type A	8-8-8	4.1	3
Erionite	8-8-8	3.6 × 5.1	3
Chabazite	8-8-8	3.8 × 3.8	3
Medium Pore			
ZSM-5	10-10-8	5.3 × 5.6	3
ZSM-11	10-10-10	5.3 × 5.4	3
Ferrierite	10-8	4.2 × 5.4	2
ZSM-48	10	5.3 × 5.6	1
ZSM-22	10	4.4 × 5.5	1
SAPO-11	10	3.9 × 6.3	1
Large Pore			
Faujasite	12-12-12	7.4	3
Beta	12-12	7.6 × 6.4	3
Mordenite	12-8	6.5 × 7.0	2
Linde Type L	12	7.1	1
ZSM-12	12	5.5 × 5.9	1
ETS-10	12-12-7	4.9 × 7.6	3
Mesopore System			
VPI-5	18	12.1	1
MCM-41	-	16-100	1

[a]Number of T or O atoms comprising smallest rings in channels

[b]Mainly crystallographic diameters

- finely dispersed oxide clusters inside/outside the pores
- bulk oxides on the external surface

To achieve the successful incorporation of metal ions in the zeolite framework during crystallization by direct hydrothermal synthesis, it is necessary to form a good metallosilicate gel. Since the final metallosilicate gel is basic (pH = 9-13), much depends on the solubility of the metal oxide/hydroxide formed. The sequence of addition in these cases is very important and the precipitation of the metal oxide/hydroxide must be prevented by a careful sequence of addition of reactants. In the synthesis of ETS-10 and ETAS-10 described in the thesis, various parameters have been optimized to improve the phase purity of the ultimate material as well as to decrease the time required for crystallization. This observation is discussed in more detail in Chapter II describing the synthesis of ETS-type materials.

1.1.4 Role of Organic Templates in Zeolite Synthesis

Lok *et al. [31]* have reviewed the role of organic compounds in the synthesis of molecular sieves. These organic molecules may be present in the zeolite void as space-fillers, as neutral species and/or as cations *[32]*. However, the exact role of organic guest molecules during zeolite formation is not yet clear. The same organic compound may lead to the formation of different zeolite structures *[33-35]* and a particular zeolite structure can be synthesized using a variety of organic molecules *[31]* having different shapes, sizes and structures. The above observations are yet to be explained fully.

1.2 MODIFICATION OF ZEOLITES

The as-synthesized zeolites usually contain substantial amounts of alkali metal ions or organic templates. To use the zeolites in acid-catalyzed reactions, they should be template

free (*i.e.*, the internal area is fully accessible) and they have to be converted into the protonic form. It may also be necessary to modify the as-synthesized zeolite to improve the thermal stability or alter the strength of the acidity or basicity. The methods of modifying zeolites and other molecular sieves are described in the following subsections.

1.2.1 Isomorphous Substitution

Barrer *[36]* has classified four types of isomorphous replacement in zeolites.

- One guest molecule by another
- One cation by another
- One element by one of its isotopes
- One element in the framework position by another

The fourth method leads to the substitution of one element by another in the zeolite lattice, essentially altering many of the properties of the zeolite.

Isomorphous substitution of the lattice silicon or aluminum atoms by other foreign elements is an interesting aspect of zeolites. In 1952, the first replacement of the zeolite framework species was reported by Goldsmith *[37]* in the synthesis of germanium-containing thomsonite, wherein Ge replaced Si in the lattice. In the past decade, the isomorphous substitution of bi-, tri-, tetra- and penta-valent elements like Be, B, Ga, In, Ge, Ti, V, Sn, Cr, Fe, Co, W, Zr, Mo, As and P into the framework of various zeolite structures has been reported *[20-30,38-48]*. It is well established that the substitution of such metal ions in the zeolite framework modifies the Brönsted acidity. Besides, the substitution by transition metal ions has extended the use of zeolites (metallosilicates) to redox reactions.

1.2.2 Cation Exchange

The cations present in the non-framework or exchange positions can be substituted by other cations through ion-exchange. The cation-exchange capacity of a zeolite is determined by its chemical composition, the density and nature of the cationic sites present and their distribution. The cations in a zeolite, present in their hydrated form, are loosely attached to the framework and have a high degree of mobility. These can be partially or completely replaced by other univalent, divalent or multivalent ions by ion-exchange, hydrothermal fusion or vapour-phase treatments *[49]*. Barrer *[50,51]*, Rees *[52]* and Sherry *[53,54]* have studied the ion-exchange equilibria in X and Y zeolites in detail. Ion Sieve Effect *[8]*, *i.e.*, the penetration of only some types of cations through the channels or cages of the zeolite, is observed in some cases. For example, Rb^+ (radius = 1.48Å) can be exchanged in analcime but not Cs^+ (radius = 1.65Å).

When the exchanged cation is an easily reducible metal such as Pt, Pd and Ni, bifunctional catalysts containing acidic and metallic functions (well dispersed) can be prepared from zeolites by ion exchanging with suitable salt solutions and subsequent reduction. In this investigation, we have prepared bifunctional Pt-ETS-10 catalysts by ion-exchanging (Na/K)-ETS-10 with $Pt(NH_3)_4(NO_3)_2$ and subsequent reduction of the material.

Other methods of loading metals over a zeolite support include solid state ion-exchange *[55]* and chemical vapour deposition *[56]*.

1.3 ACIDITY AND BASICITY IN ZEOLITES

Acidity in zeolites arises from charge compensation by protons of the negative charge on the framework arising from the presence of trivalent metal atoms such as Al, Ga and Fe present in the tetrahedral coordination *[2]*. In the case of ETS-10, the framework negative charge arises from the presence of the tetravalent metal ion Ti^{4+} in an octahedral coordination

in framework positions *[57]*. The charge compensating protons attached to the zeolite framework exhibit Brönsted acidity *[58]*. The thermal treatment of protonic zeolites causes the transformation of Brönsted acid sites into Lewis acid sites. The number of acid sites increases with increasing concentration of the trivalent metal ion in the framework position, but the strength of the acid sites tends to decrease *[59]*.

Various methods of determining and measuring the acidity of zeolites have been reviewed *[60-62]*. These are : (i) IR spectroscopy of structural hydroxyl groups and adsorbed bases like ammonia and pyridine (ii) alkane cracking (iii) temperature programmed desorption of NH_3 (iv) microcalorimetry and (v) solid-state NMR of -OH groups and sorbed bases.

Similarly, the basicity in zeolites arises from framework oxygen atoms. The extent of charge on the oxygen determines their basic strength. The application of basic zeolites in catalysis and adsorption has been reported *[63,64]*. Burthomeuf *et al.[65]* have shown that the basic strength of the zeolite depends not only on the chemical composition but also on the structural environment of the framework oxygen.

1.4 PHYSICO-CHEMICAL CHARACTERIZATION

A variety of techniques are used to characterize zeolites, a few of which are discussed briefly in the succeeding sections.

1.4.1 X-ray Diffraction

Powder X-ray diffraction is widely used in the study of zeolites. It can provide information about : (i) zeolite structure *[66,67]* (ii) phase purity (iii) degree of crystallinity (iv) unit cell parameters *[2]* and (v) crystal size. X-ray diffraction is useful in the estimation of the average Al content from the unit cell volumes of zeolite crystals *[68,69]*. Isomorphous substitution of framework positions is accompanied by a change in the unit-cell parameters of

the zeolite *[70-73]*. Synthesized zeolite materials are assumed to be pure when their X-ray patterns match exactly with the 2θ values and relative intensities reported by earlier workers *[9,66,74,75]*.

High resolution electron microscopy (HREM) is sometimes used along with XRD techniques for structure determination. The structures of VPI-5 *[76,77]*, cloverite *[78]*, MCM-22 *[79]* and ETS-10 *[57]* were established recently with the help of HREM.

1.4.2 Infrared Spectroscopy

Infrared spectroscopy is a sensitive technique for the investigation of the structural details of zeolites, isomorphous substitution, acidic properties and the nature of adsorbate-zeolite interactions *[80,81,58]*. The lattice vibrations of zeolites in the infrared spectrum are observed in the range of 300-1300 cm^{-1}. The structural hydroxyl groups and zeolite's water are observed in the range 3500-3700 cm^{-1} *[81,58]*. The framework vibrations can be classified into two groups: (i) internal vibrations of the TO_4 units or structure insensitive vibrations and (ii) vibrations due to external linkages of the TO_4 units or structure sensitive vibrations *[80,81]*. The major infra-red band assignments are given in Table 1.2.

Table 1.2 : IR bond assignments for zeolites.

Internal Tetrahedra	
Asymmetric Stretching	1250-950 cm^{-1}
Symmetric Stretching	720-650 cm^{-1}
T-O bend	420-500 cm^{-1}
External Linkages	
Pore opening	300-420 cm^{-1}
Double Ring	500-650 cm^{-1}
Symmetric Stretching	750-820 cm^{-1}
Asymmetric Stretching	1050-1150 cm^{-1}

Isomorphous substitution shifts both symmetric and asymmetric framework vibrations. The substitution of lighter elements, such as B, shifts the framework vibrations towards higher wavenumbers *[58]*, while the incorporation of heavier metal ions, such as Fe, Ga, Ti and V, shifts the vibrations to lower wavenumbers *[82]*. In the case of Ti, V and Sn silicates an additional asymmetric stretching vibration at around 960 cm^{-1} has been reported. This band has been variously attributed to Si-O-M (M = Ti, V, Sn) linkages or Si-OH vibrations at defect sites adjacent to the metal atom (M)*[83-85]*. Acidity of zeolites (Lewis and Brönsted sites) can be studied both qualitatively and quantitatively by IR spectroscopy of adsorbed bases *[86]*.

1.4.3 Nuclear Magnetic Resonance

High-resolution, solid-state MAS NMR spectroscopy is a powerful technique to characterize the framework and non-framework elements in zeolites *[87-91]*. In the zeolite system, most of the Q-units are Q^4 type units, *i.e.*, $Si(OT)_4$, where the T atom is either Si or Al or a mixture of these. Five different Q^4 units are possible, namely, Si(0Al)(4Si), Si(1Al)(3Si), Si(2Al)(2Si), Si(3Al)(1Si) and Si(4Al)(0Si). The ^{29}Si NMR spectrum of the zeolite may consist of one to five possible Si(nAl)((4-n)Si) environments in the zeolite framework. With increasing number of Al atoms (n) in the first coordination sphere of the silicon atom, the ^{29}Si NMR signals are systematically shifted to a lower field, each Al substitution contributing to a shift of about 5 ppm *[92]*. The ^{29}Si chemical shift values for various Si(nAl) environments in Q^4 aluminosilicate are in the range of δ = -80 to -125 ppm with respect to TMS.

The isotropic ^{27}Al chemical shifts of aluminosilicates are primarily determined by the coordination number of the aluminum atom *[93]*. The chemical shift ranges observed (with

reference to $[Al(H_2O)_6]^{3+}$) are about +50 to +80 ppm for tetrahedral AlO_4, about -10 to +20 ppm for octahedral AlO_6 and about +30 to +40 ppm for the relatively rare, tetragonal bipyramidal AlO_5 units *[88]*.

1.4.4 Sorption and Diffusion in Zeolites

Zeolites are porous, crystalline materials with ability to sorb selected molecules inside their channels and cavities. Sorption measurements using probe molecules of different critical dimensions have been used to gauge the effective size of these pores *[94,95]*. By suitable choice of sorbate molecules which have different critical dimensions and shapes, the shape of the pore, circular or elliptical, may be differentiated *[96,97]*.

Zeolites are also used as selective adsorbents due to their high sorption capacity *[8]* and their ability to separate molecules based upon size and orientation with respect to the size of their pores. Different isotherm equations such as Langmuir, Brunauer-Emmett and Teller (BET), Freundlich, Dubinin and Sips have been used to analyze sorption in zeolites *[98-101]*. From these equations, surface area, pore volume, isosteric heats and the chemical potential of sorption processes could be calculated. These isotherm equations are summarized in Table 1.3 and the main assumptions associated with each are mentioned.

In heterogeneous catalysis, adsorption and diffusion properties control the observable rate of chemical reactions at catalytic sites. The theory and the role of diffusion in heterogeneous catalysis were developed by Thiele *[102]* and Wheeler *[103]*. Diffusion in zeolite catalysts may be divided into three types:

(i) Bulk Diffusion : In bulk diffusion, molecular translational velocity is proportional to the square root of the temperature and inversely proportional to the square root of the molecular weight of the diffusing molecules.

Table 1.3 : Isotherm equations and their main assumptions.

Type	Equation	Main assumption
Langmuir	$\frac{P}{V} = \frac{1}{V_m} + \frac{1}{bV_m}$	Monolayer Adsorption
BET	$\frac{\left(P/P_o\right)}{V\left(1 - P/P_o\right)} = \frac{1}{CV_m} + \left(\frac{P}{P_o} \times \frac{(C-1)}{CV_m}\right)$	Multilayer Adsorption
Dubinin	$\log(W) = \log(W_o) - \left(\frac{B}{2.303\beta^2} \times \left[T.\log\left(P/P_o\right)\right]^2\right)$	Pore Filling Theory
Sips	$\log\left[\frac{\theta}{(1-\theta)}\right] = \log A + c \log P$	Similar to Langmuir's Model

V = Volume adsorbed at equilibrium pressure P

V_m = Monolayer volume

b = Constant

P_o = Saturation vapour pressure of adsorbate

C = Differential heat of adsorption

W = Amount sorbed at equilibrium pressure P

W_o = Total sorption capacity

B = Constant, dependent on temperature T (K) and characteristic of the sorbent pore structure

β = Affinity coefficient

A and c = Constants

θ = Coverage at an equilibrium pressure P.

(ii) Knudsen diffusion : In Knudsen diffusion, a molecule within a pore on an average, will collide with the pore wall more often than it collides with a second molecule. The Knudsen diffusion coefficient is $(D_k) = \sqrt{T/M} \cdot r$, where M = molecular weight of the diffusing species and r is the radius of the pore.

(iii) Confugurational diffusion : This type of diffusion occurs when the diameter of the pores approaches the dimensions of the molecules. Diffusion is extremely slow and the diffusion rate is highly susceptible to even minor changes (of a fraction an Å) in the pore or molecular dimensions *[104]*.

1.5 ZEOLITES IN CATALYSIS

The industrial use of zeolites as catalysts started in the beginning of the 1960s. Since then, they have been used in many commercial processes such as the isomerization of xylenes and n-paraffins, cracking and hydrocracking of heavy oils, the dewaxing of petroleum oils, the transformation of methanol to gasoline, olefin oligomerization and alkylation of benzene. The main advantages in the use of zeolites as catalysts *[105]* are listed below :

- high internal surface area,
- uniform pores of one or more discrete sizes,
- good thermal stability,
- ability to sorb and concentrate hydrocarbons at the surface,
- shape selective properties,
- tailoring of acidity of zeolites through various methods such as changing Si/Al ratio and ion-exchange with rare earth ions,
- zeolites can also be converted into solid bases through ion-exchange with alkali metal cations such as Cs^+ and Rb^+ *[106]* and by impregnating with sodium azide *[107]* or with cesium acetate *[108]*,

- zeolites can be used as selective oxidation catalysts by substituting metal ions such as Ti, V, Sn, Cr, Zr in the framework *[27,29,42,45,109]* and
- well defined crystal structure enabling better quality control of preparations.

1.6 TITANOSILICATE MOLECULAR SIEVES

The titanosilicate, TS-1 possessing the MFI structure was reported by Taramasso *et al.* in 1983 *[110]*. Since then, other titanosilicates, such as TS-2 (MEL) *[111]*, Ti-beta *[112,113]*, Ti-ZSM-48 *[114,115]*, Ti-MCM-41 *[24,116]* and Ti-HMS *[25]* have also been synthesized. In all the above molecular sieves, the Ti^{4+} ions are believed to be present in tetrahedral coordination along with Si^{4+} ions, bridged by oxygen linkages. Due to charge equivalence of the ions (Si^{4+} and Ti^{4+}), these molecular sieves cannot theoretically possess any Brönsted acid sites. These materials oxifunctionalize/oxidize a variety of organic molecules *[26,117-122]* in the presence of hydrogen peroxide or *tert*-butylhydroperoxide (TBHP). The uniformly distributed and tetrahedrally coordinated Ti^{4+} is reported to be responsible for the catalytic activity of these materials in oxidation reactions. According to Notari *[84]*, a possible representation of the active site in TS-1 is :

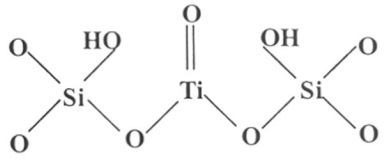

However, others believe that the Ti^{4+} ions are present as regular $[TiO_4]^{4-}$ tetrahedra corner sharing with four $[SiO_4]^{4-}$ units in the framework *[123]* or in the defect sites in the structure *[124]*. Evidence suggests that TS-1 contains an appreciable number of isolated, active titanyl centers uniformly distributed within the crystal. Each Ti^{4+} center is surrounded by Si^{4+} and is isolated from other titanyl centers by long Si-O-Si-O sequences *[84]*. This

isolation of the Ti^{4+} centers is presumed to be responsible for the high selectivities observed with TS-1 *[125]* and may be related to a significantly reduced rate for H_2O_2 decomposition (*i.e.*, to O_2) *[84]*. The critical importance of structurally isolated active sites for achieving high selectivity in oxidation catalysis was first recognized by Grasselli *et al. [126,127]*. The isolation of titanyl centers may also inhibit their oligomerization, a deactivating tendency which occurs in many reactions of oxometals in solution *[125]*. Sheldon *[125]* also observed that the catalytic characteristics of TS-1 resemble those of a Ti^{4+}/SiO_2 catalyst where isolated titanyl sites were thought to be involved. Notari *[84]* noted the high affinity of H_2O_2 for TS-1 and also suggested that the addition of H_2O_2 leads to the formation of surface titanium peroxo compounds, which could either be in the hydrated (Fig. 1.1a) or dehydrated (Fig. 1.1b) forms.

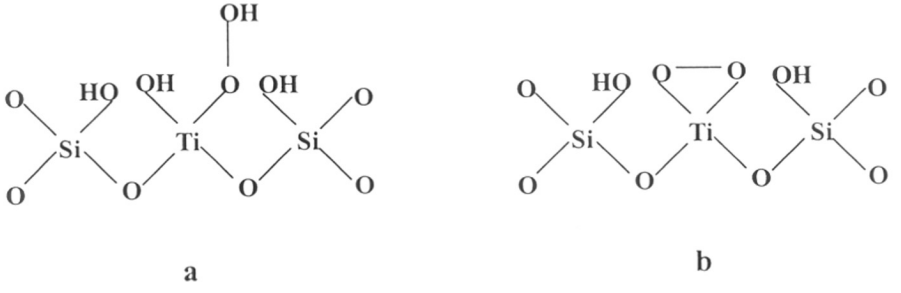

Fig. 1.1 : Likely structures of peroxo complexes in titanosilicate molecular sieves.

The precise catalytic mechanisms associated with TS-1 are not yet fully resolved *[128]*, but the key event may be the transfer of peroxidic oxygen to the substrate to be oxidized *[129]*.

There has been some success recently in synthesizing microporous materials with framework atoms in different coordinations. The notable ones are the microporous titanosilicates, ETS (Engelhard titanosilicates) *[130-135]* and molybdenum phosphates

(MOPOs) *[136]*. Both the above titanosilicates and MOPOs contain both tetrahedral and octahedral framework atoms incorporated in stoichiometric quantities and not as dopants. In most minerals, titanium adopts an octahedral coordination while silicon adopts a tetrahedral coordination. Zorite *[137,138]* is a rare naturally occurring microporous octahedral/ tetrahedral titanosilicate. Zorite has a highly disordered framework with a two-dimensional channel system. Cacoxenite *[139]* is a naturally occurring octahedral/tetrahedral phosphate structure with one of the largest pores ever observed.

1.7 STRUCTURE OF ETS-10

COMPUTERISED

A crystal structure model of ETS-10 has been proposed by Anderson *et al.[57,140,141]* based on chemical analysis, structural modeling, XRD, HREM and high resolution MAS NMR studies. ETS-10 is a particularly important structure as it possesses a three-dimensional 12-ring pore system. Very few zeolite structure types have such an open pore geometry, the most important other examples being zeolite Y (FAU) *[142]* and zeolite β (BEA) *[143]*. Neither disorder nor faulting in ETS-10 should result in pore-system blockage; indeed, some type of planar faults increase pore access.

The framework of ETS-10 is composed of tetrahedral $[SiO_4]^{4-}$ and octahedral $[TiO_6]^{8-}$ units. The TiO_6 units (Fig. 1.2a) are connected to each other to form a -Ti-O-Ti-O-Ti- chain (Fig. 1.2b). The structure can be envisaged to be constructed from rods consisting of two chains of silicate 5-rings connected by octahedral titanate units, as shown in Figure 1.2c. Each titanium atom is linked via oxygen to four silicon atoms in two 3-rings and also via oxygen to other titanium atoms. The framework structure of ETS-10 is shown in Figure 1.2d. All silicon atoms, except those at the apex of each 5-ring, are connected to three silicon atoms and one titanium atom via oxygen [Si(3Si, 1Ti)]. The apical silicon in each 5-ring is a [Si(4Si, 0Ti)] unit. Two rods of Ti perpendicular to each other join together by forming 7-membered rings (Figure 1.2d). The complex of the rods is regularly arranged along x- and y-axis with a period of 15Å and a large channel with a 12-membered ring aperture is formed.

Two ordered polymorphs of ETS-10, polymorph A and B, analogous to β *[143]* have been described by Anderson *et al. [57,140]*. The 12-membered ring having a zigzag arrangement, forming polymorph A, is shown in Figure 1.3a. Polymorph A has either $P4_1$ or $P4_3$ symmetry and has a tetragonal lattice with unit-cell parameters, a = b = 14.84Å, c = 27.08Å and $\alpha = \beta = \gamma = 90°$. Consequently, polymorph A has a screw axis and therefore will

RR
66.097.3(043)
DAS

TH-1080

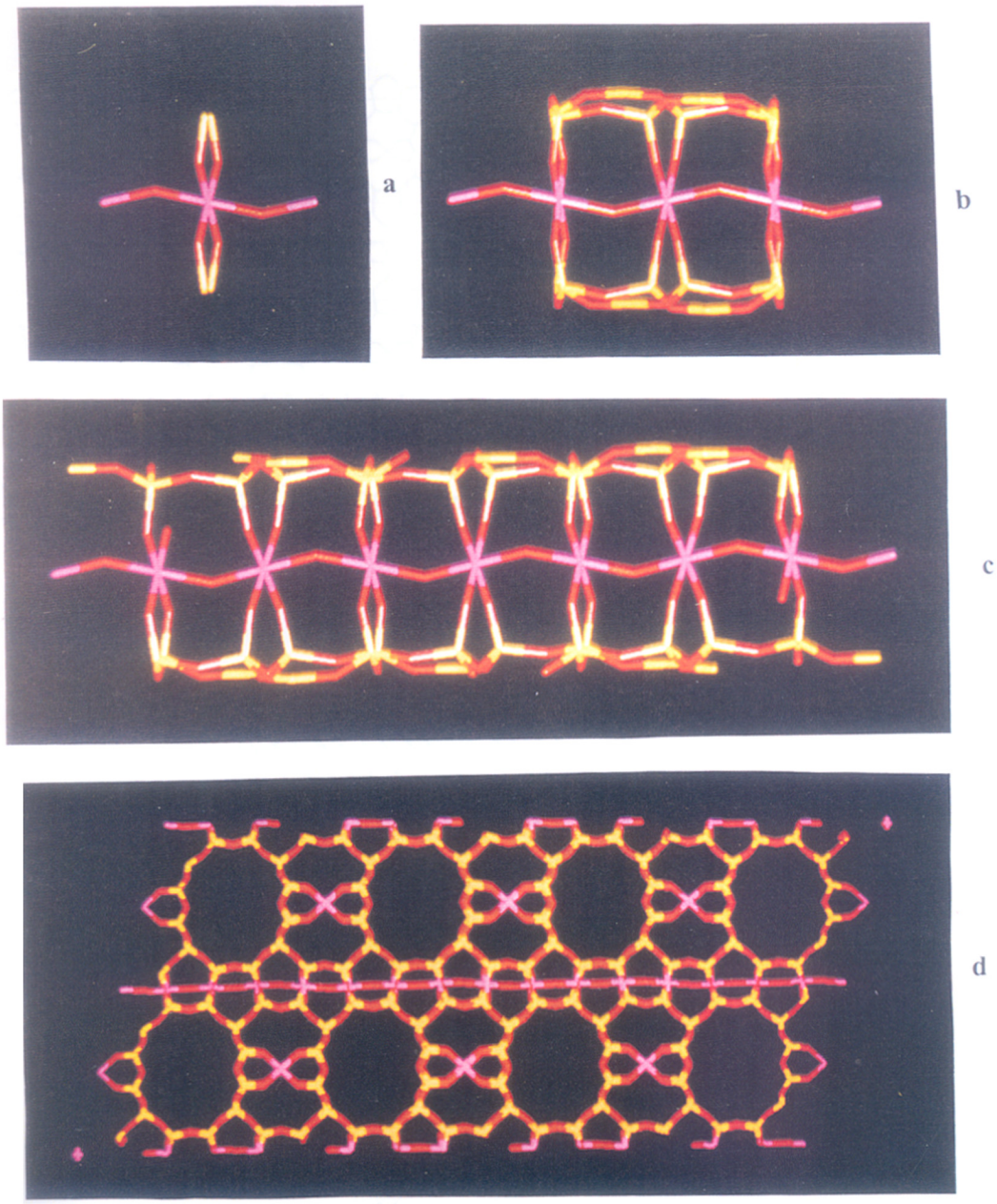

Fig. 1.2 : Structural components and the framework of ETS-10 :

a, One octahedral TiO_6 unit,

b, Three octahedral TiO_6 units connected,

c, Ti-O-Ti-O-Ti chain and

d, Framework structure of ETS-10.

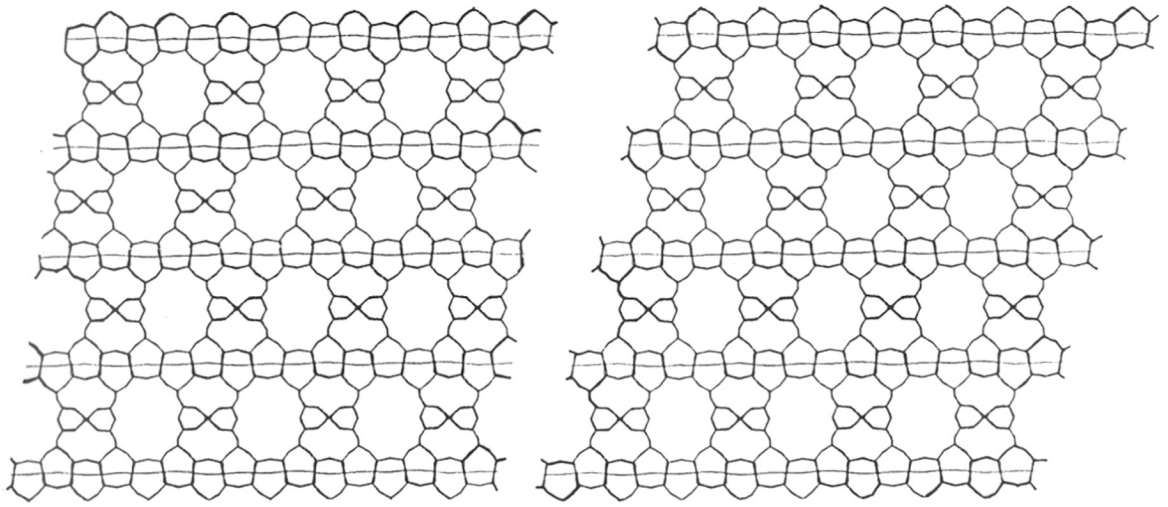

a b

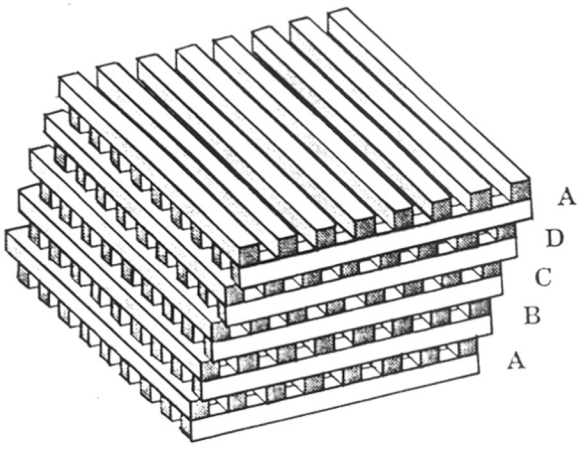

c

Fig. 1.3 : Schematic diagrams of the structure of ETS-10 polymorphs :
a, Polymorph A,
b, Polymorph B and
c, Rod stacking model for polymorph B.

display chiral symmetry. In fact there is a spiral channel along the c-direction, with a pitch of 27.08Å. In polymorph A, there are four crystallographically different Ti-sites and 20 Si-sites.

Polymorph B (Figure 1.3b) has a C2/c symmetry and has a monoclinic lattice with unit-cell parameters, a = b = 21.00Å, c = 14.51Å, $\alpha = \gamma = 90°$ and $\beta = 111.12°$. The main straight 12-membered ring dimension is 4.9Å x 7.6Å. In polymorph B, there are three crystallographically different Ti-sites and 11 Si-sites. A schematic drawing of the stacking of sheets consisting of rods for perfect ABCD stacking for the construction of polymorph B is shown in Figure 1.3c. The unit-cell composition of ETS-10 is $[Si_{80}Ti_{16}O_{208}]^{32-}$ presented in Figure 1.4.

The connectivity of different Si- and Ti-sites, bond angles and bond length of the polymorph B calculated using a Silicon Graphics Indigo II Work Station and reported crystal structure *[57,140]*, are given in Tables 1.4 and 1.5, respectively. These bond angles and bond lengths are discussed in detail in Chapter III.

It is important to note that the titanium atoms are not accessible to the main channels, which prevents the use of ETS-10 as a redox catalyst.

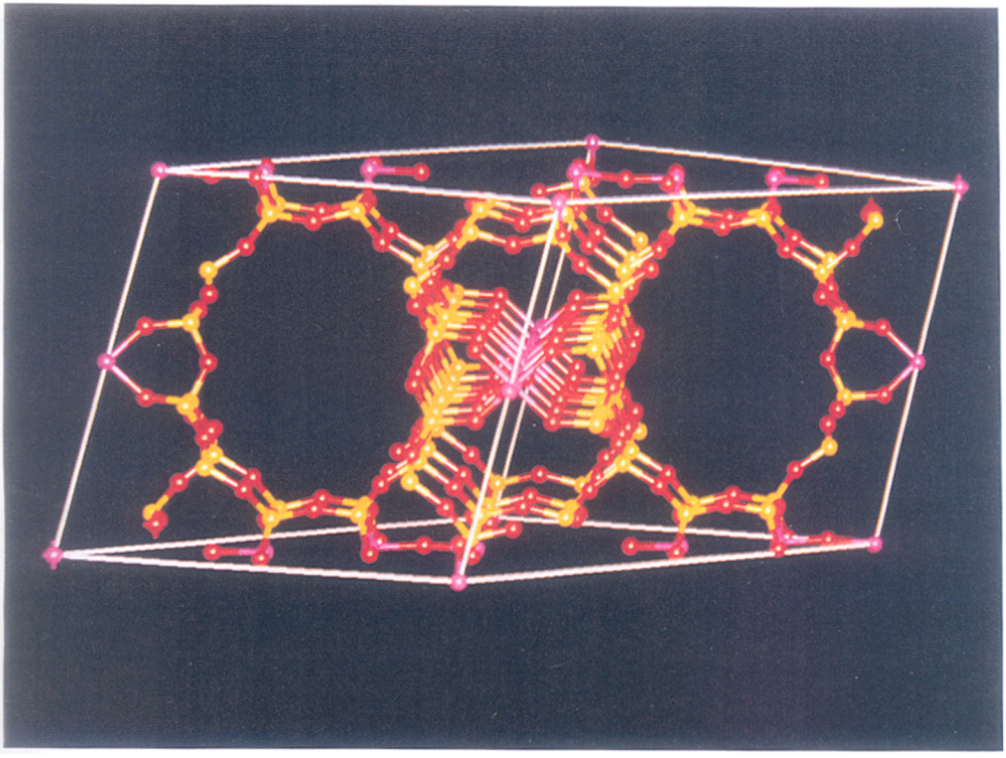

Fig. 1.4 : Unit cell of ETS-10.

Table 1.4 : Si-O and Ti-O distances in ETS-10.

Bond	Bond distance (Å)	Average bond distance (Å)	Bond	Bond distance (Å)	Average bond distance (Å)
Si1-O14	1.58		Si9-O4	1.59	
Si1-O14	1.58	1.5750	Si9-O13	1.55	1.5775
Si1-O15	1.57		Si9-O19	1.59	
Si1-O15	1.57		Si9-O25	1.58	
Si2-O1	1.57		Si10-O1	1.57	
Si2-O2	1.59	1.5775	Si10-O5	1.58	1.5775
Si2-O3	1.56		Si10-O21	1.57	
Si2-O4	1.59		Si10-O26	1.59	
Si3-O5	1.58		Si11-O24	1.57	
Si3-O6	1.59	1.5775	Si11-O24	1.57	1.5800
Si3-O7	1.55		Si11-O25	1.59	
Si3-O23	1.59		Si11-O25	1.59	
Si4-O8	1.59		Ti1-O10	1.90	
Si4-O12	1.59	1.5775	Ti1-O10	1.90	
Si4-O15	1.56		Ti1-O11	1.87	1.8867
Si4-O22	1.57		Ti1-O11	1.87	
Si5-O11	1.59		Ti1-O19	1.89	
Si5-O12	1.59	1.5775	Ti1-O19	1.89	
Si5-O13	1.56		Ti2-O6	1.89	
Si5-O26	1.57		Ti2-O6	1.89	
Si6-O3	1.57		Ti2-O9	1.90	1.8867
Si6-O16	1.59	1.5800	Ti2-O9	1.90	
Si6-O20	1.59		Ti2-O18	1.87	
Si6-O21	1.57		Ti2-O18	1.87	
Si7-O7	1.57		Ti3-O2	1.89	
Si7-O14	1.57	1.5800	Ti3-O8	1.88	
Si7-O18	1.59		Ti3-O9	1.90	1.8833
Si7-O20	1.59		Ti3-O10	1.90	
Si8-O17	1.59		Ti3-O16	1.87	
Si8-O22	1.56	1.5775	Ti3-O17	1.89	
Si8-O23	1.59				
Si8-O24	1.57				

Table 1.5 : Si-O-Si and Si-O-Ti angles in ETS-10.

Connectivity	Angles (degrees)	Average angles (degrees)	Connectivity	Angles (degrees)	Average angles (degrees)
Si1-O15-Si4	148.45		Si9-O4-Si2	149.13	
Si1-O15-Si4	148.45	149.7000	Si9-O13-Si5	132.67	143.7625
Si1-O14-Si7	150.95		Si9-O25-Si11	151.31	
Si1-O14-Si7	150.95		Si9-O19-Ti1	141.94	
Si2-O3-Si6	132.38		Si10-O1-Si2	149.01	
Si2-O4-Si9	149.13	142.8200	Si10-O5-Si3	151.66	150.7725
Si2-O1-Si10	149.01		Si10-O26-Si5	150.39	
Si2-O2-Ti3	140.76		Si10-O21-Si6	152.03	
Si3-O7-Si7	131.86		Si11-O24-Si8	153.07	
Si3-O23-Si8	147.55	142.6525	Si11-O24-Si8	153.07	152.1900
Si3-O5-Si10	151.66		Si11-O25-Si9	151.31	
Si3-O6-Ti2	139.54		Si11-O25-Si9	151.31	
Si4-O12-Si5	149.20		Ti1-O11-Si5	141.53	
Si4-O22-Si8	139.20	144.3525	Ti1-O11-Si5	141.53	
Si4-O15-Si1	148.45		Ti1-O19-Si9	141.94	145.9900
Si4-O8-Ti3	140.56		Ti1-O19-Si9	141.94	
Si5-O12-Si4	149.20		Ti1-O10-Ti3	154.50	
Si5-O13-Si9	132.67	143.4475	Ti1-O10-Ti3	154.50	
Si5-O26-Si10	150.39		Ti2-O6-Si3	139.54	
Si5-O11-Ti1	141.53		Ti2-O6-Si3	139.54	
Si6-O3-Si2	132.38		Ti2-O18-Si7	139.60	144.6867
Si6-O21-Si10	152.03	143.1475	Ti2-O18-Si7	139.60	
Si6-O20-Si7	147.62		Ti2-O9-Ti3	154.92	
Si6-O16-Ti3	140.56		Ti2-O9-Ti3	154.92	
Si7-O7-Si3	131.86		Ti3-O17-Si8	140.74	
Si7-O14-Si1	150.95	142.5075	Ti3-O16-Si6	140.56	
Si7-O20-Si6	147.62		Ti3-O10-Ti1	154.50	145.3400
Si7-O18-Ti2	139.60		Ti3-O8-Si4	140.56	
Si8-O23-Si3	147.55		Ti3-O9-Ti2	154.92	
Si8-O22-Si4	139.20	145.1400	Ti3-O2-Si2	140.76	
Si8-O24-Si11	153.07				
Si8-O17-Ti3	140.74				

1.8 SCOPE OF THE THESIS

A new family of microporous titanosilicate molecular sieves called ETS-4 and ETS-10 was discovered at Engelhard in 1990. Eventhough, the synthesis of ETS-10 has been reported in the literature, investigations on its synthesis, characterization and catalytic properties have not been published in a unified manner. ETS-10 has a Si/Ti ratio of 5, with a double negative charge imparted on the framework by each Ti ion, the negative charges being compensated by cations. The cation density in ETS-10 is, therefore, approximately equivalent to that in a zeolite with Si/Al = 2.5 such as zeolite Y. This makes ETS-10 potentially a very interesting material both for cation exchange and catalysis. With regard to catalysis, the high framework charge and cation exchange capacity impart basic properties to the cationic form while the protonic form possesses acidic properties. Besides, the large pores (12 MR) and the open pore system make this molecular sieve potentially useful in catalyzing reactions involving large molecules.

Additionally, the synthesis of ETS-10 has been reported to be slow requiring the use of ETS-4 seeds. It was therefore interesting to study the synthesis, characterization and catalytic properties of ETS-10 in detail.

Two different methods of synthesis will be studied : (1) synthesis using $TiCl_3$ in the absence and presence of templates and (2) synthesis using $TiCl_4$. The kinetics of crystallization of the above two synthesis methods will also be carried out. The influence of temperature and compositional variations on the nucleation and crystallization of the molecular sieve, as well as size and shape of the molecular sieve crystals will be examined. The synthesis of aluminium substituted ETS-10 (ETAS-10) will also be carried out.

Physico-chemical characterization of the ETS-10 samples synthesized by the different methods will be carried out using instrumental techniques such as XRD, SEM, FTIR,

TGA/DTA, UV-Visible, NH_3-temperature programmed desorption, Pt-dispersion by H_2 chemisorption and MAS NMR. MAS NMR studies will be carried out in detail to obtain information regarding the different silicon environments in ETS-10. Besides, the location of Al in ETAS-10 will be investigated by MAS NMR and computer modeling techniques.

Sorption kinetics of different probe molecules like water, n-hexane and 1,3,5-trimethylbenzene will be carried out to find out the approximate pore diameter of ETS-10. Sorption isotherms of alkali metal exchanged ETS-10 samples will be studied using different probe molecules like water, m-xylene and p-xylene. The sorption isotherm data will be examined using Langmuir and Dubinin isotherm equations to calculate chemical affinities and isosteric heats.

Catalytic test reactions, such as m-xylene and 1,3,5-trimethylbenzene isomerization and alcohol dehydration will be carried out over H-ETS-10 samples to characterize pore dimensions and acidity. The hydroisomerization of n-hexane will be carried out over Pt-H-ETS-10 to study its performance as an isomerization catalyst. The aromatization of n-hexane over alkali metal (Li, Na, K, Rb and Cs) and alkaline earth metal (Mg, Ca, Ba) exchanged Pt-M-ETS-10 will be investigated as the above materials are basic in nature and their catalytic properties might be similar to those of the basic Pt-L catalysts.

1.9 REFERENCES

1. Cronstedt, A.F., *Adak. Handl. Stockholm,* **17**, 120 (1756).
2. Barrer, R.M., "Hydrothermal Chemistry of Zeolites", Academic Press, New York, (1982).
3. Szostak, R., "Molecular Sieves, Principles of Synthesis and Identification", Van Nostrand Reinhold Catalysis Series, New York, (1989).
4. Loewenstein, W., *Am. Mineral.,* **39**, 92 (1954).
5. Wilson, S.T., Oak, S., Lok, B.M., Flanigen, E.M., and Plains, W., US Pat., 4,310,440 (1982).
6. Lok, B.M., Messina, C.A., Gajek, R.T., Cannan, T.R., and Flanigen, E.M., US Pat., 4,440,871 (1984).
7. Wilson, S.T., Oak, S., and Flanigen, E.M., US Pat., 4,567,029 (1986).
8. Breck, D.W., "Zeolite Molecular Sieves : Structure, Chemistry and Use", London, Wiley, (1974).
9. Meier, W.H., Olson, D.H., "Atlas of Zeolite Structure Types", London, Butterworths-Heinemann, Boston, MA, 3rd Ed., p. 1-200 (1992).
10. Bragg, W.L., "The Atomic Structure of Minerals", Cornell University Press, Ithaca, New York, (1937).
11. Meier, W.M., "Molecular Sieves, Soc. of Chem. Ind., London, 10 (1968).
12. Flanigen, E.M., "in Proceedings of the 5th International Conference on Zeolites", (L.V.C. Rees, Eds.) Naples, Italy, June 2-6, 760 (1980).
13. Sand, L.B., Econ. Geol., 191 (1967).
14. Barrer, R.M., "Zeolites and Clay Minerals as Sorbents and Molecular Sieves", Academic Press, New York, London, Ch. 2 (1978).
15. Venuto, P.B., *Microporous Mater.,* **2**, 297 (1994).
16. Chen, N.Y., Gardwood, W.E., and Dwyer, F.G., "Shape Selective Catalysis in Industrial Applications", Marcel Dekker (Ed.), New York (1996).

17. Flanigen, E.M., Lok, B.M., Patton, R.L., and Wilson, S.T., *Stud. Surf. Sci. Catal.*, **28**, 103 (1986).

18. Haag, W.O., and Chen, N.Y., Catalyst Design Process and Perspectives, Hegedus, L.L. (Ed.), John Wiley and Sons, New York, Ch. 6 (1987).

19. Guth, J.L., Kessler, H., Higel, J.M., Lamberlin, J.M., Patarim, J., Sieve, A., Chezean, J.M., and Wey, R., *ACS Symposium Ser.*, Washington D.C., **398**, 176 (1989).

20. Mueller, U., and Steck, W., *Stud. Surf. Sci. Catal.*, **84**, 203 (1994).

21. Zones, S.I., and Nakagawa, Y., *Microporous Mater.*, **2**, 543 (1994).

22. Kotasthane, A.N., Shiralkar, V.P., Hegde, S.G., and Kulkarni, S.B., *Zeolites*, **6**, 253 (1986).

23. Yuan, Z.Y., Liu, S.Q., Chen, T.H., Wang, J.Z., and Li, H.X., *J. Chem. Soc. Chem. Commun.*, 973 (1995).

24. Franke, O., Rathousky, J., Schulz-Ekloff, G., Starek, J., and Zukal, A., *Stud. Surf. Sci. Catal.*, **84**, 77 (1994).

25. Tanev, P.T., Chibwe, M., and Pinnavaia, T.J., *Nature*, **368**, 321 (1994).

26. Camblor, M.A., Costantini, M., Corma, A., Gilbert, L., Esteve, P., Martinez, A., and Valencia, S., *J. Chem. Soc. Chem. Commun.*, 1339 (1996).

27. Reddy, J.S., Sivasanker, S., and Ratnasamy, P., *J. Mol. Catal.*, **70**, 335 (1991).

28. Rao, P.R.H.P., Ramaswamy, A.V., and Ratnasamy, P., *J. Catal.*, **141**, 604 (1993).

29. Das, T.K., Chaudhari, K., Chandwadkar, A.J., and Sivasanker, S., *J. Chem. Soc. Chem. Commun.*, 2495 (1995).

30. Mal, N.K., Ramaswamy, V., Ganapathy, S., and Ramaswamy, A.V., *J. Chem. Soc. Chem. Commun.*, 1933 (1994).

31. Lok, B.M., Cannan, T.R., and Messina, C.A., *Zeolites*, **3**, 282 (1983).

32. Engelhard G., and Michel, D., "High Resolution Solid State NMR of Silicates and Zeolites", (John Wiley, New York), 348 (1987).

33. Barrer, R.M., and Denny, P.J., *J. Chem. Soc.*, 971 (1961).

34. Barrer, R.M., Denny, P.J., and Flanigen, E.M., US Pat. 3,306,922 (1967).

35. Daniels, R.H., Kerr, G.T., and Rollmann, L.D., *J. Am. Chem. Soc.*, **100**, 3097 (1978).

36. Barrer, R.M., in "Proc. of 6th International Zeolite Conference", (D.H. Olson and A. Bisio, Eds.), Reno, July 10-15, 1983, Butterworth Ltd., UK, 870 (1984).

37. Goldsmith, J.R., *Min. Mag.*, **29**, 952 (1952).

38. Cheng, C-F., and Klinowski, J., *J. Chem. Soc., Faraday Trans.*, **92(2)**, 289 (1996).

39. Anderson, M.W., Philippou, A., Lin, Z., Ferreira, A., and Rocha, J., *Angew. Chem. Int. Ed. Engl.*, **34**, 1003 (1995).

40. Kwak, B.S., and Sachtler, W.M.H., *J. Catal.*, **145**, 456 (1994).

41. Chapus, T., Tuel, A., Taarit, Y.B., and Naccache, C., *Zeolites*, **14**, 349 (1994).

42. Ulagappan, N., and Rao, C.N.R., *J. Chem. Soc. Chem. Commun.*, 1047 (1996).

43. Jentys, A., Pham, N.H., Vinek, H., Englisch, M., and Lercher, J.A., *Microporous Mater.*, **6**, 13 (1996).

44. Lok, B.M., Messina, C.A., Patton, R.L., Gajek, R.T., Cannan, T.R., and Flanigen, E.M., *J. Am. Chem. Soc.*, **106**, 6092 (1984).

45. Tuel, A., Gontier, S., and Teisser, R., *J. Chem. Soc. Chem. Commun.*, 651 (1996).

46. Dongare, M.K., Singh, P., Moghe, P.P., and Ratnasamy, P., *Zeolites*, **11**, 690 (1991).

47. Bhaumik, A., and Kumar, R., *J. Chem. Soc. Chem. Commun.*, 869 (1995).

48. Wilson, S.T., and Flanigen, E.M., *ACS Symp. Ser.*, **298**, 329 (1988).

49. Barrer, R.M., and Hinds, L., *J. Chem. Soc. Chem. Commun.*, 1879 (1953).

50. Barrer, R.M., Davis, J.A., and Rees, L.V.C., *J. Inorg. Nucl. Chem.*, **31**, 2599 (1969).

51. Barrer, R.M., Bartholomew, R., and Rees, L.V.C., *J. Phys. Chem. Solids*, **24**, 309 (1963).

52. Rees, L.V.C., and Rao, A., *J. Chem. Soc. Faraday Trans.*, **62**, 2103 (1966).

53. Sherry, H.S., *J. Phys Chem.*, **72**, 4086 (1968).

54. Sherry, H.S., *J. Collid. Interface Sci.*, **28**, 288 (1968).

55. Kucherov, A.V., and Slinkin, A.A., *Zeolites*, **7**, 43 (1987) and **7**, 583 (1987).

56. Niwa, M., Itoh, H., Kato, M., Hattori, T., and Murakami, Y., *J. Chem. Soc. Chem.*

Commun., 819 (1982).

57. Anderson, M.W., Terasaki, O., Ohsuna, T., Philippou, A., Mackay, S.P., Ferreira, A., Rocha, J., and Lidin, S., *Nature,* **367**, 347 (1994).

58. Ward, J.W., *"Zeolites Chemistry and Catalysis"*, (J.A. Rabo Eds.), ACS, monograph, Ch.2, **171**, 118 (1976).

59. Chu, C.T., Kuehl, G.H., Lago, R.M., and Chang, C.D., *J. Catal.*, **93**, 451 (1985).

60. Farneth, W.E., and Georte, R.J., *J. Chem. Rev.*, **95**, 615 (1995).

61. Van Hoof, J.H.C., and Roelofsen, J.W., *Stud. Surf. Sci. Catal.*, **58**, 242 (1991).

62. Karge, H., *Stud. Surf. Sci. Catal.*, **65**, 133 (1991).

63. Yashima, T., Sato, K., Hayasaki, T., and Hara, N., *J. Catal.*, **26**, 303 (1972).

64. Ono, Y., *Stud. Surf. Sci. Catal.*, **5**, 19 (1980).

65. Barthomeuf, D., *Stud. Surf. Sci. Catal.*, **65**, 157 (1991).

66. Von Balmoos, R., "Collection of Simulated XRD Poder Pattern for Zeolite", Butterworths, London, (1984).

67. Meier, W.M., Olson, D.H., and Baerlocher, Ch., *Zeolites,* **17**, 16 (1996).

68. Bibby, D.M., Aldridge, L.P., and Milestone, N.B., *J. Catal.*, **72**, 373 (1981).

69. Dempsey, E., Kuhl, G.H., and Olson, D.H., *J. Phys. Chem.*, **73**, 387 (1969).

70. Meyers, B.L., Ely, S.R., Kutz, N.A., Kaduk J.A., and Van der Bossche, E., *J. Catal.*, **91**, 352 (1985).

71. Szostak, R., and Thomas, T.L., *J. Catal.*, **100**, 555 (1986).

72. Simmons, D.K., Szostak, R., Agarwal, P.K., and Thomas, T.L., *J. Catal.*, **106**, 287 (1987).

73. Perego, G., Bellussi, G., Corno, C., Taramasso, M., Buonomo, F., and Esposito, A., *Stud. Surf. Sci. Catal.*, **28**, 129 (1986).

74. Meier, W.M., and Olson, D.H., *Zeolites,* **12**, 17 (1992).

75. Treacy, M.M.J., Higgins, J.B., and Von Ballmoos, R., *Zeolites,* **16**, 340 (1996).

76. Davis, M.E., Saldarriaga, C., Montes, C., Garces, J., and Crowder, C., *Nature,* **331**,

968 (1988).

77. Davis, M.E., Saldarriaga, C., Montes, C., Garces, J., and Crowder, C., *Zeolites,* **8**, 362 (1988).

78. Estermann, M., McCusker, L.B., Baerlocher, Ch., Merrouche, A., and Kessler, H., *Nature,* **352**, 320 (1991).

79. Leonowicz, M.L., Lawton, J.A., Lawton, S.L., and Rubin, M.K., *Science,* **264**, 1910 (1994).

80. Flanigen, E.M., Khatani, H., and Szymanski, H.A., *ACS Symp. Ser.,* Washington D.C., **101**, 201 (1971).

81. Flanigen, E.M., *ACS Monograph,* Rabo, J.A., (Eds.), Washington D.C., **171**, 80 (1976).

82. Kutz, N.A., "Heterogeneous Catalysis-II", Ed. B.L. Shapiro *et al.*, 121 (1984).

83. Huybrechts, D.R.C., Vaesen, I., Li, H.X., and Jacobs, P.A., *Catal. Lett.,* **8**, 237 (1991).

84. Notari, B., *Stud. Surf. Sci. Catal.,* **37**, 413 (1989).

85. Kraushaar, B., and Van Hooff, J.H.C., *Catal. Lett.* **1**, 81 (1989).

86. Jacobs, P.A., "Carboniogenic Activity of Zeolites", Elsevier, Amsterdam, 39 (1977).

87. Lippmaa, E., Magi, M., Samoson, A., Engelhardt, G., and Griner, A.R., *J. Am. Chem. Soc.,* **102**, 4889 (1980).

88. Engelhardt, G., and Michel, D., "High Resolution Solid State NMR of Silicates and Zeolites", (John Wiley, New York), 348 (1987).

89. Engelhardt, G., Lippmaa, E., and Magi, M., *J. Chem. Soc. Chem. Commun.,* 712 (1981).

90. Ramdas, S., Thomas, J.M., Klinowski, J., Fyfe, C.A., and Hartman, J.S., *Nature.* **292**, 228 (1981).

91. Thomas, J.M., Fyfe, C.A., Ramdas, S., Klinowski, J., and Gobbi, G.C., *J. Phys Chem.,* **86**, 3061 (1982).

92. Engelhardt, G., Lohse, U., Lippmaa, E., Tarmak, M., and Magi, M., *Z. Anorg. Allg. Chem.,* **482**, 49 (1981).

93. Fyfe, C.A., Gobbi, G.C., Klinowski, J., Thomas, J.H., and Ramdas, S., *Nature,* **296**, 530 (1982).

94. Chen, N.Y., and Garwood, W.E., *J. Catal.,* **52**, 453 (1978).

95. Olson, D.H., Kokotailo, G.T., Lawton, S.L., and Meier, W.M., *J. Phys Chem.,* **85**, 2238 (1981).

96. Chester, A.W., Chen, P., and Rohrbaugh, W.J., "Relationship Between Measuring Zeolite Pore sizes and Catalytic Performance", Paper presented at the 10th North american Catal. Soc. Mtg., San Diego, (1987).

97. Wu, E.L., Landolt, G.R., and Chester, A.W., Proc. 7th Int. Zeol. Conf., Murakami, Y., Iijima, A., and Ward, J.W., Eds., Kodausha/Elsevier Tokyo/Amsterdam, 547 (1986).

98. Barrer, R.M., *Pure and Appl. Chem.,* **52**, 2143 (1980).

99. Mirajkar, S.P., Thangaraj, A., and Shiralkar, V.P., *J. Phys. Chem.* **96**, 3073 (1992).

100. Joshi, P.N., and Shiralkar, V.P., *J. Phys. Chem.,* **97**, 619 (1993).

101. Joshi, P.N., Eapen, M.J., and Shiralkar, V.P., *J. Chem. Soc., Faraday Trans.,* **90(2)** 387 (1994).

102. Thiele, E.W., *Ind. Eng. Chem.,* **31**, 916 (1939).

103. Wheeler, A., *"Advances in Catalysis and Related Materials",* **3**, 249 (1951).

104. Weisz, P.B., *Chem. Tech.*, **3**, 498 (1973).

105. Jacobs, P.A., and von Ballmoos, R., *J. Phys. Chem.,* **86**, 3050 (1982).

106. Chen, N.Y., and Degnan, J.F., *Chem. Eng. Progr.,* **84**, 32 (1988).

107. Yashima, T., Sato, K., Hayasaki, T., and Hara, N., *J. Catal.,* **26**, 303 (1972).

108. Martens, L.R.M., Grobet, P.J., and Jacobs, P.A., *Nature,* **315**, 568 (1985).

109. Thangaraj, A., Kumar, R., and Ratnasamy, P. *J. Catal.,* **131**, 294 (1991).

110. Taramasso, M., Perego, G., and Notari, B., US Pat. 4,410,501 (1983).

111. Reddy, J.S., and Kumar, R., *J. Catal.,* **130**, 440 (1991).

112. Camblor, M.A., Corma, A., Martinez, A., and Perez-Pariente, *J., J. Chem. Soc. Chem. Commun.,* 589 (1992).

113. Camblor, M.A., Corma, A., and Perez-Pariente, J., *Zeolites*, **13**, 82 (1993).

114. Serrano, D.P., Hong-Xin, L., and Davis, M.E., *J. Chem. Soc. Chem. Commun.*, 745 (1992).

115. Reddy, K.M., Kaliaguine, S., and Sayari, S., *Catal. Lett.*, **23**, 169 (1994).

116. Corma, A., Navarro, M.T., and Perez-Pariente, J., *J. Chem. Soc. Chem. Commun.*, 147 (1994).

117. Thangaraj, A., Kumar, R., Mirajkar, S.P., and Ratnasamy, P., *J. Catal.*, **130**, 1 (1991).

118. Reddy, J.S., Kumar, R., and Ratnasamy, P., *Appl. Catal.*, **58**, L1 (1990).

119. Corma, A., Esteve, P., Martinez, A., and Valencia, A., *J. Catal.*, **152**, 18 (1995).

120. Reddy, K.M., Kaliaguine, S., Sayari, S., Ramaswamy, A.V., Reddy, V.S., and Bonneviot, L., *Catal. Lett.*, **23**, 175 (1994).

121. Corma, A., Iiglesias, M., and Sanchez, F., *J. Chem. Soc. Chem. Commun.*, 1635 (1995).

122. Corma, A., Navarro, M.T., Perez-Pariente, J., and Sanchez, F., *Stud. Surf. Sci. Catal.*, **84**, 69 (1994).

123. Bellussi, G., Fattore, V., *Stud. Surf. Sci. Catal.*, **69**, 79 (1991).

124. Bonneviot, L., On, D.T., and Lopez, A., *J. Chem. Soc. Chem. Commun.*, 685 (1993).

125. Sheldon, R.A., *Stud. Surf. Sci. Catal.*, **66**, 573 (1991).

126. Callahan, J.L., and Grasselli, R.K., *AIChE J.*, **9**, 755 (1963).

127. Grasselli, R.K., and Burrington, J.D., *Adv. Catal.*, **141**, 140 (1993).

128. Hoelderich, W.F., and van Bekkum, H., *Stud. Surf. Sci. Catal.*, **58**, 686 (1991).

129. Roffia, P., Leofanti, G., Cesana, A., Mantegazza, M., Padovan, M., Petrini, G., Tonti, S., and Gervasutti, P., *Stud. Surf. Sci. Catal.*, **55**, 43 (1990).

130. Kuznicki, S.M., Indian Pat. 171379 (1988).

131. Kuznicki, S.M., Indian Pat. 171483 (1988).

132. Kuznicki, S.M., Us Pat. 4,853,202 (1989).

133. Kuznicki, S.M., and Thrush, K.A., EP Pat. 0405978A1 (1990).

134. Kuznicki, S.M., US Pat. 5,011,589 (1991).

135. Kuznicki, S.M., and Thrush, K.A., US Pat. 5,208,006 (1993)

136. Haushalter, R.C., and Mundi, L.A., *Chem. Mater.*, **4**, 31 (1992).

137. Sandomirskii, P.A., Belov, N.V., *Sov. Phys. Crystallogr.*, **24**, 686 (1979).

138. Chapman, D.M., and Roe, A.L., *Zeolites,* **10**, 730 (1990).

139. Moore, P.B., and Shen, J., *Nature,* **306**, 356 (1983).

140. Anderson, M.W., Tarasaki, O., Ohuna, T., Malley, P.J.O., Philippou, A., Mackay, S.P., Ferreira, A., Rocha, J., and Lidin, S., *Philos. Mag. B,* **71**, 813 (1995).

141. Ohuna, T., Tarasaki, O., Watanabe, D., Anderson, M.W., and Lidin, S., *Stud. Surf. Sci. Catal.*, **84**, 413 (1994).

142. Baur, W.H., *Am. Miner,* **49**, 697 (1964).

143. Newsham, J.M., Treacy, M.M.J., Koetsier, W.T., and De Gruyter, C.B., *Proc. R. Soc. Lond. A.,* **420**, 375 (1988).

CHAPTER II

SYNTHESIS AND MODIFICATION OF ETS-10

2.1 PART - I : SYNTHESIS OF ETS-10

2.1.1 Introduction

The first information on microporous titanosilicates appeared in 1967 when Young *[1]* reported the synthesis of titanium silicates under conditions similar to aluminosilicates. These materials were called *titanium zeolites*. In 1973 a naturally occurring alkaline titanosilicate identified as zorite was discovered *[2]* in trace quantities in the Siberian tundra. In 1988 and 1990 two independent reports by Kuznicki *[3,4]* and Chapman and Roe *[5]* discussed synthetic structures that appeared to mimic zorite. Comparisons with the natural mineral were largely based upon similarities between x-ray diffraction (XRD) patterns of the synthetic materials and those reported for zorite. This synthetic material, which was referred to as ETS-4 (Engelhard Titanosilicate-4), was not very thermally stable and had poor adsorption characteristics.

Subsequently, it was realized that a new family of titanosilicate molecular sieves containing tetrahedral and octahedral framework atoms had been discovered *[3,4, 6-13]*. Two titanosilicate members of this family are ETS-4 and ETS-10. ETS-10 is a large pore member of this class and has attracted interest due to its unique pore structure and charge distribution *[14-20]*. An interesting application, *viz.*, its use as a desiccant for manufacturing CFC-free air conditioning systems *[21]*, has also been reported. The crystal structure model of ETS-10 has recently been proposed by Anderson *et al. [14-16]*. It is believed that the framework of ETS-10 consists of corner-sharing tetrahedrally coordinated silicon and octahedrally coordinated titanium linked through bridging oxygens. The main pore system is a three-dimensional 12-membered ring channel network.

Though the synthesis of ETS-10 has been reported in the literature, a detailed kinetic study of its synthesis has so far not been reported. The use of the organic template,

tetramethyl ammonium chloride (TMACl) in ETS-10 synthesis was first reported by Valtchev *et al.[22-24]*. Recently, Liu *et al. [25]* reported the synthesis of ETS-10 using TiO_2 as the titanium source. Luca *et al. [26]* have reported the use of tetralkylammonium salts as templating agents in the synthesis of ETS-10. Most of the published reports have used $TiCl_3$ as the titanium source, though the use of Ti(IV) compounds have also been reported occasionally *[22,23]*.

This chapter recounts the synthesis of ETS-10 along with the kinetic studies of the crystallization process under various synthesis conditions *[27,28]*. The above studies were carried out using mostly $TiCl_3$ as the Ti-source. Besides, the influence of the various factors during the synthesis on the size and shape of the molecular sieve crystals, is reported. The synthesis of ETS-10 using templates other than TMACl *[29,30]* and also $TiCl_4$ as the titanium source *[31]* is also described. The use of choline chloride and the bromide salt of hexaethyl diquat-5 as templates is also presented.

2.1.2 Experimental

Hydrothermal syntheses of ETS-10 samples were carried out in stainless steel autoclaves at autogenous pressure under static conditions or using a high pressure stirred reactor (Parr Instruments, USA). The autoclaves were cleaned with aqueous hydrofluoric acid (40 wt.%) and polished with a carbon brush prior to use. The raw materials used in the syntheses and the modification of the titanosilicates are summarized in Table 2.1. The reactants used in the various catalytic tests are also listed in the table. The typical synthesis procedures are described in the following sections.

Table 2.1 : Specifications of the materials used in the study.

Reagent and Source	Chemical Formula or Composition	Purity (%)
Sodium silicate (UCIL, India)	28.6% SiO_2, 8.82% Na_2O, 62.58% H_2O	98
Titanium trichloride (Loba Chemie, India)	$TiCl_3$, 15 wt.% solution in 15% HCl	99
Titanium tetrachloride (Aldrich, USA)	$TiCl_4$	99
Sodium hydroxide (S.D. Fine Chemicals, India)	NaOH	99
Potassium Fluoride (Loba Chemie, India)	$KF.2H_2O$	98
1,5-Dibromopentane (Aldrich, USA)	$Br\text{-}(CH_2)_5\text{-}Br$	99
Triethyl amine (Loba Chemie, India)	$(C_2H_5)_3N$	98
Choline chloride (Loba Chemie, India)	$(CH_3)_3(OHCH_2CH_2)N^+Cl^-$	98
Hexaethyl diquat-5 (Self made, NCL, India)	$Br^-(C_2H_5)_3N^+\text{-}(CH_2)_5\text{-}N^+(C_2H_5)_3Br^-$	98
Ammonium nitrate (S.D. Fine Chemicals, India)	NH_4NO_3	99
Sodium chloride (S.D. Fine Chemicals, India)	NaCl	99
Lithium nitrate (S.D. Fine Chemicals, India)	$LiNO_3$	98
Sodium nitrate (S.D. Fine Chemicals, India)	$NaNO_3$	98
Potassium nitrate (S.D. Fine Chemicals, India)	KNO_3	98
Rubidium nitrate (Aldrich, USA)	$RbNO_3$	98
Cesium nitrate (Loba Chemie, India)	$CsNO_3$	98
Magnesium nitrate (S.D. Fine Chemicals, India)	$Mg(NO_3)_2.6H_2O$	98
Calcium nitrate (S.D. Fine Chemicals, India)	$Ca(NO_3)_2.xH_2O$	98
Barium nitrate (S.D. Fine Chemicals, India)	$Ba(NO_3)_2$	98
Lanthanum nitrate (Merck, Germaney)	$La(NO_3)_3.3H_2O$	99
Tetraamine platinum(II) nitrate (Aldrich, USA)	$Pt(NH_3)_4(NO_3)_2$	99.9
1-Butanol (S.D. Fine Chemicals, India)	$CH_3\text{-}(CH_2)_2\text{-}CH_2\text{-}OH$	98
2-Butanol (S.D. Fine Chemicals, India)	$CH_3\text{-}CH(OH)\text{-}CH_2\text{-}CH_3$	98
iso-Butanol (S.D. Fine Chemicals, India)	$CH_3\text{-}CH(CH_3)\text{-}CH_2\text{-}OH$	98
t-Butanol (S.D. Fine Chemicals, India)	$(CH_3)_3\text{-}C\text{-}OH$	98
m-Xylene (Aldrich, USA)	$C_6H_4(CH_3)_2$	99
1,3,5-Trimethylbenzene (Aldrich, USA)	$C_6H_3(CH_3)_3$	99.9
n-Hexane (S.D. Fine Chemicals, India)	C_6H_{14}	99.9

2.1.2.1 Synthesis using $TiCl_3$

2.1.2.1(i) Synthesis in the Absence of Templates

A. Synthesis of ETS-4 (seed) :

Solution (A) comprising 63.0 g of sodium silicate (28.6% SiO_2, 8.82% Na_2O, 62.58% H_2O) was stirred vigorously. 11.4 g NaOH pellets were added to the above solution (A) and the gel was stirred for a further ten minutes. 54.4 g of titanium trichloride ($TiCl_3$, 15% solution in HCl) was added dropwise to this solution and the mixture was stirred for half an hour to get a blackish paste (B). Finally, 9.4 g potassium fluoride dihydrate ($KF.2H_2O$) was added to (B) and the mixture was stirred for one hour at room temperature to get a homogeneous gel (pH = ~11.0).

The molar composition of the gel in terms of oxides was as follows :

4.42 Na_2O : 0.95 K_2O : TiO_2 : 5.71 SiO_2 : 81.88 H_2O.

The gel was transferred to a stainless steel autoclave; it was then capped tightly and crystallization was carried out in static condition at 423K for 7 days. The pH of the mother liquor was 10.7 at the end of the synthesis. The solid material was filtered off and washed with deionized water. The product was then dried and identified as the crystalline small pore titanosilicate (ETS-4) with the X-ray diffraction pattern presented in Fig. 2.1(a).

B. Synthesis of ETS-10 using seeds of ETS-4 :

Solution (A) comprising 63 g of sodium silicate (28.6% SiO_2, 8.82% Na_2O, 62.58% H_2O) and 20 g distilled water was stirred vigorously. Solution (B) was prepared by dissolving 8.4 g of NaOH pellets in 58.8 g distilled water and added slowly to the above solution (A) with stirring. The gel was stirred for 15-20 minutes and 54.4 g $TiCl_3$ (15% solution in HCl) was added dropwise taking care to avoid sputtering of the above stirred gel. The paste-like blackish material (C) was stirred for half an hour. 9.4 g $KF.2H_2O$ was added

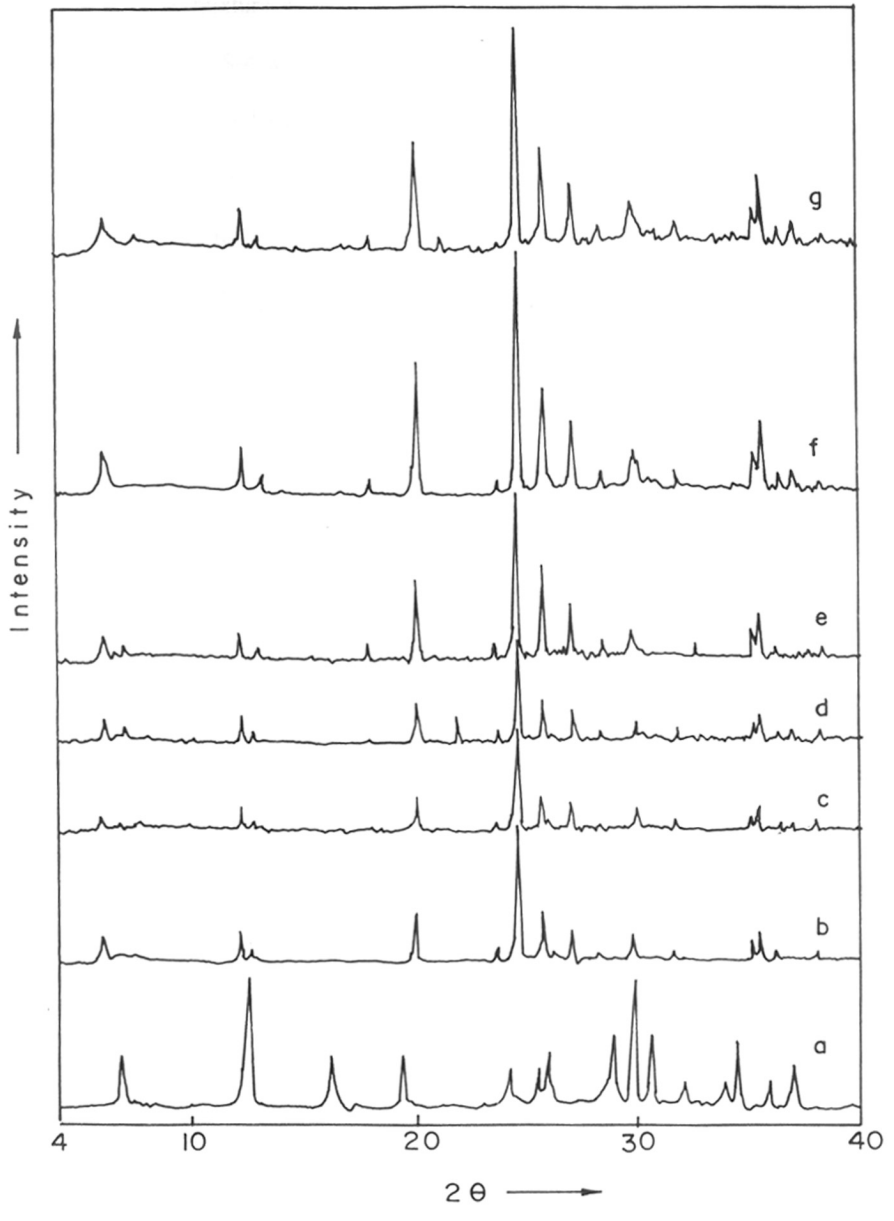

Fig. 2.1 : X-ray diffraction patterns of the as-synthesized samples :

a, ETS-4; b, ETS-10(A); c, ETS-10(B); d, ETS-10(C); e, ETS-10(D); f, ETS-10(E) and g, ETAS-10.

to paste (C) and the mixture was stirred for one hour to get paste (D). Finally 1.3 g of titanosilicate seeds of ETS-4 was added to paste (D) very slowly and stirred vigorously for another hour till the mixture became homogeneous (pH = 10.8-11.0) at room temperature. The molar composition of the gel in terms of oxides was as follows :

3.70 Na_2O : 0.95 K_2O : TiO_2 : 5.71 SiO_2 : 171 H_2O.

It was then transferred to a stainless steel autoclave. The autoclave was capped tightly and crystallization was carried out at 443K for 10 days. The pH of the mother liquor was 10.6 at the end of the crystallization. The solid material was filtered off and washed with deionized water. The product was then dried and identified as the crystalline large pore titanosilicate (ETS-10) with the X-ray diffraction pattern presented in Fig. 2.1(b). The yield was 80%-85%. The sample is designated as ETS-10(A).

C. Synthesis of ETS-10 without seeds of ETS-4 :

Solution (A) comprising 63 g of sodium silicate (28.6% SiO_2, 8.82% Na_2O, 62.58% H_2O) and 60 g distilled water was stirred vigorously. Solution (B) was prepared by dissolving 9.9 g of NaOH pellets in 77.7 g distilled water and added slowly to the above solution (A) with stirring. The gel was stirred for 15-20 minutes. 54.4 g $TiCl_3$ (15% solution in HCl) was added dropwise to the above stirred gel. The paste-like blackish material (C) was stirred for half an hour. 9.4 g $KF.2H_2O$ was added to paste (C) and the mixture was stirred for one hour to get paste (D). Finally 5.5 g of NaCl dissolved in 20 g deionized water was added to paste (D). The mixture was stirred for one hour till it became homogeneous (pH = 11-11.5) at room temperature and then it was transferred to a stainless steel autoclave. The molar composition of the gel in terms of oxides was as follows :

4.95 Na_2O : 0.95 K_2O : TiO_2 : 5.71 SiO_2 : 342.85 H_2O.

The autoclave was capped tightly and crystallization was carried out at 473K for 10 days. When crystallization was complete, the pH of the mother liquor was found to be 11.0.

The solid material was filtered off and washed with deionized water. The product was then dried and identified as ETS-10. Its X-ray diffraction pattern is presented in Fig. 2.1(c). The yield was 70% to 76%. The sample is designated as ETS-10(B).

2.1.2.1(ii) Synthesis in the Presence of Templates

A. Synthesis of ETS-10 using choline chloride :

Solution (A) comprising 63 g sodium silicate (28% SiO_2, 8.82% Na_2O, 62.58 H_2O) and 35 g distilled water was stirred vigorously. Solution (B) was prepared by dissolving 8.4 g NaOH pellets in 70 g distilled water and added slowly to the above solution (A) under stirring. The gel was stirred for 15 minutes and 16.3 g choline chloride dissolved in 52.6 g deionized water was added slowly. The mixture was stirred for half hour (C). 54.4 g $TiCl_3$ (15% solution in HCl) was added dropwise to the above gel under stirring, followed by the addition of 9.4 g $KF.2H_2O$ in small amounts. The final sticky grey gel (pH = 11.3-11.5) was stirred for one hour at room temperature and then transferred to a stainless steel autoclave. The molar composition of the gel in terms of oxides was as follows :

$$1.14\ R_2O : 3.70\ Na_2O : 0.95\ K_2O : TiO_2 : 5.71\ SiO_2 : 256.9\ H_2O,$$

where R = choline chloride.

The autoclave was capped tightly and crystallization was carried out at 473K for 7 days. When the crystallization was over (pH of the mother liquor = 10.7-10.8), the solid material was filtered off and washed with deionized water. The product was then dried and identified as the crystalline large pore titanosilicate ETS-10 with the X-ray diffraction pattern presented in Fig. 2.1(d). The yield was 78% to 84%. The sample was designated as ETS-10(C).

B. Synthesis of ETS-10 using the bromide salt of hexaethyl diquat-5 :

Synthesis of the template :

The organic template hexaethyl diquat-5 (*N,N,N,N′,N′,N′*-hexaethylpentane-diammonium dibromide) used in the synthesis was prepared by the following procedure :

Triethylamine (25 g) and acetone (50 g) were taken in a 250 ml RB flask. To this mixture, 1,3-dibromopentane (30 g; Aldrich, 99%) was added. The homogeneous reaction mixture was refluxed for 10 hours. After completion of the reaction, a white salt (diquaternary salt; highly hygroscopic) was formed in >90% yield. This was separated from the reaction mixture and dried in vacuum. The white solid was characterized by ^{1}H and ^{13}C NMR spectroscopy (200 MHz, D_2O as a solvent) and mass spectrometry.

Synthesis of ETS-10(D) :

Solution (A) which comprised of 63 g sodium silicate (28% SiO_2, 8.82% Na_2O, 62.58% H_2O) and 10 g of distilled water was stirred vigorously. Solution (B) was prepared by dissolving 8.4 g NaOH pellets in 48 g distilled water and added slowly to the above stirred solution (A). The gel was stirred for 15 minutes and 51.8 g hexaethyl diquat-5 (bromide salt) dissolved in 20.8 g deionized water was added slowly and then the mixture was stirred for half hour (C). 54.4 g $TiCl_3$ (15% solution in HCl) was added dropwise to the above stirred gel, followed by the addition of 9.4 g $KF.2H_2O$. The final sticky grey gel (pH = 11.3-11.5) was stirred for one hour at room temperature and the stirred gel was transferred to a stainless steel autoclave.

The molar composition of the gel in terms of oxides was as follows :

$$1.14\ R_2O : 3.70\ Na_2O : 0.95\ K_2O : TiO_2 : 5.71\ SiO_2 : 171.4\ H_2O,$$

where R = bromide salt of hexaethyl diquat-5.

The autoclave was capped tightly and the crystallization carried out at 473K for 5 days. When the crystallization was over (pH of the mother liquor = 10.7-10.8), the solid material was filtered off and washed with deionized water. The product was then dried and identified as the crystalline large pore titanosilicate ETS-10 with the X-ray diffraction pattern presented in Fig. 2.1(e). The yield of the sample was 80% to 85%. The sample is designated as ETS-10(D).

2.1.2.2 Synthesis using $TiCl_4$

The hydrothermal synthesis of ETS-10(E) using $TiCl_4$ was carried out with a gel of the following molar composition:

3.70 Na_2O : 0.95 K_2O : TiO_2 : 5.71 SiO_2 : 171 H_2O.

In a typical synthesis, a solution of 9.3 g NaOH in 40 g distilled water was added to a vigorously stirred solution of 52.5 g sodium silicate (28.6% SiO_2, 8.82% Na_2O, 62.58% H_2O) and 40 g distilled water. This was followed by the dropwise addition of 32.75 g of a $TiCl_4$ solution (25.42 wt.% $TiCl_4$, 25.92 wt.% HCl, 48.60 wt.% H_2O) to this mixture (colourless gel) with rapid stirring. 7.8 g $KF.2H_2O$ was then added to the above gel (pH = 11.2 ± 0.1) and the mixture was stirred well. The mixture was then transferred to a stirred stainless steel autoclave (Parr Instruments, USA) and crystallization carried out at 473K with a stirrer speed of 300 r.p.m for 14-16 hours. After crystallization, the products were filtered and washed with deionized water till the pH of the filtrate was 10.7-10.8. It was dried at 373K for 8-10 hours. The product was identified as ETS-10 with the x-ray pattern presented in Fig. 2.1(f). The yield of the sample was 85% to 90%.

2.1.3 Results and Discussion

2.1.3.1 Kinetic Studies of Syntheses using $TiCl_3$

2.1.3.1(i) Kinetics of Crystallization in the Absence of Template

A. Influence of Temperature on Crystallization

To study the effect of temperature on the formation of the titanosilicate, the kinetics of crystallization were studied in the range 423-473K by comparing the extent of crystallization of the gel mixture at different intervals of synthesis time. The extent of crystallization is conventionally evaluated either by sorption of water vapour/nitrogen at a fixed relative pressure on a completely dehydrated zeolite or by the ratio of the sum of the areas of the intense XRD peaks of the sample under consideration to that of the most crystalline sample obtained during the study *[32-34]*. In the present study, the XRD technique was used. The extent of crystallization was evaluated by comparing the ratio of the sums of the areas of the most intense XRD peaks (2θ = 24.65° to 27.5°) of the sample under study with that of the most crystalline sample obtained during the study. The curves depicting the influence of the temperature on the crystallization kinetics of ETS-10(A) are presented in Fig. 2.2. The composition of the gel used in the study was 3.70 Na_2O : 0.95 K_2O : TiO_2 : 5.71 SiO_2 : 171 H_2O. The intercept made by the curve on the time axis (abscissa) is defined as the induction period (the time needed to form crystallization centers or nuclei). In accordance with thermodynamic expectations, it is found from Fig. 2.2 that the induction period is inversely proportional to the temperature. The rate of nucleation may be assumed to be proportional to the reciprocal of the induction period; hence, it varies directly with the crystallization temperature. The induction period is followed by the formation of the crystalline material, the rate of crystallization increasing with time up to about 60-70% crystallinity and then

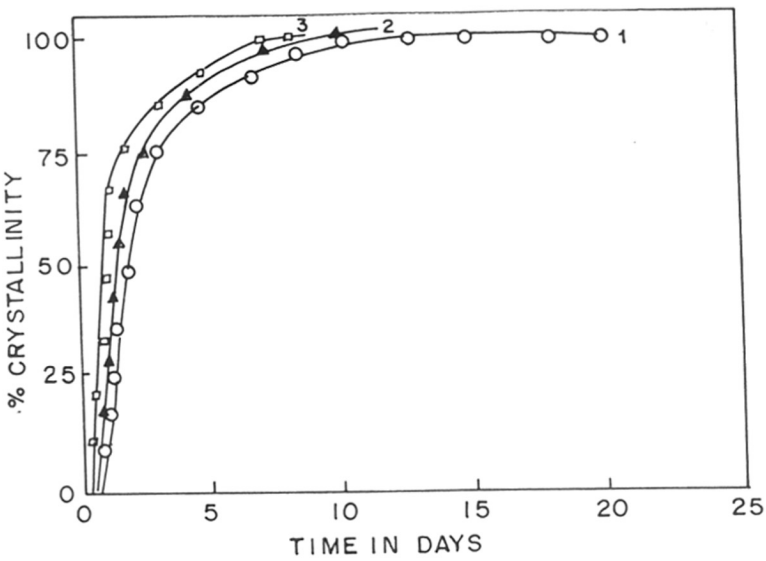

Fig. 2.2 : Effect of temperature on the kinetics of crystallization of ETS-10(A) (seed = 7.0%); curves 1-3 correspond to 423K, 443K and 473K, respectively.

slowing down. Nearly, 100% crystallization occurs after about 7 days. The phase purity (ETS-10) or crystallinity was not affected even after autoclaving for 25 days.

Linear plots were obtained on applying the Arrhenius equation (Fig. 2.3). The values of the activation energy obtained from slope of the linear plots for nucleation (E_n) (applying the relation $d\ln(1/\theta)/d\ln(1/T) = -E_n/R$, where θ is the induction period in hours at the reaction temperature T and R is the molar gas constant) and crystallization (E_c) (applying the relation $d\ln(1/K)/d(1/T) = -E_c/R$, where K is the time in hour required for 50% crystallization at the crystallization temperature T) are 76.5 and 38.3 KJ $mole^{-1}$, respectively. Thompson has recently pointed out the shortcomings of the applicability of the Arrhenius equation to zeolite crystallization data *[35]*. Similarly, den Ouden and Thompson have pointed that the assumptions made to arrive at the rate of nucleation and crystal growth in order to apply the Arrhenius equation to evaluate the apparent activation energies the nucleation (E_n) and crystal growth (E_c) may not be realistic *[36]*. In spite of the short comings, the above analysis is useful in comparing different synthesis procedures.

B. Influence of water content of the gel

Water plays an important role in the hydrothermal synthesis of molecular sieves. Studies were carried out by changing the water content in the overall synthesis gel. Only the water content was changed and the relative ratios of the other components kept the same in all the batches (gel composition, 3.70 Na_2O : 0.95 K_2O : TiO_2 : 5.71 SiO_2 : x H_2O, where x = 85.65 to 342.6). For convenience, we will be expressing the water content with respect to SiO_2 as H_2O/SiO_2 ratio. The influence of water content of the gel on crystallization is presented in Fig. 2.4A and Fig. 2.4B, respectively, for the titanosilicate prepared by the seed method [ETS-10(A)] (seed content = 7.0%) at 443K and that prepared directly without seeds [ETS-10(B)] at 473K. The dilution of the gel affects the rate of nucleation only marginally

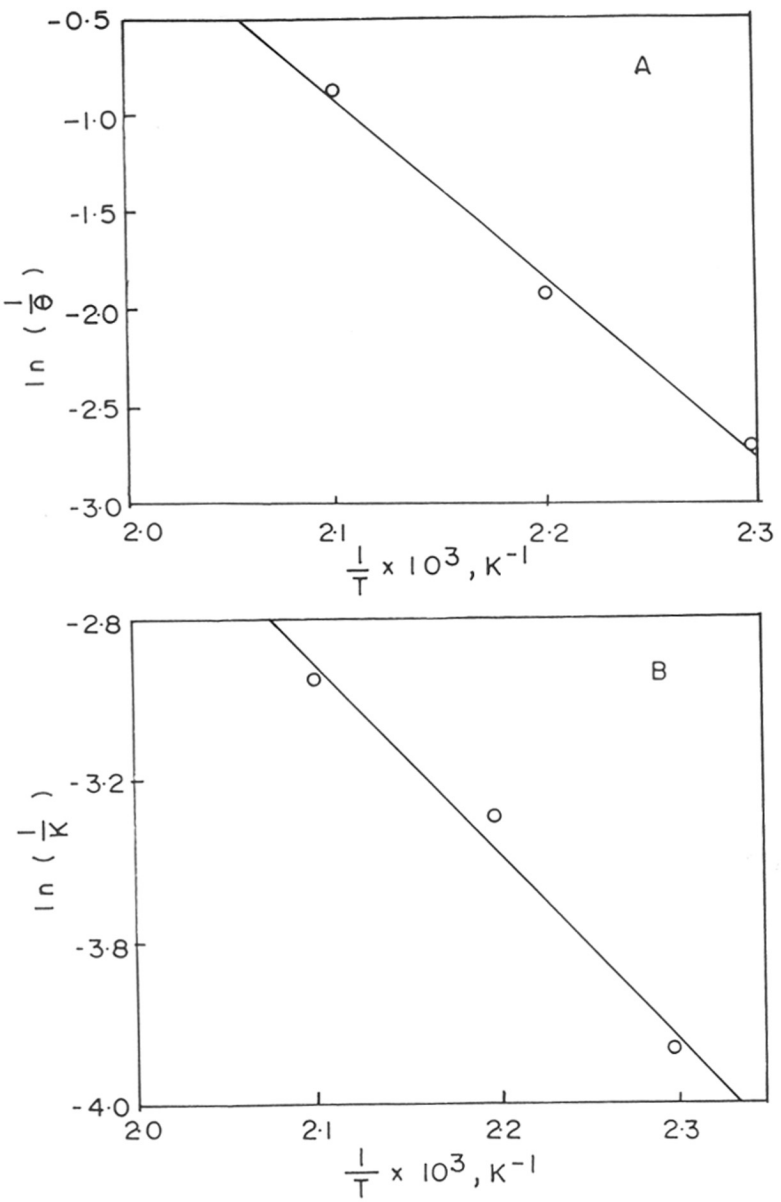

Fig. 2.3 : Arrhenius plots derived from the crystallization kinetics of ETS-10(A) : A, nucleation (E_n) and B, crystallization (E_c).

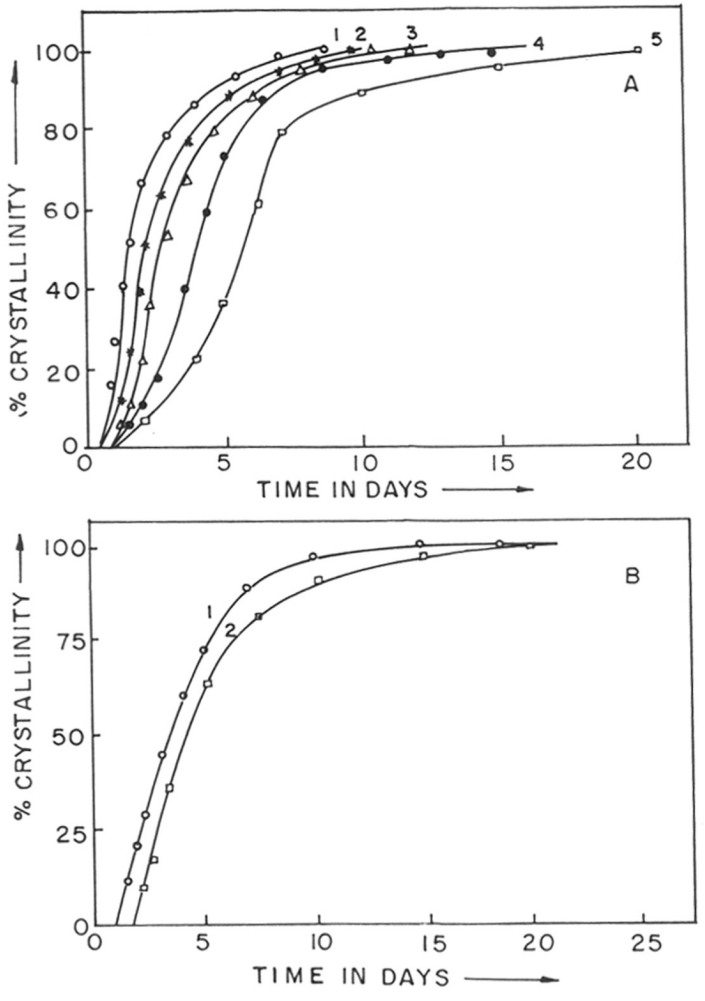

Fig. 2.4 : The influence of H_2O/SiO_2 ratio on the kinetics of crystallization of ETS-10.

A : ETS-10(A) (seed = 7.0%); curves 1-5 correspond to H_2O/SiO_2 values of 15, 30, 40, 50 and 60, respectively; Temp. = 443K.

B : ETS-10(B); curves 1 and 2 correspond to H_2O/SiO_2 values of 30 and 60, respectively; Temp. = 473K.

but influences the rate of crystallization appreciably. Figure 2.4A shows that the crystallization rate is enhanced when the water content is lower (H_2O/SiO_2 = 15) (curve 1). When the H_2O/SiO_2 ratio is increased from 15 to 40 (curves 1-3), the crystallization period increases from 7 to 10 days. On increasing the H_2O/SiO_2 ratio further up to 60 (curves 4 and 5), the crystallization period increases to 12 days and it takes 20 days to obtain fully crystalline material. For H_2O/SiO_2 = 15, two impurity peaks (2θ = 7.6 and 9.1) were observed in the XRD pattern. When the H_2O/SiO_2 ratio was lower than 15, the water content was found to be too low to obtain a homogeneous gel and hence crystallization was not attempted. An increase in the rate of crystallization at lower water content is also observed (Fig. 2.4B) for the titanosilicates [ETS-10(B)], prepared in the absence of seeds. Curves 1 and 2 correspond to H_2O/SiO_2 = 30 and 60, respectively. A fully crystalline sample is obtained between 18-20 days. These studies show that the crystallization rate increases with a decrease in H_2O/SiO_2 ratio whether seeds are present or not.

The water content of the synthesis gel has the most influence on the size and morphology of the ETS-10 crystals (Figs. 2.5 and 2.6). In the case of ETS-10(A), as the dilution is increased from H_2O/SiO_2 = 30 to 50, the size of the cuboid crystals increases (Fig. 2.6C for H_2O/SiO_2 = 30 and Fig. 2.5A for H_2O/SiO_2 = 50, respectively). However, on further dilution to H_2O/SiO_2 = 60, the crystal morphology changes and elongated crystals of 4-8 μm are obtained (Fig. 2.5B). The faster rates of crystallization found in the more concentrated systems (see above) and larger crystal sizes in dilute solutions are commonly observed in zeolite synthesis *[37]*.

In the case of the titanosilicate synthesized in the absence of seeds [ETS-10(B)] using H_2O/SiO_2 = 30, very prominent cuboidal layered particles of 5-7 μm are observed (Fig.

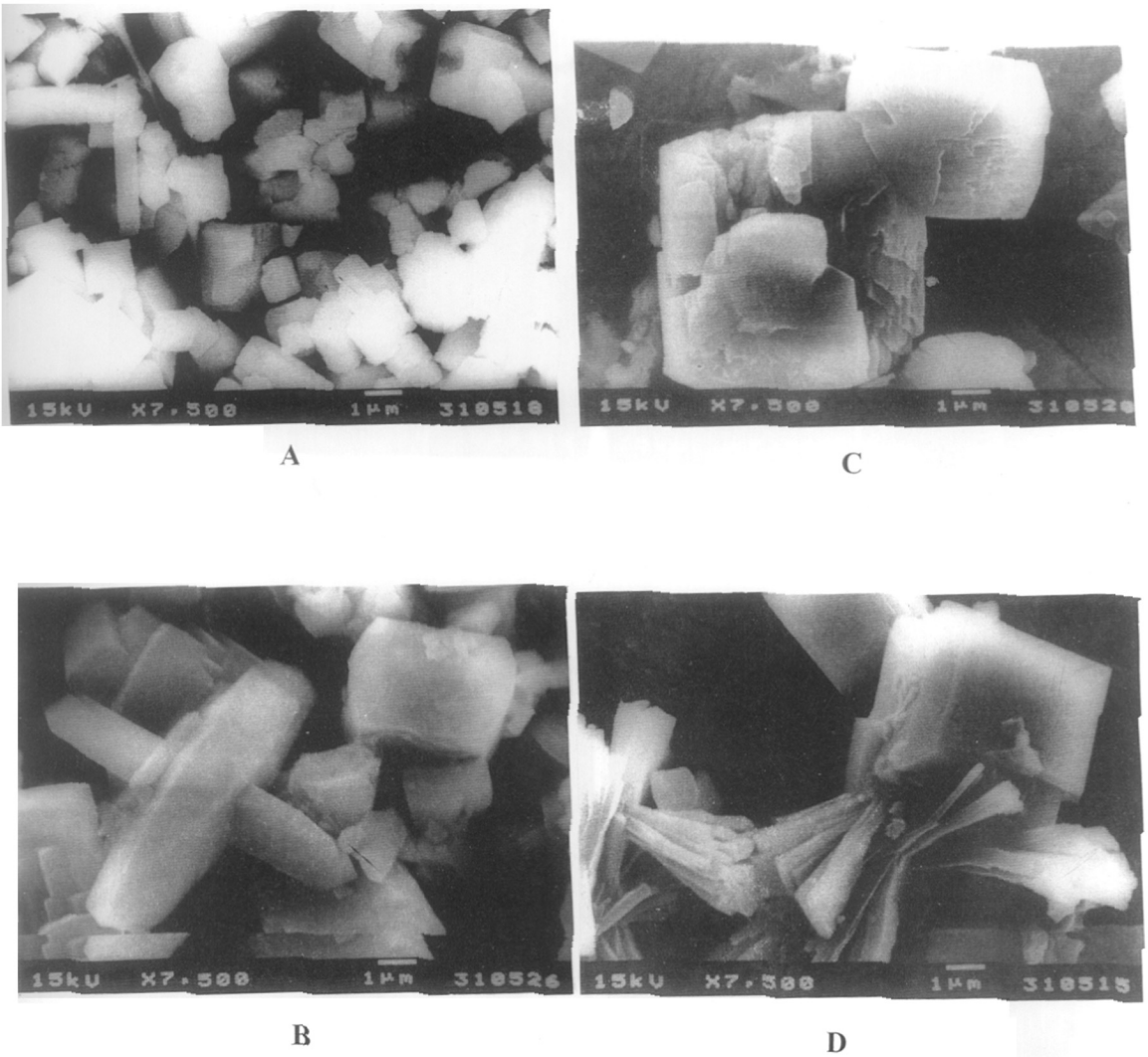

Fig. 2.5 : Influence of water content, H_2O/SiO_2 (X), of the gel on morphology of ETS-10 crystals.

A : ETS-10(A) (seed = 7.0%), X = 50; B : ETS-10(A) (seed = 7.0%), X = 60; C : ETS-10(B), X = 30 and D : ETS-10(B), X = 60.

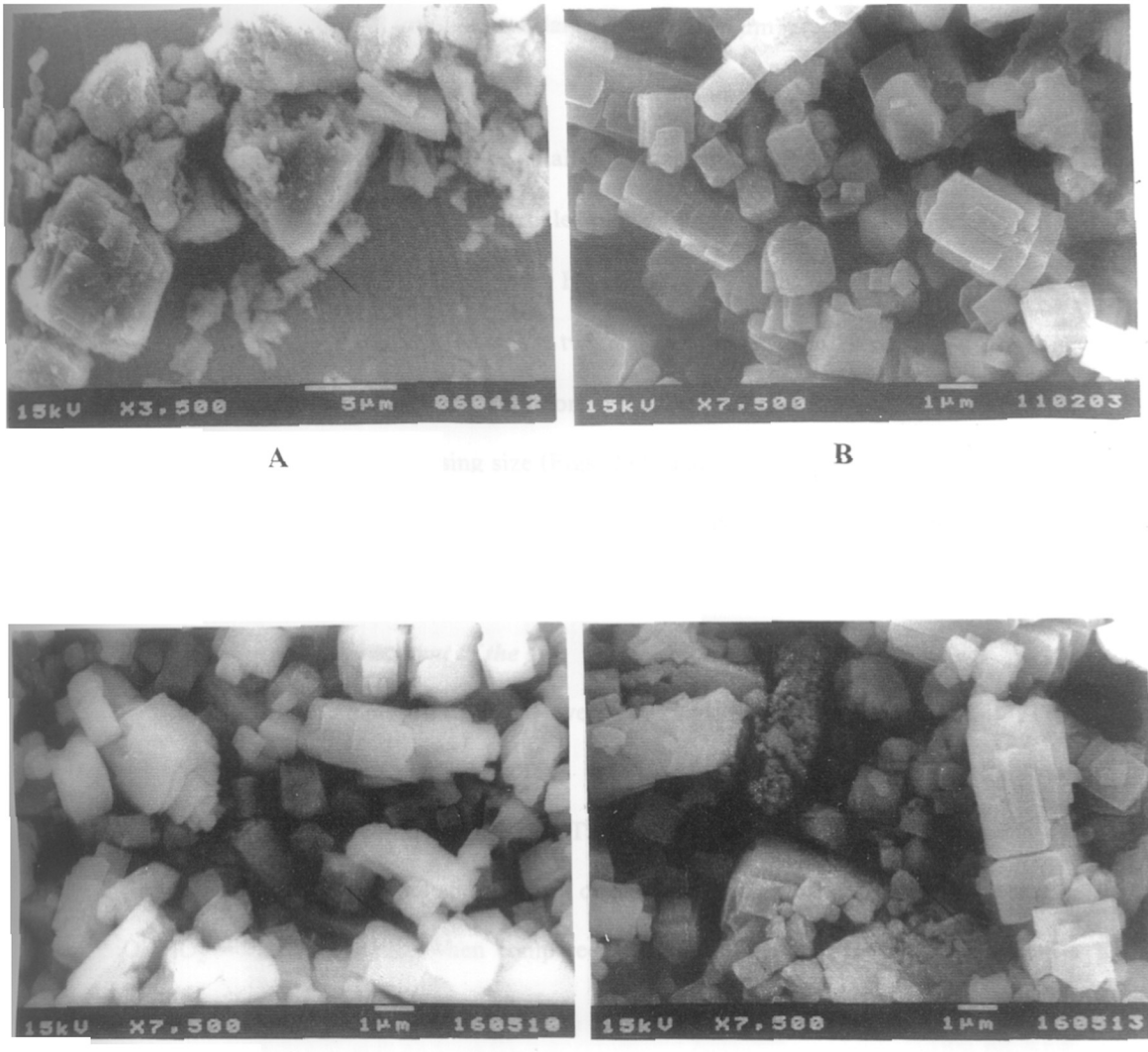

Fig. 2.6 : Influence of seed content on morphology of crystals.

A : ETS-4 (seed); B : ETS-10(A) (14.0% seed); C : ETS-10(A) (7.0% seed) and D : ETS-10(A) (0.9% seed).

2.5C). But when the water content is increased (H_2O/SiO_2 = 60), mixtures of sheaf-like bundles of narrow strips (~8 μm long) and large cuboids (6-8 μm) are seen (Fig. 2.5D).

C. Influence of seed concentration

SEM photographs show that the small pore titanosilicate (ETS-4) used as seed in the present study has irregular undefined particles ranging in size from 1-8 μm (Fig. 2.6A). On the other hand, ETS-10 synthesized (with H_2O/SiO_2 = 30) using ETS-4 seeds (14.0 wt% based on SiO_2 input) crystallizes as sharp, twinned cuboids in the size range 1-4 μm (Fig. 2.6B). On decreasing the seed concentration to 7.0, 3.5, 1.7 and 0.9%, individual cuboids tend to form clusters with increasing size (Figs. 2.6C and 2.6D, respectively, for 7.0 and 0.9 wt% seeds). The crystallinity (XRD) of the samples was not significantly influenced by the quantity of the seeds used.

D. Influence of titanium content of the gel

Titanosilicate samples [ETS-10(A)] were also prepared using input ratio of SiO_2/TiO_2 = 3, 4 and 7.5 and using seeds of ETS-4 (7.0%) by the above procedure. The X-ray diffraction patterns showed mixed phases (ETS-4 + ETS-10) and less crystalline products in the case of SiO_2/TiO_2 = 3 and 4 and also less crystalline (50% to 70%) ETS-10 in the case of SiO_2/TiO_2 = 7.5 (input ratio) when compared to ETS-10(A) prepared using a gel with a SiO_2/TiO_2 ratio of 5.7.

2.1.3.1(ii) Kinetics of Crystallization in the Presence of Templates

The computer graphics (CG) visualization of ETS-10 and the generation of the template models were carried out on a Silicon Graphics Indigo2 workstation using Insight II software package supplied by Biosym Technologies Inc., USA. The ETS-10 lattice was modeled from the crystal structure reported by Anderson *et al. [14,15]* for the polymorph B. The two templates used in the synthesis of ETS-10, choline chloride and hexaethyl diquat-5 are shown

in the Fig. 2.7 (A and B, respectively). Choline chloride is small enough to fit into the 12-membered ring of ETS-10 (Fig. 2.8A). Hexaethyl diquat-5 fits exactly into two 12-membered rings connected through a 7-membered channel (Fig. 2.8B). The $-(CH_2)_5-$ segment of hexaethyl diquat-5 passes through the 7-membered ring. Three molecules of hexaethyl diquat-5 can thus be fitted into each unit cell of ETS-10 (Fig. 2.8B) which is confirmed from chemical analysis (Chapter III, Table 3.2). Fig. 2.8B represents two fully occupied molecules of hexaethyl diquat-5 and four one fourth portions of four hexaethyl diquat-5 molecules (two at the top are shown while the two at the bottom are not shown in the Fig. 2.8B) fitted in the ETS-10 unit cell.

A. Influence of temperature on crystallization

To study the effect of temperature on the formation of the titanosilicate, the kinetics of crystallization were studied in the range 423-473K by comparing the extent of crystallization of the gel mixture at different intervals of synthesis time using a gel composition 1.14 R_2O : 3.70 Na_2O : 0.95 K_2O : TiO_2 : 5.71 SiO_2 : x H_2O, where x = 256.9 for choline chloride and 171.4 for hexaethyl diquat-5. The curves for the crystallization kinetics of ETS-10 for the above gel composition are presented in Fig. 2.9. The curves typically exhibit a continuous increase of crystallization with respect to time. The rate of crystallization is slower for ETS-10(C) [H_2O/SiO_2 = 45] when compared to ETS-10(D) [H_2O/SiO_2 = 30] (Fig. 2.9, curves 3C and 3D for ETS-10(C) and ETS-10(D), respectively). Also, the induction period for ETS-10(C) is larger, suggesting that the formation of the nuclei is slower when choline chloride is used as the template. As a result, 70-75% crystalline ETS-10(C) and ETS-10(D) are obtained after 5 days and 3 days respectively; 7 and 5 days (respectively) are required to get ~100% crystalline material at 473K (Fig. 2.9, curves 3C and 3D, respectively, for ETS-10(C) and ETS-10(D)). Fully crystalline (100%) titanosilicate could not be obtained at 423K (Fig. 2.9, curves 1C and 1D) even on prolonging the period of crystallization to 30 days.

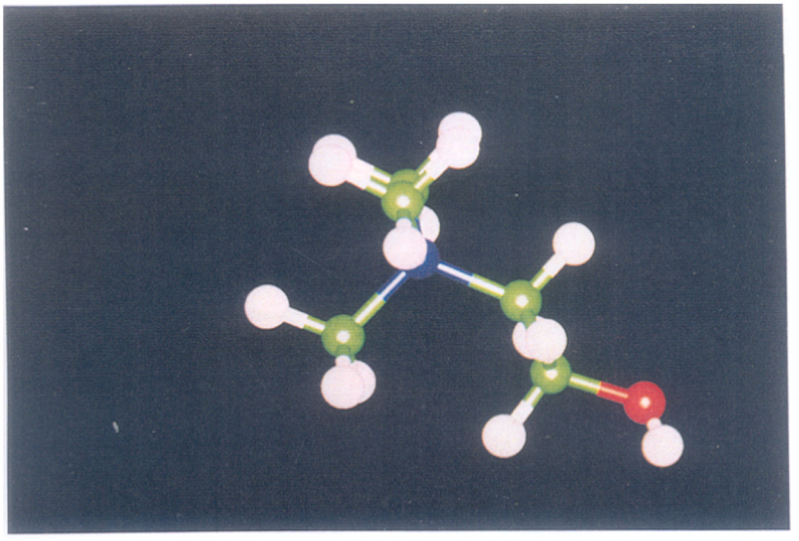

A

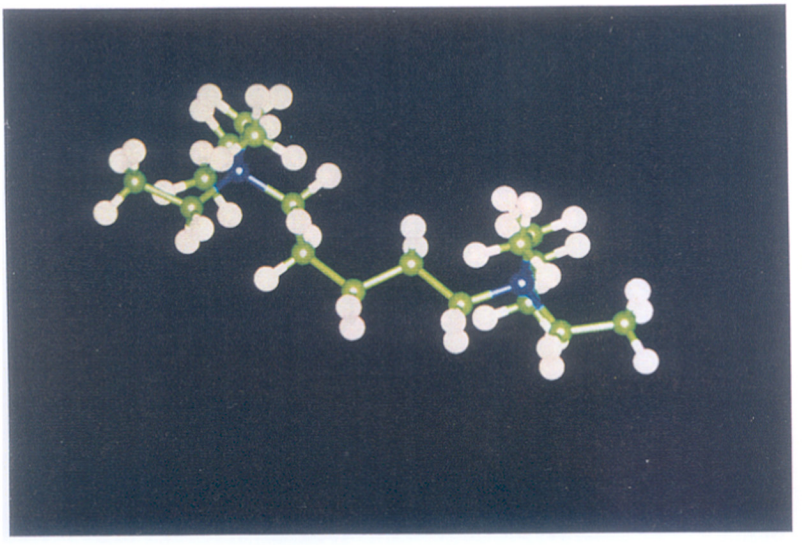

B

Fig. 2.7 : Structure of the organic templates used in ETS-10 synthesis.

A : Choline chloride and

B : Hexaethyl diquat-5.

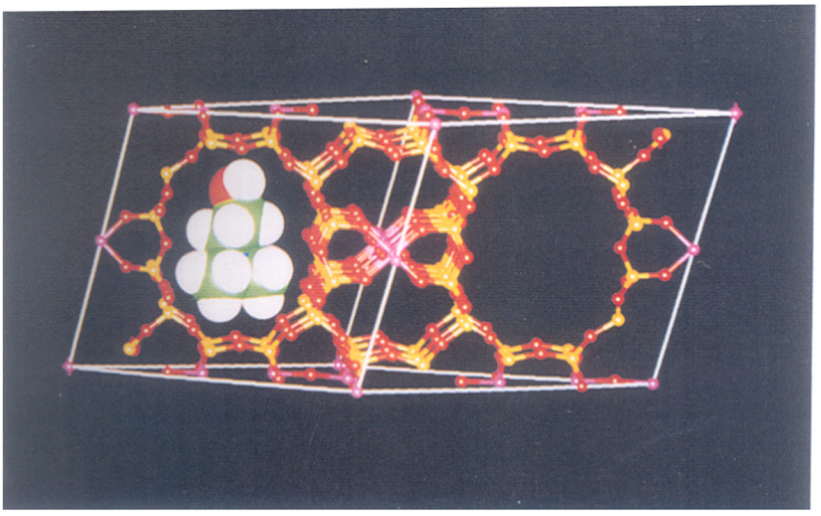

A

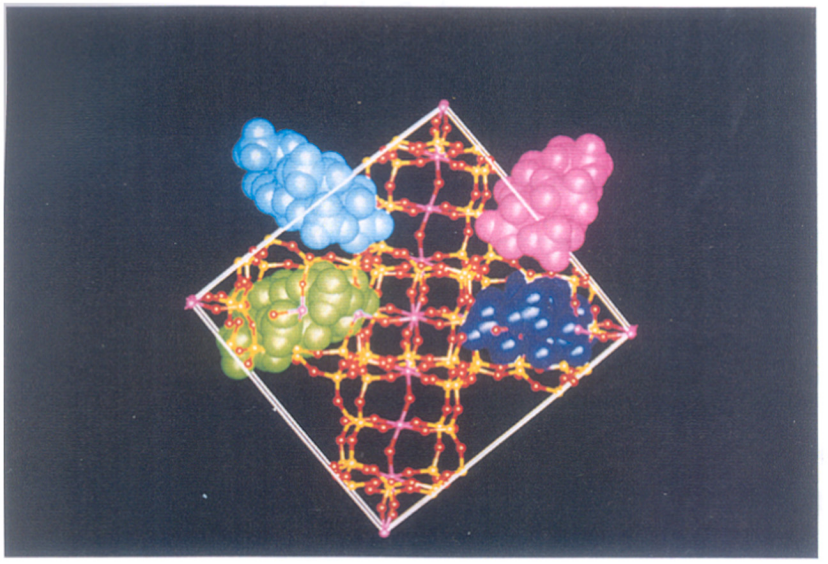

B

Fig. 2.8 : Location of the organic templates in ETS-10 structure.

A : Choline chloride in ETS-10 unit cell and

B : Hexaethyl diquat-5 in ETS-10 unit cell.

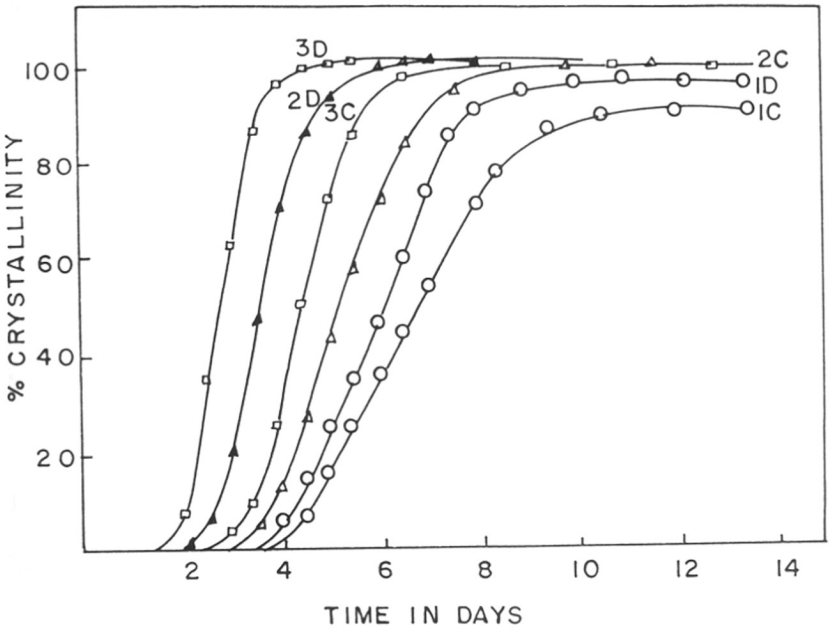

Fig. 2.9 : Effect of temperature on the kinetics of crystallization of ETS-10(C) and ETS-10(D); curves 1-3 correspond to 423K, 443K and 473K, respectively.

Applying the Arrhenius equation, the activation energies for nucleation (E_n) and crystallization (E_c) were found to be 17.4 and 13.1 KJ/mole for ETS-10(C) and 22.7 and 20.1 KJ/mole for ETS-10(D) (Fig. 2.10). These values are lower than the values reported for ETS-10 synthesized in the absence of templates *[28]*.

B. Influence of water content of the gel

The influence of water content of the gel (1.14 R_2O : 3.70 Na_2O : 0.95 K_2O : TiO_2 : 5.71 SiO_2 : x H_2O, where x = 171.4-342.6) on the crystallization is presented in Fig. 2.11 for ETS-10(C) and ETS-10(D) at 473K. Dilution of the gel influences the rate of nucleation and also the rate of crystallization appreciably. Figure 2.11 shows that the crystallization rate is enhanced when the water content is lowered (curves 1C and 1D). However, only 92% crystalline material is obtained (Fig. 2.11, curve 1C) even on prolonged heating up to 20 days at 473K, when choline chloride is used as the template. Besides, an impurity peak (XRD) at $2\theta = 21.8°$ is also observed. When H_2O/SiO_2 ratio is increased from 30 to 45, the crystallization improves and 98% crystallinity is observed in about 7 days (Fig. 2.11, curve 2C). Further increase in crystallinity could not, however, be noticed even after 30 days. The magnitude of the impurity peak at $2\theta = 21.8°$ is smaller when $H_2O/SiO_2 = 45$. Thus, good ETS-10(C) can be obtained only when the H_2O/SiO_2 ratio is 45 or 60 (Fig. 2.11, curves 2C and 3C, respectively). An increase in the rate of crystallization at lower water contents is also observed (Fig. 2.11) in the case of ETS-10(D). Curves 1D, 2D and 3D in Fig. 2.11 correspond to H_2O/SiO_2 ratios of 30, 45 and 60, respectively. 100% crystalline material is obtained in 5, 7 and 10 days, when the H_2O/SiO_2 ratios are 30, 45 and 60, respectively.

C. Influence of template concentration

Studies were carried out by changing the concentrations of choline chloride and the bromide salt of hexaethyl diquat-5 in the synthesis gel, keeping the relative ratios of the other

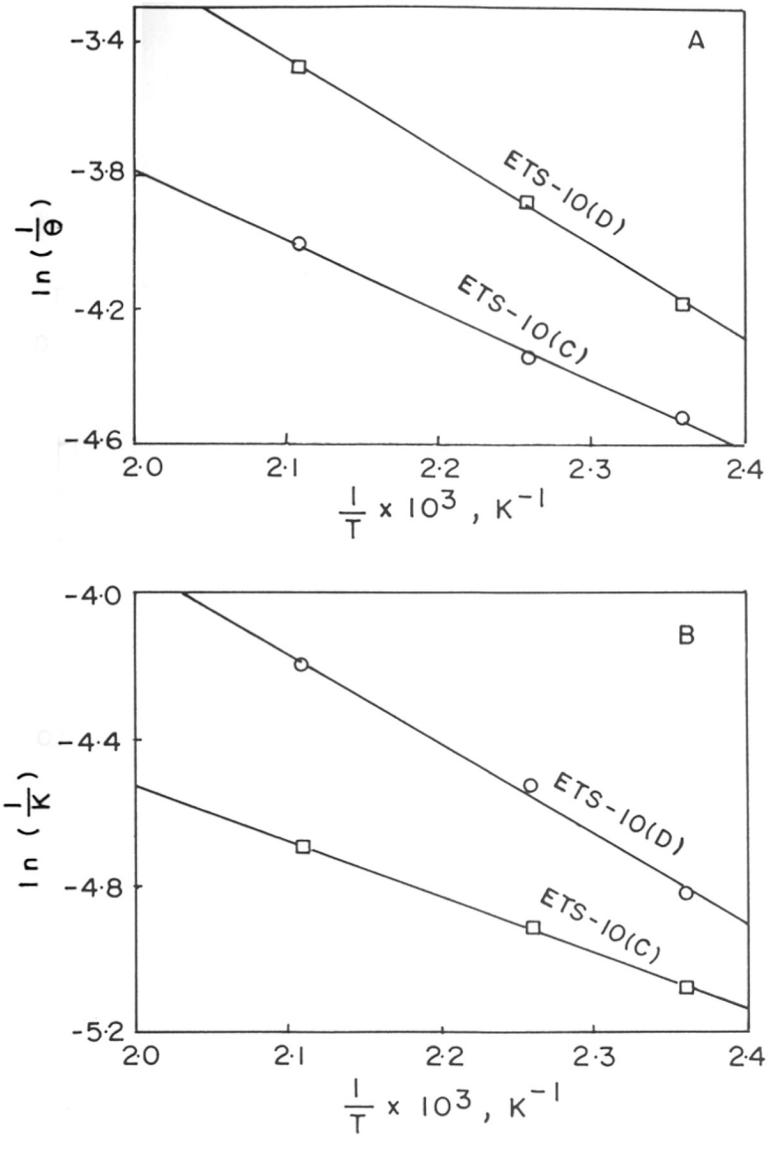

Fig. 2.10 : Arrhenius plots derived from the crystallization kinetics of ETS-10. A, nucleation (E_n) and B, crystallization (E_c).

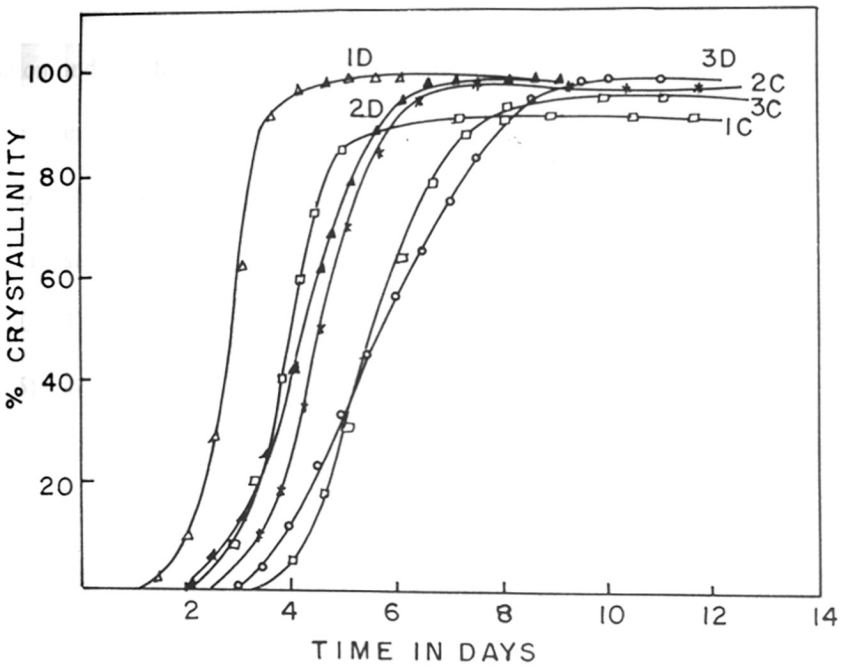

Fig. 2.11 : The influence of H_2O/SiO_2 ratio on the kinetics of crystallization of ETS-10(C) and ETS-10(D); curves 1-3 correspond to H_2O/ SiO_2 values of 30, 45 and 60, respectively; Temp. = 473K.

components constant and as required for obtaining the most crystalline material (gel composition, y R_2O : 3.70 Na_2O : 0.95 K_2O : TiO_2 : 5.71 SiO_2 : x H_2O, where x = 256.9 for choline chloride and 171.4 for hexaethyl diquat-5, and y = 2.28-3.42). For convenience, we will be expressing the template content (with respect to SiO_2) as R/SiO_2 ratio. The influence of the template concentration of the gel on the crystallization rate is presented in Fig. 2.12 for ETS-10(C) and ETS-10(D) at 473K and H_2O/SiO_2 = 45 and 30, respectively. The rate of nucleation and crystallization were both influenced appreciably by changing the template concentration. 98% crystalline material was obtained in 7 days for ETS-10(C) at 473K and H_2O/SiO_2 = 45 when R/SiO_2 = 0.4 (Fig. 2.12, curve 1C). On increasing R/SiO_2 from 0.4 to 0.6, the crystallinity of the material obtained even after 30 days was only 90% (Fig. 2.12, curve 2C). Figure 2.12 also shows that crystallization is faster when the template (hexaethyl diquat-5) content is lower, *i*.e., R/SiO_2 = 0.4 (Fig. 2.12, curve 1D). When R/SiO_2 is 0.6 (Fig. 2.12, curve 2D), 100% crystallinity is achieved in 6 days at 473K. On the other hand, when R/SiO_2 was decreased to 0.2, both ETS-10(C) and ETS-10(D) did not crystallize at all. This suggests that the above templates play a positive role in the synthesis of ETS-10.

D. Influence of titanium content of the gel

Studies were carried out by changing the titanium content in the synthesis gel, keeping the other components the same (gel composition, 1.14 R_2O : 3.70 Na_2O : 0.95 K_2O : z TiO_2 : 5.71 SiO_2 : x H_2O, where x = 256.9 for choline chloride and 171.4 for hexaethyl diquat-5, and z = 1.9 - 0.63). The influence of titanium concentration (SiO_2/TiO_2) in the gel on crystallization (at 473K) is presented in Fig. 2.13 for ETS-10(C) and ETS-10(D). As noted earlier in the case of the other parameters, both the rate of nucleation and crystallization are affected significantly when the SiO_2/TiO_2 ratio is changed; 98% crystalline titanosilicate material is obtained in 7 and 8 days, respectively, for SiO_2/TiO_2 ratio of 5.71 and 9 [ETS-10(C); curves 2C and 3C, respectively], whereas 90% crystallinity is the upper limit when SiO_2/TiO_2 = 3 [ETS-10(C); curve 1C]. On the other hand, 5 and 7 days are

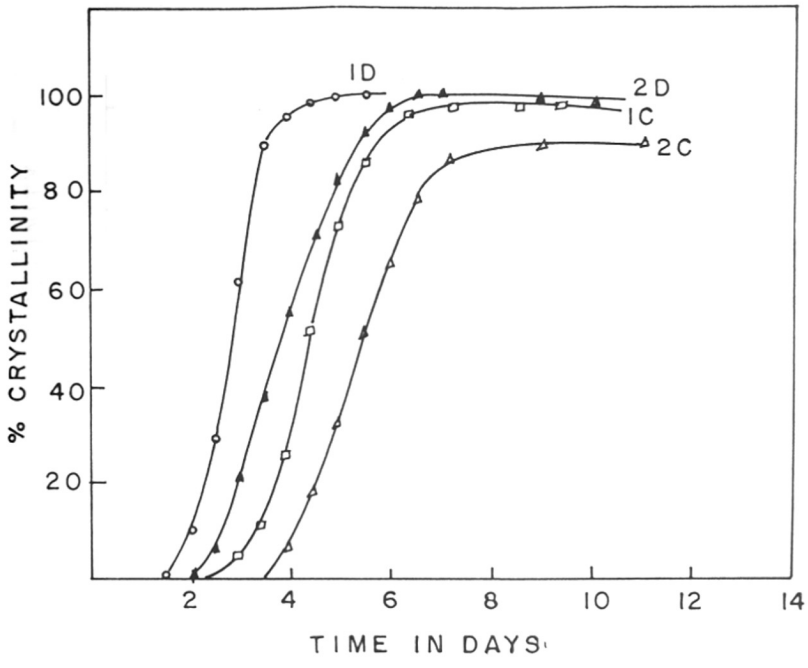

Fig. 2.12 : The influence of R/SiO_2 ratio on the kinetics of crystallization of ETS-10(C) and ETS-10(D) at 473K; curves 1 and 2 correspond to R/SiO_2 values of 0.4 and 0.6, respectively.

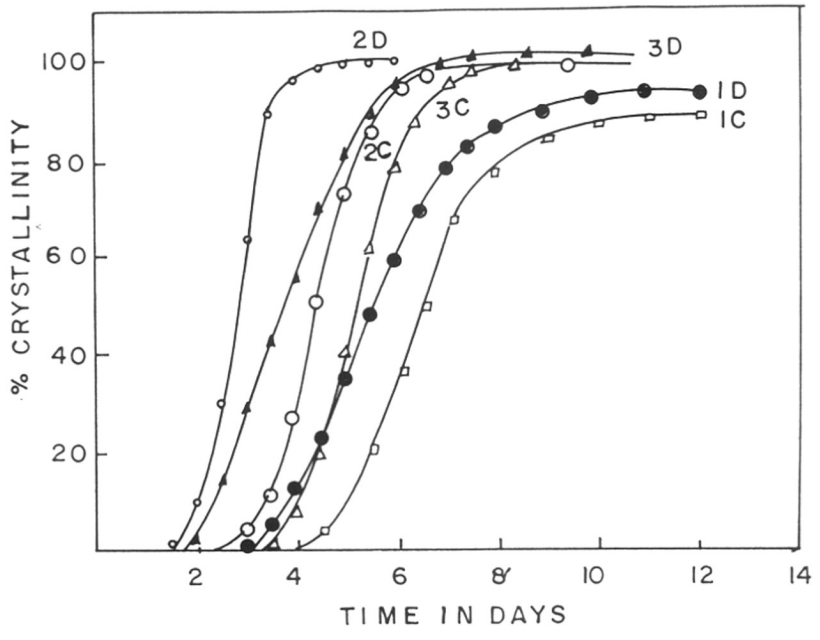

Fig. 2.13 : The influence of SiO_2/TiO_2 ratio on the kinetics of crystallization of ETS-10(C) and ETS-10(D) at 473K; curves 1-3 correspond to SiO_2/TiO_2 values of 3, 5.7 and 9, respectively.

sufficient to get good crystalline material for SiO_2/TiO_2 ratios of 5.71 and 9, respectively, for ETS-10(D) (curves 2D and 3D, respectively), and almost 95% crystalline material for SiO_2/TiO_2 = 3 (curve 1D). When the titanium content was increased further (*i.e.*, SiO_2/TiO_2 < 3), the material did not crystallize at all. However, the ETS-10 materials synthesized using SiO_2/TiO_2 ratios 3.0 and 9.0 were not pure in the case of both the templates. These materials contained ETS-4 impurity.

2.1.3.2 Kinetics of Crystallization during Synthesis using $TiCl_4$

A. Influence of temperature on crystallization

To study the effect of temperature on the formation of the titanosilicate, the kinetics of crystallization were studied in the range 423-473K by comparing the extent of crystallization of the gel mixture (3.70 Na_2O : 0.95 K_2O : TiO_2 : 5.71 SiO_2 : 171 H_2O) at different intervals of synthesis time. The curves (based on XRD estimation of crystallinity) for the crystallization kinetics of ETS-10(E) for the gel composition mentioned earlier are presented in Fig. 2.14. The induction period is followed by the formation of crystalline material, the rate of crystallization increasing with time up to about 70-80% crystallinity and then slowing down. Nearly, 100% crystallization occurs after 15 hours.

Linear plots were obtained applying the Arrhenius equation (Fig. 2.15). The values of activation energies calculated from the slope of the linear plots for nucleation (E_n) and crystallization (E_c) are 32.8 KJ/mole and 27.9 KJ/mole, respectively.

B. Influence of Water Content of the gel

The influence of water content of the gel on the crystallization is presented in Fig. 2.16. The dilution of the gel affects the rate of nucleation as well as the rate of crystallization. When the H_2O/SiO_2 ratio is increased from 15 to 45 (curves 1-3), the crystallization period increases from 12 to 27 hours. At H_2O/SiO_2 ratios of 15 and 45 (curves 1 and 3) the maximum crystallinity obtained was 95%, whereas when the H_2O/SiO_2 was 30, 100% crystalline material was obtained (curve 2).

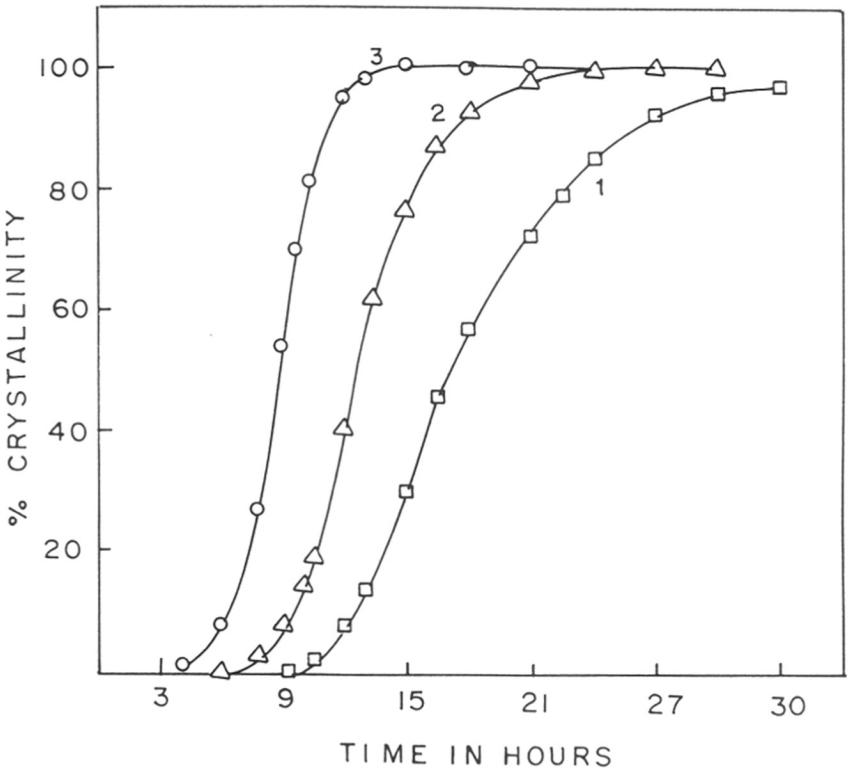

Fig. 2.14 : Effect of temperature on the kinetics of crystallization of ETS-10(E); curves 1-3 correspond to 423K, 448K and 473K, respectively.

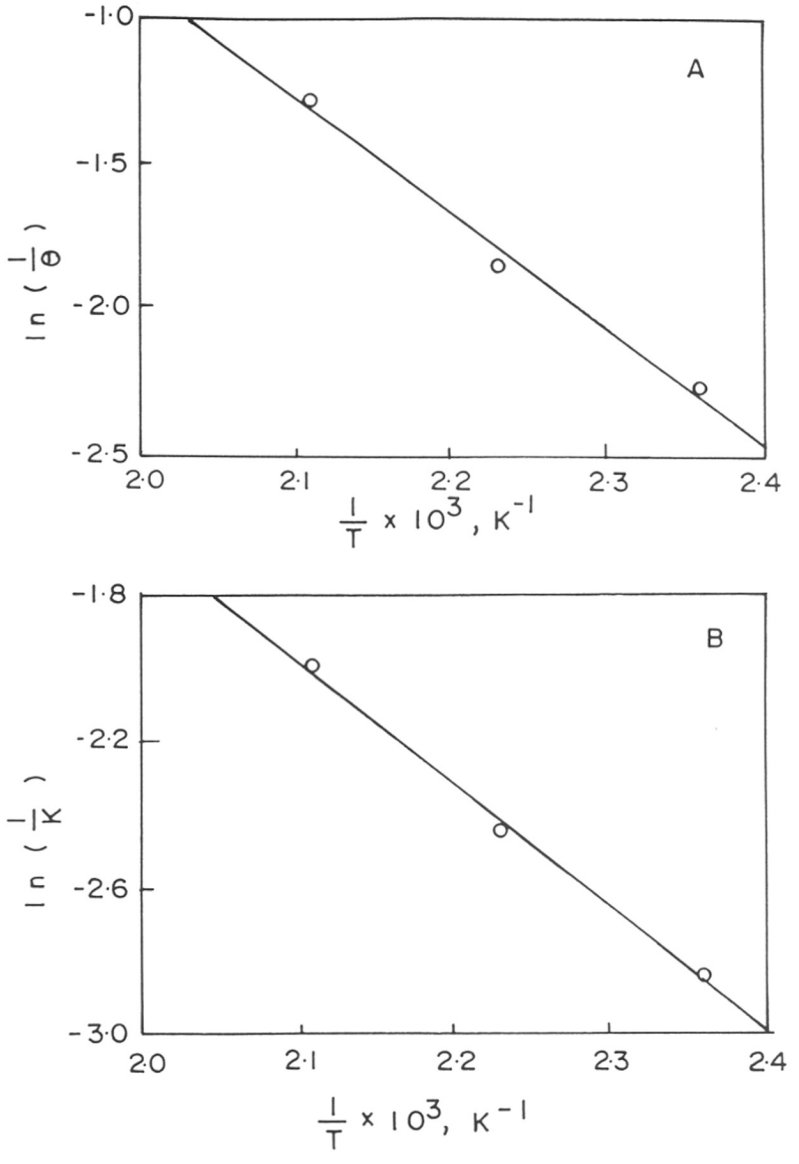

Fig. 2.15 : Arrhenius plots derived from the kinetics of crystallization of ETS-10(E) : A, nucleation (E_n) and B, crystallization (E_c).

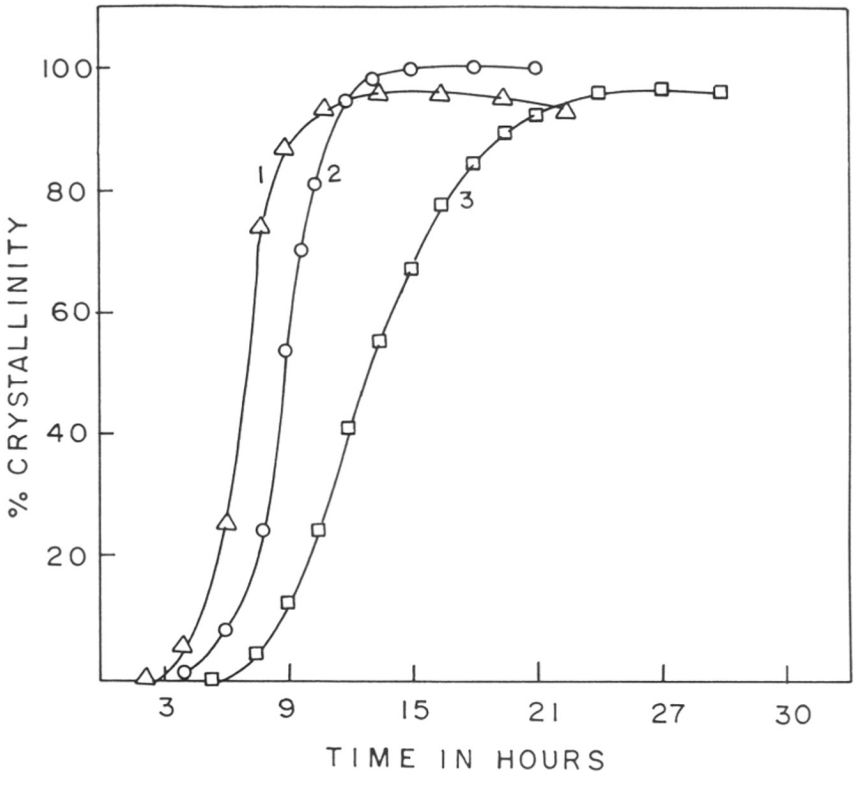

Fig. 2.16 : Influence of H_2O/SiO_2 ratio on the kinetics of crystallization of ETS-10(E); curves 1-3 correspond to H_2O/SiO_2 ratio of 15, 30 and 45, respectively; Temp. = 473K.

2.2 PART - II : MODIFICATION OF ETS-10

2.2.1 Introduction

One of the emerging trends in the area of zeolite catalysis is the isomorphous substitution of Al^{3+} or Si^{4+} by different bivalent (Be), trivalent (B, Ga, Fe or Cr), tetravalent (Ti, V, Sn or Zr) and pentavalent (P or V) elements in the framework positions and the application of these isomorphous materials in various catalytic reactions *[38-46]*. The substitution of Si^{4+} in ETS-10 by Al^{3+} *[20,47,48]* and Ga^{3+} *[19,48]* has been reported recently.

The adsorption and catalytic properties of zeolites are modified to a considerable extent by the replacement of Na^{+} ions with other alkali *[49]* and multivalent cations *[50]*. The Y type zeolite exchanged with rare earth cations are widely used as catalysts in many reactions of the industrial importance *[51]*. The surface acidity of the rare earth zeolite is different from that of the parent zeolite *[52]*.

The unique properties of zeolites, *viz.*, the large ion exchange capability and crystalline structure with uniform pore diameters, allow the preparation of highly dispersed supported metals with narrow particle size distributions *[53]*.

2.2.2 Preparation of Modified ETS-10

2.2.2.1 Isomorphous Substitution

The synthesis of aluminum containing ETS-10 (ETAS-10) has been reported in the literature *[20,47,48]*. In this section, a new method of synthesizing ETAS-10 has been described. The ETAS-10 samples with Si/Al ratios of 22.4, 42.3 and 62.5 were prepared by this method. A typical synthesis procedure for obtaining ETAS-10 with Si/Al = 25 is described below :

Synthesis of ETAS-10

The hydrothermal synthesis of ETAS-10 using $TiCl_4$ was carried out with a gel of the following molar composition:

3.72 Na_2O : 0.95 K_2O : TiO_2 : 5.71 SiO_2 : 0.115 Al_2O_3 : 172 H_2O.

In a typical synthesis, a solution of 9.3 g NaOH in 40 g distilled water was added to a vigorously stirred solution of 52.5 g sodium silicate (28.6% SiO_2, 8.82% Na_2O, 62.58% H_2O) and 40 g distilled water. This was followed by the dropwise addition of 32.75 g of a $TiCl_4$ solution (25.42 wt.% $TiCl_4$, 25.92 wt.% HCl, 48.60 wt.% H_2O) to this mixture (colourless gel) with rapid stirring. 7.8 g $KF.2H_2O$ was next added to the above gel (pH = 11.2 ± 0.1) and the mixture was stirred well. Finally 1.2 g sodium aluminate (43.68% Al_2O_3, 39.0% Na_2O, 17.3% H_2O) dissolved in 16 g water was added to the above mixture and stirred for 1 hour. The mixture was then transferred to a stirred stainless steel autoclave (Parr Instruments, USA) and crystallization was carried out at 473K with a stirrer speed of 300 r.p.m for 14-16 hours. After crystallization, the products were filtered and washed with deionized water till the pH of the filtrate was 10.7-10.8. It was then dried at 373K for 8-10 hours. The XRD pattern is presented in Figure 2.1(g).

2.2.2.2 Cation Exchange

The calcined ETS-10 samples were converted to catalytically active protonic forms by exchanging with ammonium nitrate thrice (20 ml of 1 M solution/g of catalyst at 373K for 10 h), filtering, drying at 383K and calcining at 623K for 5 hour. The ETS-10(E) sample was converted into different ion-exchanged forms by exchanging thrice with the required metal nitrate solutions (20 ml of 1 M solution/g of catalyst at 373K for 3h). After washing, filtering and drying, the M-ETS-10 samples (M = Li, Na, K, Rb, Cs, Mg, Ca, Ba, La) were calcined at 773K for 2h.

2.2.2.3 Impregnation with Platinum

The metal loading of different metal exchanged ETS-10(E) samples and H-ETS-10(E) was carried out by wet impregnation with tetraamine platinum(II) nitrate (Aldrich, 99% purity) to get different Pt-loadings between 0.1 to 0.5 wt.%. A known amount of ETS-10 was added to a concentrated aqueous salt solution containing the amount necessary to obtain the desired weight loading. After impregnation, the materials were dried in air at 383K for 4h and finally calcined at 773K (623K for H-ETS-10) for 3h in air and reduced at 623K for 4h in hydrogen.

2.3 REFERENCES

1. Young, G., US Pat. 3,329,481 (1967).
2. Sandomirskii, P.A., and Belov, N.V., *Sov. Phys. Crystallogr.*, **24**, 686 (1979).
3. Kuznicki, S.M., US Pat. 4,853,202 (1989).
4. Kuznicki, S.M., and Thrush, K.A., Eur. Pat. 0405978A1 (1990).
5. Chapman, D.M., Roe, A.L., *Zeolites,* **10**, 730 (1990).
6. Kuznicki, S.M., Indian Pat. 171379 (1988).
7. Kuznicki, S.M., Indian Pat. 171483 (1988).
8. Kuznicki, S.M., US Pat. 5,011,591 (1991).
9. Kuznicki, S.M., and Thrush, K.A., US Pat. 4,994,191 (1991).
10. Kuznicki, S.M., and Thrush, K.A., US Pat. 5,208,006 (1993).
11. Garfinkel, H.M., Kuznicki, S.M., and Thrush, K.A., WO Pat. 9300152 (1993); EP Pat. 544892 (1993).
12. Blosser, P.W., and Kuznicki, S.M., US Pat., 5,453,263 (1995).
13. Kuznicki, S.M., Dang, D., Hayhurst, D.T., and Thrush, K.A., US Pat. 5,346,535 (1994).
14. Anderson, M.W., Terasaki, O., Ohsuna, T., Philippou, A., Mackay, S.P., Ferreira, A., Rocha, J., and Lidin, S., *Nature,* **367**, 347 (1994).
15. Anderson, M.W., Tarasaki, O., Ohuna, T., Malley, P.J.O., Philippou, A., Mackay, S.P., Ferreira, A., Rocha, J., and Lidin, S., *Philos. Mag. B,* **71**, 813 (1995).
16. Ohuna, T., Tarasaki, O., Watanabe, D., Anderson, M.W., and Lidin, S., *Stud. Suf. Sci. Catal.*, **84**, 413 (1994).
17. Sommerfeld, D.A., Ellis, W.R., Jr., Eyring, E.M., Kuznicki, S.M., and Thrush, K.A., *J. Phys. Chem.*, **96**, 9975 (1992).
18. Kuznicki, S.M., Thrush, K.A., Allen, F.M., Levine, S.M., Hamil, M.M., Hayhurst, D.T., and Mansour, M., *Synth. Microporous Mater.*, **1**, 427 (1992).
19. Rocha, J., Lin, Z., Ferreira, A., and Anderson, M.W., *J. Chem. Soc. Chem. Commun.*,

867 (1995).

20. Anderson, M.W., Philippou, A., Lin, Z., Ferreira, A., and Rocha, *J., Angew. Chem. Int. Ed. Engl.*, **34**, 1003 (1995).

21. A review article titled : Looming Ban on Production of CFCs, Halons Spurs Switch to Substitutes, *C & E News;* No. **15**, 12-18 (1993).

22. Valtchev, V., *J. Chem. Soc. Chem. Commun.*, 261 (1994).

23. Valtchev, V., and Mintova, S., *Zeolites,* **14**, 697 (1994).

24. Bozhilov, K.N., Valtchev, V., *Mat. Res. Bull.*, **28**, 1209 (1993).

25. Liu, X., and Thomas, J.K., *J. Chem. Soc. Chem. Commun.*, 1435 (1996).

26. De Luca, P., and Nastro, A., *International Zeolite Conference,* Korea, (1996)

27. Das, T.K., Chandwadkar, A.J., and Sivasanker, S., *Mater. Res. Bull.*, **17**, 1143 (1994).

28. Das, T.K., Chandwadkar, A.J., Budhkar, A.P., Belhekar, A.A., and Sivasanker, S., *Microporous Mater.*, **4**, 195 (1995).

29. Das, T.K., Chandwadkar, A.J., Budhkar, A.P., and Sivasanker, S., *Microporous Mater.*, **5**, 401 (1996).

30. Das, T.K., Chandwadkar, A.J., and Sivasanker, S., *J. Mol. Catal.*, **107**, 199 (1996).

31. Das, T.K., Chandwadkar, A.J., and Sivasanker, S., *J. Chem. Soc. Chem. Commun.*, 1105 (1996).

32. Tsitsishvilli, G.V., Krupeniikov, A. Yu., Mamulashvili, M.V., and Urushadze, M.V., *Russ. J. Phys. Chem.*, **53**, 975 (1979).

33. Domine, D., and Quobex, J., J. Mol. Sieves, Soc, Chem. Ind. London, 78 (1968).

34. Chao, K.J., Tasi, T.C., Chen., M.S., and Wang, I., *J. Chem. Soc., Faraday Trans.*, **77**, 547 (1981).

35. Thompson, R.W., *Zeolites,* **12**, 680 (1992).

36. Den Ouden, C.J.J., and Thompson, R.W., *Ind. Eng. Chem. Res.*, **31**, 369 (1992).

37. Ernst, S., Jacobs, P.A., Martens, J.A., and Weitkamp, J., *Zeolites,* **7**, 46 (1987).

38. Barrer, R.M., "Hydrothermal Chemistry of Zeilites" Academic Press, London, 251

(1982).

39. Mueller, U., and Steck, W., *Stud. Surf. Sci. Catal.*, **84**, 203 (1994).

40. Kwak, B.S., and Sachtler, W.M.H., *J. Catal.*, **145**, 456 (1994).

41. Yuan, Z.Y., Liu, S.Q., Chen, T.H., Wang, J.Z., and Li, H.X., *J. Chem. Soc. Chem. Commun.*, 973 (1995).

42. Ulagappan, N., and Rao, C.N.R., *J. Chem. Soc. Chem. Commun.*, 1047 (1996).

43. Thangaraj, A., Kumar, R., and Ratnasamy, P., *J. Catal.*, **131**, 294 (1991).

44. Sen, T., Ramaswamy, V., Ganapathy, S., Rajamohanan, P.R., and Sivasanker, S., *J. Phys. Chem.*, **100**, 3809 (1996).

45. Das, T.K., Chaudhari, K., Chandwadkar, A.J., and Sivasanker, S., *J. Chem. Soc. Chem. Commun.*, 2495 (1995).

46. Dongare, M.K., Singh, P., Moghe, P.P., and Ratnasamy, P., *Zeolites*, **11**, 690 (1991).

47. Deeba, M., Keweshan, C.F., Koermer, G.S., Kuznicki, S.M., and Madon, R.S., in M. Dekker (Ed.) "Catalysis of Organic Reactions", 383, (1994).

48. Anderson, M.W., Rocha, J., Lin, Z., Philippou, A., and Orion, I., Ferreira, A., *Microporous Mater*, **6**, 195 (1996).

49. Zheng, J., Dong, J-L., Xu, Q-H., Liu, Y., and Yan, A-Z., *Appl. Catal.*, **126**, 141 (1995).

50. Tsitsishvilli, G.V., and Andronikashvili, T.G., *"Molecular Sieves Zeolites-II"*, Adv. Chem. Ser., Amer. Chem. Soc., Washington D.C., **102**, 217 (1971).

51. Venuto, P.B., and Landis, P.S., *Adv. Catal.*, **18**, 259 (1968).

52. Naccache, C., Primet. M., and Mathieu, M.V., *"Molecular Sives-II"*, Adv. Chem. Ser., Amer. Chem. Soc., Washington D.C., **121**, 266 (1973).

53. Breck, D.W., "Zeolites Molecular Sieves", Wiley, New York, (1974).

CHAPTER III

PHYSICO-CHEMICAL CHARACTERIZATION OF ETS-10

3.1 INTRODUCTION

Samples of titanosilicates, synthesized *[1-5]* as described in Chapter II, have been characterized using various physico-chemical techniques.

This chapter summarizes the results of the physico-chemical characterization of the titanosilicate samples. The discussion focuses on XRD, SEM, FTIR, MAS NMR, thermal analysis, UV-Visible, NH_3-TPD and Pt-dispersion by H_2 chemisorption of these materials.

3.2 EXPERIMENTAL

3.2.1 Chemical Analysis

Wet chemical methods were used to determine the chemical composition of the gel and the crystalline materials. A known amount of the sample (W_1) was taken in a platinum crucible with a lid and heated at a high temperature (1073K) for 5 hours. The sample was then cooled in a desiccator and weighed (W_2). The difference in weights (W_1-W_2) gave the weight loss on ignition. The dry weight was noted. The sample was then treated with 4 drops of sulphuric acid and 5 ml of HF (48 wt.%) and evaporated on the hot plate to remove silicon in the form of H_2SiF_6. This procedure was repeated twice to ensure that all the silicon species had been removed. The crucible was then heated over a Bunsen flame to red heat for 4 hours. It was then cooled in a desiccator and weighed. The loss in the weight of the sample indicated the content of silica.

The residue was dissolved in 5 ml HCl (1:1) and 2 drops of HF and diluted to a known volume. The solution was then analyzed for Ti, Al, Na, K and other elements by atomic absorption spectroscopy (Hitachi, Model Z-8000). Ti estimation was also carried out by a spectroscopic method *[6]*. In this method, a known volume of the solution was taken in a volumetric flask and 2 ml dilute hydrogen peroxide (5 ml 30 wt.% H_2O_2 diluted to 50 ml)

added to it in order to get a yellow colour. In this procedure titanium(IV) forms a complex with hydrogen peroxide $[Ti(H_2O_2)]^{4+}$ which is yellow in colour. The intensity of the colour is proportional to the amount of Ti^{4+} present. Enough H_2SO_4 was present in the final solution (H_2SO_4 concentration of about 1.5 to 3.5 (N)) to prevent hydrolysis to a basic sulphate and to prevent condensation to metatitanic acid. The colour intensity was slightly dependent on temperature and hence the solutions were kept at the same temperature (25°C). Na and K estimations were carried out using a flame photometer.

3.2.2 X-ray Diffraction

Powder X-ray diffraction patterns of all the samples were recorded using Rigaku (Model D/Max III VC, Japan) x-ray diffractometer with Ni filtered Cu-K_α radiation (λ = 1.5404 Å). The sample was first ground and dried at 383K for 2 hours and equilibrated over a saturated $CaCl_2$ solution at room temperature for 6 hours prior to measurements. All the samples were scanned in the 2θ range 4-40° at the scan rate of 0.25° $min.^{-1}$. Based on the synthesis experiments, the sample with a highest crystallinity was taken as a reference sample to compare the phase purity and crystallinity of the other samples. Peak areas were calculated from the collected data, using a semi-quantitative software programme provided with the instrument. Silicon was used as the internal standard for calibrating the 2θ° values.

3.2.3 Infrared Spectroscopy

KBr pellets containing the sample (1 mg) and KBr (300 mg) were used for framework IR analysis. Fourier transform infrared (FTIR) spectra were recorded with a Nicolet FTIR spectrometer (Model 60 X B). FTIR spectra in the 450 cm^{-1} to 1300 cm^{-1} framework region were obtained in the diffuse reflectance mode. The hydroxyl as well as the pyridine absorption region were scanned in transmittance mode. The powder sample was pressed into

a self supporting wafer containing ~6 mg/cm^2 of the material, mounted in an IR cell and evacuated at 598K for 6 hours to a pressure of 10^{-6} Torr. The cell was then closed, the sample was allowed to cool down to room temperature and the IR spectra was recorded. Afterwards, pyridine vapour (vapour pressure = 10 mm of Hg) was admitted into the cell. Then the temperature of the sample was increased to 373K and the pyridine allowed to adsorb for 1 hour. Finally, the excess pyridine was desorbed by evacuating the sample at the required temperature for 2 hours. The sample was cooled to room temperature and the spectra were recorded. For hydroxyl region experiments, the samples were evacuated at 313K, 373K and 473K, while for pyridine region experiments, the samples were evacuated at 373K, 473K and 573K. Each spectrum was averaged over 1000 scans and had a spectral resolution of 4 cm^{-1}.

3.2.4 UV-Visible Spectroscopy

UV-Vis diffuse reflectance spectra of the samples were recorded on a Shimadzu UV-Visible spectrophotometer (Model UV 210PC) in the reflectance mode using barium sulphate as a reference.

3.2.5 Thermal Analysis

Simultaneous TGA-DTA analysis of the as-synthesized samples was carried out using a computer controlled thermal analyzer (Setaram, France, Model TG-DTA 92). A linear rate of heating of 10K min^{-1} from room temperature to 1173K in an air flow (30 ml min^{-1}) was employed to find out the temperature of decomposition of the organic additive, the thermal stability of the molecular sieves and weight loss. Usually, 30 mg of the samples were used in the experiments and inert α-alumina was used as the reference sample.

3.2.6 Solid-State MAS NMR Spectroscopy

The solid-state magic-angle spinning (MAS) NMR spectra of ^{29}Si, ^{27}Al and ^{23}Na were recorded at 298K using a Bruker MSL-300 FT NMR spectrometer. Bloch decays were averaged 2400 times before Fourier transformation to obtain spectra with a sufficient signal-to-noise ratio. The magic angle was precisely set using KBr and maximizing the rotational echo intensities of the satellite transitions of ^{81}Br. While acquiring the ^{29}Si spectra, a recycle time of 4s was found to be sufficient to give fully relaxed spectra. ^{29}Si spectra were recorded at Larmor frequency (γ) = 59.62 MHz using tetramethylsilane (TMS) as the primary reference. An excitation pulse (t pulse) of 2 μs was used with 2000 scans (NS). ^{27}Al spectra was obtained using 0.25s recycle time, Larmor frequency of 78.172 MHz and 3 μs pulse. The spectra were collected over 600 scans with 0.1 M $[Al(H_2O)_6]^{3+}$ as the external reference. Typically, 2000 transients were accumulated before they were remotely processed on a Silicon Graphics Indigo2 Work Station using the Bruker UXNMR software package. Resolution enhancement using a sine bell window function and spectral deconvolution, assuming a Gaussian function, were carried out for accurate estimation of the ^{29}Si chemical shifts and the integrated intensities. While acquiring the ^{23}Na spectra, a recycle time of 1s was found to be sufficient to give fully relaxed spectra. ^{23}Na spectra were measured using a Larmor frequency of 79.39 MHz, excitation pulse of 2 μs, 200 NS and sodium chloride as the primary reference.

3.2.7 Molecular Modeling

The computer graphics (CG) visualization of ETS-10, the cluster model generation and the semi-empirical quantum chemical calculations were performed on Silicon Graphics Indigo2 workstation using Insight II software package supplied by Biosym Technologies Inc., USA. The ETS-10 lattice was modeled from the crystal structure reported by Anderson *et al.*

[7,8] for the polymorph B. The unit cell of ETS-10 has a stoichiometry of $[M_{96}O_{208}]^{32-}$ (where M = Si or Ti), or precisely $[(SiO_2)_{80}(TiO_3)_{16}]^{32-}$, where the Si/Ti ratio is 5.

A computer graphics view of the asymmetric unit cell showing the various Si and Ti sites is shown in Fig. 3.1. There are 11 distinct Si sites and 3 distinct Ti sites in the asymmetric unit cell of ETS-10 (polymorph B). All the Ti sites are octahedrally coordinated, where 2 oxygen atoms are bridging to adjacent Ti sites and the remaining 4 oxygen atoms are bridging to Si sites. All the Si sites are tetrahedrally coordinated and there are basically two types of silicons; there are silicons [Si(4Si)] where all the 4 oxygen atoms are bridging to adjacent Si sites and silicons [Si(3Si,1Ti)] where 3 oxygen atoms are bridging to adjacent Si-sites and the remaining oxygen atom is bridging to adjacent Ti site. The average M-O distances and M-O-M angles (where M = Si or Ti), calculated from the reported crystal structure are given in Table 3.1. Semi-empirical quantum chemical calculations using a standard MNDO procedure were carried out on cluster models representing the Si sites in ETS-10 to understand the electronic structure, preferred locations for Al substitution and resulting acidity.

3.2.8 Scanning Electron Microscopy

The crystallite size and morphology of the as-synthesized and calcined samples were determined by a scanning electron microscope (Model JSM 5200, JEOL, Japan) equipped with energy dispersive X-ray analysis (EDX). The samples were sputtered with gold to prevent surface charging and to protect from thermal damage from the electron beam.

3.2.9 Temperature Programmed Desorption of NH_3

NH_3-TPD measurements were performed using a commercial instrument (Sorbstar, Model 200, Institute of Isotopes, Hungary). In this measurement, 200 mg of the sample was taken in a U tube and heated at 673K for 3h in an argon atmosphere. After the bed was cooled down to room temperature, anhydrous ammonia was passed (5 ml/min.) through the

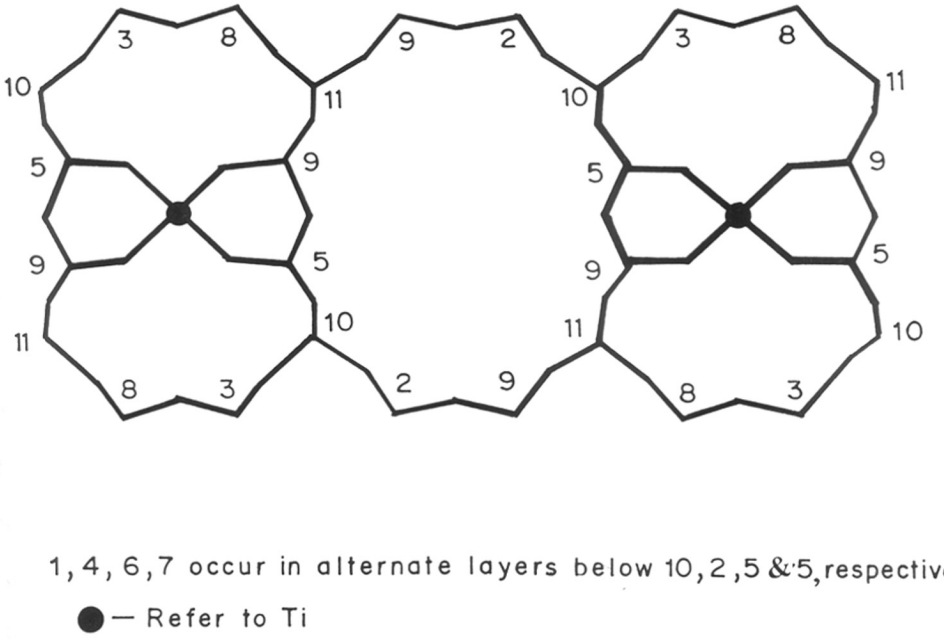

Fig. 3.1 : The topographical distribution of the 11 crystallographically different Si sites of polymorph B in the ETS-10 lattice.

Table 3.1 : The geometric data of the polymorph B of ETS-10 structure.

Site (M)	M-O distance[a]	M-O-M angle[b]	Connectivity[c]
Ti_1	1.8867	145.9900	Si_5, Si_5, Si_9, Si_9, Ti_3, Ti_3
Ti_2	1.8867	144.6867	Si_3, Si_3, Si_7, Si_7, Ti_3, Ti_3
Ti_3	1.8833	145.3400	Si_8, Si_6, Ti_1, Si_4, Ti_2, Si_2
Si_1	1.5750	149.7000	Si_4, Si_4, Si_7, Si_7
Si_2	1.5775	142.8200	Si_6, Si_9, Si_{10}, Ti_3
Si_3	1.5775	142.6525	Si_7, Si_8, Si_{10}, Ti_2
Si_4	1.5775	144.3525	Si_5, Si_8, Si_1, Ti_3
Si_5	1.5775	143.4475	Si_4, Si_9, Si_{10}, Ti_1
Si_6	1.5800	143.1475	Si_2, Si_{10}, Si_7, Ti_3
Si_7	1.5800	142.5075	Si_3, Si_1, Si_6, Ti_2
Si_8	1.5775	145.1400	Si_3, Si_4, Si_{11}, Ti_3
Si_9	1.5775	143.7625	Si_2, Si_5, Si_{11}, Ti_1
Si_{10}	1.5775	150.7725	Si_2, Si_3, Si_5, Si_6
Si_{11}	1.5800	152.1900	Si_8, Si_8, Si_9, Si_9

[a]The M-O distances are the average of six Ti-O distances for TiO_6 octahedra and the average of four Si-O distances for SiO_4 tetrahedra.

[b]The M-O-M angles are the average of six Ti-O-M (where M = Ti or Si) angles for the TiO_6 octahedral and the average of four Si-O-M (where M = Ti or Si) angles for SiO_4 tetrahedra.

[c]Connectivity as derived from the structure reports.

bed for 1h. The bed was then flushed with argon for 2h at 313K. The temperature-programmed desorption experiment was carried out with a heating rate of 8K/min. in the temperature range 313K to 673K. The NH_3 desorbed was detected by a TCD.

3.2.10 Pt-dispersion Measurement by H_2 Chemisorption

The platinum dispersion of the catalyst was determined by hydrogen chemisorption at room temperature *[9]*. 3 g of the calcined catalyst was loaded in a pyrex-glass U shape sample holder. The sample was reduced at 623K for 2h and degassed at 773K (598K for H-ETS-10) for 5h under vacuum (10^{-5} Torr). Under the same vacuum, the temperature of the sample was brought to the ambient temperature. High purity hydrogen was adsorbed in the equilibrium pressure range between 5 to 200 Torr. After this, the sample was evacuated at 10^{-5} Torr at ambient temperature to remove the weakly adsorbed hydrogen. A second adsorption isotherm was carried out at ambient temperature in the same pressure range as the first one. The difference between the two adsorption isotherms after extrapolating to zero pressure provides the amount of chemisorbed hydrogen *[9]*. The Pt-dispersion was estimated assuming dissociative adsorption of hydrogen on the metal.

3.3 RESULTS AND DISCUSSION

3.3.1 Chemical Analysis

The unit cell compositions (in the hydrated form) of ETS-4, all the as-synthesized ETS-10 and the modified ETS-10 samples, obtained from chemical analysis are reported in Table 3.2. The protonic form of all the ETS-10 samples and 0.5 M H_2SO_4 extracted ETS-10(C) and ETS-10(D) are also given in Table 3.2. The chemical compositions were not significantly altered by variations in the seed concentration (0.9-14.0%, input SiO_2 basis). The chemical analysis shows that the SiO_2/TiO_2 ratio is influenced by the templating agent.

Table 3.2 : Unit cell composition of as-synthesized ETS-10 samples (hydrated form).

Sample	Unit cell composition
ETS-4	$Na_{37.95}K_{13.62}(Ti_{24.33}Si_{75.67}O_{224.33})$ 77.37 H_2O (Not unit cell)
ETS-10(A)	$Na_{23.43}K_{10.85}(Ti_{14.28}Si_{81.72}O_{206.28})$ 44.43 H_2O
ETS-10(B)	$Na_{25.30}K_{3.45}(Ti_{14.37}Si_{81.63}O_{206.37})$ 104.62 H_2O
ETS-10(C)	$(Choline)_{3.83}Na_{20.64}K_{4.60}(Ti_{14.52}Si_{81.48}O_{206.52})$ 19.73 H_2O
ETS-10(D)	$(diquat)_{3.15}Na_{21.32}K_{3.32}(Ti_{15.07}Si_{80.93}O_{207.07})$ 10.47 H_2O
ETS-10(E)	$Na_{22.60}K_{8.90}(Ti_{15.73}Si_{80.26}O_{207.71})$ 65.38 H_2O
H-ETS-10(A)	$Na_{6.82}K_{0.92}(Ti_{14.28}Si_{81.72}O_{206.28})$ 44.43 H_2O
H-ETS-10(B)	$Na_{6.95}K_{1.02}(Ti_{14.37}Si_{81.63}O_{206.37})$ 62.42 H_2O
H-ETS-10(C)	$Na_{6.30}K_{0.25}(Ti_{14.52}Si_{81.48}O_{206.52})$ 19.73 H_2O
H-ETS-10(D)	$Na_{7.72}K_{0.31}(Ti_{15.07}Si_{80.93}O_{207.07})$ 25.70 H_2O
H-ETS-10(E)	$Na_{7.24}K_{1.04}(Ti_{15.74}Si_{80.26}O_{207.74})$ 45.64 H_2O
ETS-10(C) [acid extracted]	$Na_{7.80}K_{1.09}(Ti_{12.08}Si_{83.92}O_{204.08})$ 18.46 H_2O
ETS-10(D) [acid extracted]	$Na_{8.21}K_{0.81}(Ti_{12.52}Si_{83.47}O_{204.50})$ 24.60 H_2O
Li-ETS-10(E)	$Li_{13.60}\,Na_{14.20}\,K_{3.70}\,(Ti_{15.73}\,Si_{80.26}\,O_{208})$ 65.38 H_2O
Na-ETS-10(E)	$Na_{29.54}\,K_{1.96}\,(Ti_{15.73}\,Si_{80.26}\,O_{208})$ 65.38 H_2O
K-ETS-10(E)	$Na_{11.23}\,K_{20.27}\,(Ti_{15.73}\,Si_{80.26}\,O_{208})$ 65.38 H_2O
Rb-ETS-10(E)	$Rb_{14.41}\,Na_{14.40}\,K_{2.69}\,(Ti_{15.73}\,Si_{80.26}\,O_{208})$ 65.38 H_2O
Cs-ETS-10(E)	$Cs_{12.85}\,Na_{15.85}\,K_{2.80}\,(Ti_{15.73}\,Si_{80.26}\,O_{208})$ 65.38 H_2O
Mg-ETS-10(E)	$Mg_{11.92}\,Na_{4.46}\,K_{3.17}\,(Ti_{15.73}\,Si_{80.26}\,O_{208})$ 65.38 H_2O
Ca-ETS-10(E)	$Ca_{13.06}\,Na_{2.65}\,K_{2.70}\,(Ti_{15.73}\,Si_{80.26}\,O_{208})$ 65.38 H_2O
Ba-ETS-10(E)	$Ba_{11.00}\,Na_{8.18}\,K_{1.26}\,(Ti_{15.73}\,Si_{80.26}\,O_{208})$ 65.38 H_2O
La-ETS-10(E)	$La_{7.60}\,Na_{3.91}\,K_{4.04}\,(Ti_{15.73}\,Si_{80.26}\,O_{208})$ 65.38 H_2O

It also indicates that choline chloride or hexaethyl diquat-5 ions replace the hydrated potassium ions in the ETS-10 structure, while the TMA (tetramethyl ammonium) ions were reported to replace mainly the hydrated sodium ions *[10]*. When the SiO_2/TiO_2 molar ratio of the synthesis gel (standard) was 5.71, the SiO_2/TiO_2 ratio of the crystalline product was 5.61 for ETS-10(C) and 5.37 for ETS-10(D).

3.3.2 X-ray Diffraction

The phase purity and crystallinity of the samples were determined by powder X-ray diffraction. The XRD patterns of ETS-4 and ETS-10 synthesized by different methods have already been reported in Chapter II (Fig. 2.1). From the XRD patterns it is clear that ETS-10(E) is more crystalline than the other samples. Figure 3.2 shows that there is a slight decrease in the intensity of the peaks of the as-synthesized ETS-10(A) after calcination at 623K for 3 hours in air and then it remains the same on further heating from 623K to 873K indicating that it is stable at 873K, which is also confirmed from TGA/DTA. When the NH_4-form of the ETS-10(A) was similarly heated at different temperatures (Fig. 3.3), near collapse of the structure occurred at 673K. Apparently, the structure is stabilized by the Na/K-ions present in the as-synthesized sample. The NH_4-form of ETS-10(E) is stable at 673K, but, its structure collapses at 723K (Fig. 3.4). It appears, therefore, that H-ETS-10(E) is more stable than H-ETS-10(A). The Na/K content of H-ETS-10(E) is slightly more than that of H-ETS-10(A). It is not, therefore, clear if the greater stability of H-ETS-10(E) is a result of larger alkali ion content, or due to its greater purity. The XRD patterns of the different alkali metal exchanged ETS-10(E) are presented in Figure 3.5. As the atomic weight of the alkali metal increases, the intensity of the peaks decreases.

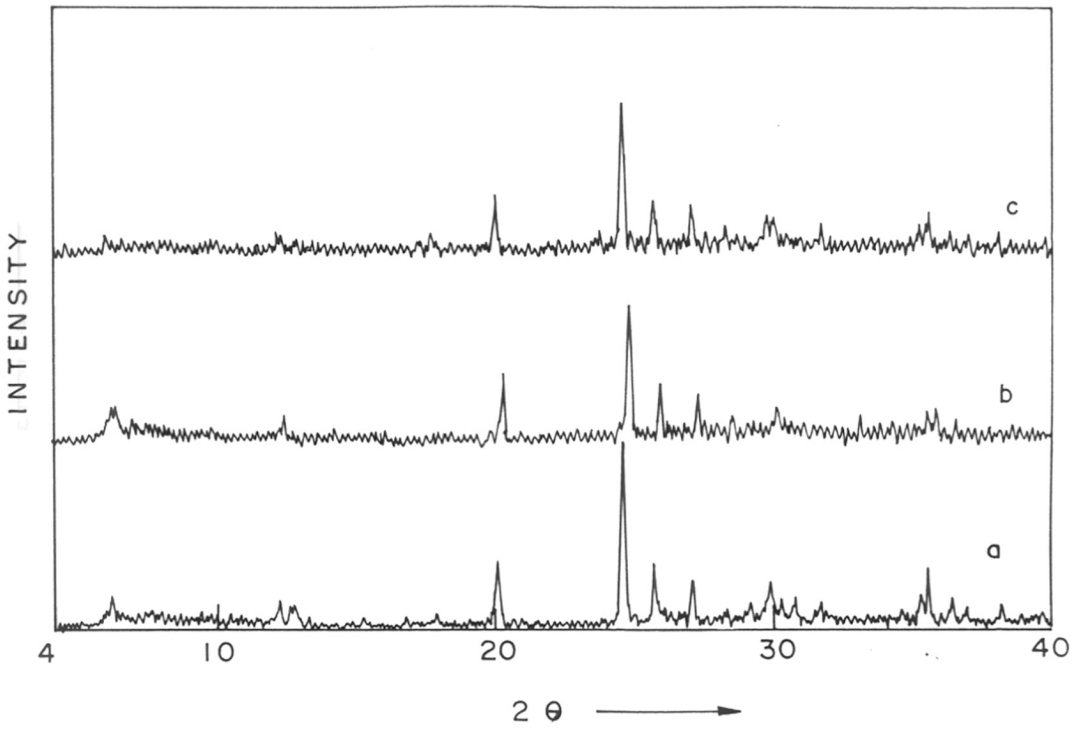

Fig. 3.2 : Powder XRD patterns of ETS-10(A) :

(a) As-synthesized; after calcination for 4h at (b) 623K and (c) 873K.

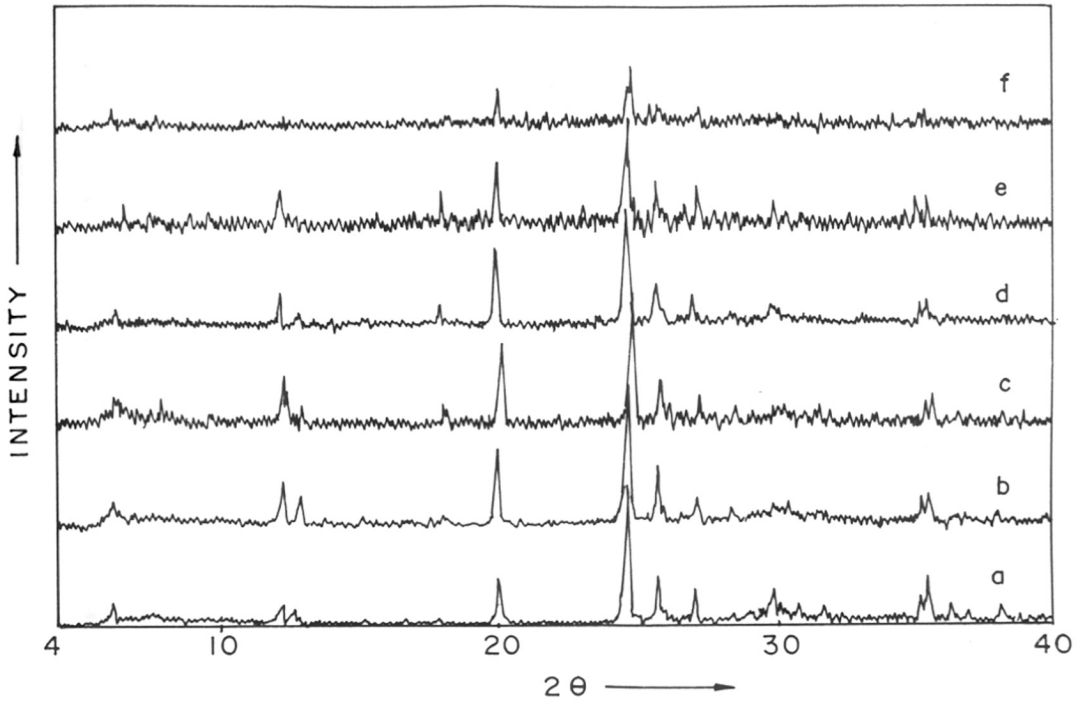

Fig. 3.3 : Powder XRD patterns of ETS-10(A); (a) As-synthesized, (b) NH_4-form and after calcination in air for 4h at (c) 473K, (d) 598K, (e) 623K and (f) 673K.

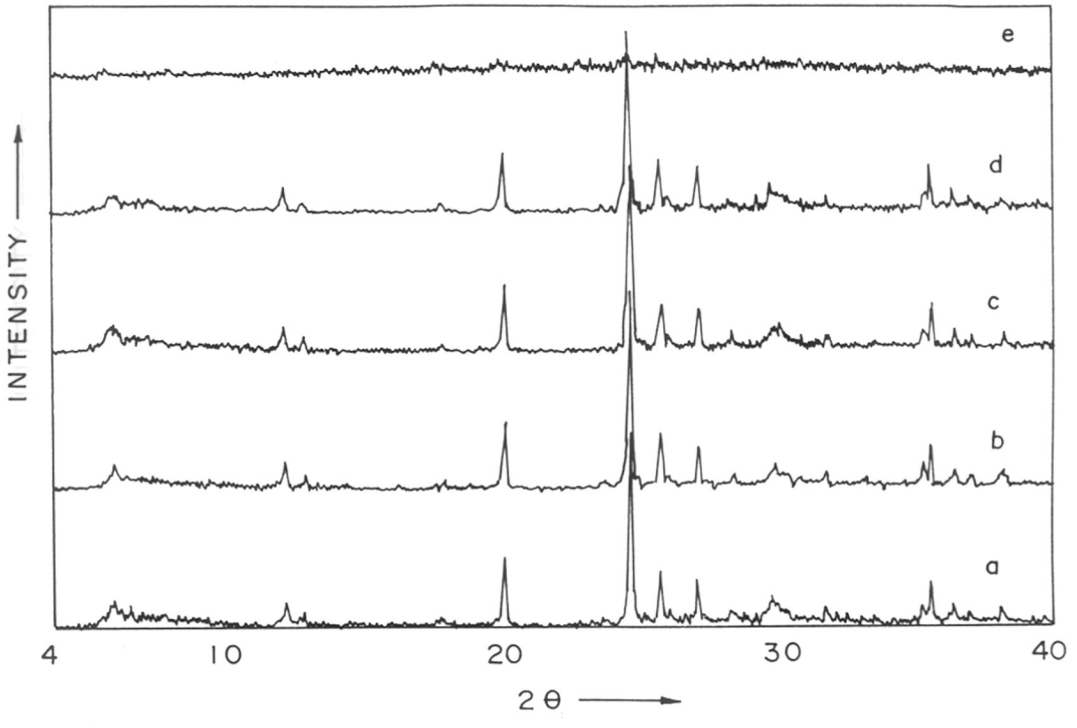

Fig. 3.4 : Powder XRD patterns of ETS-10(E); (a) As-synthesized and after calcination of NH_4-form in air for 4h at (b) 523K, (c) 623K, (d) 673K and (e) 723K.

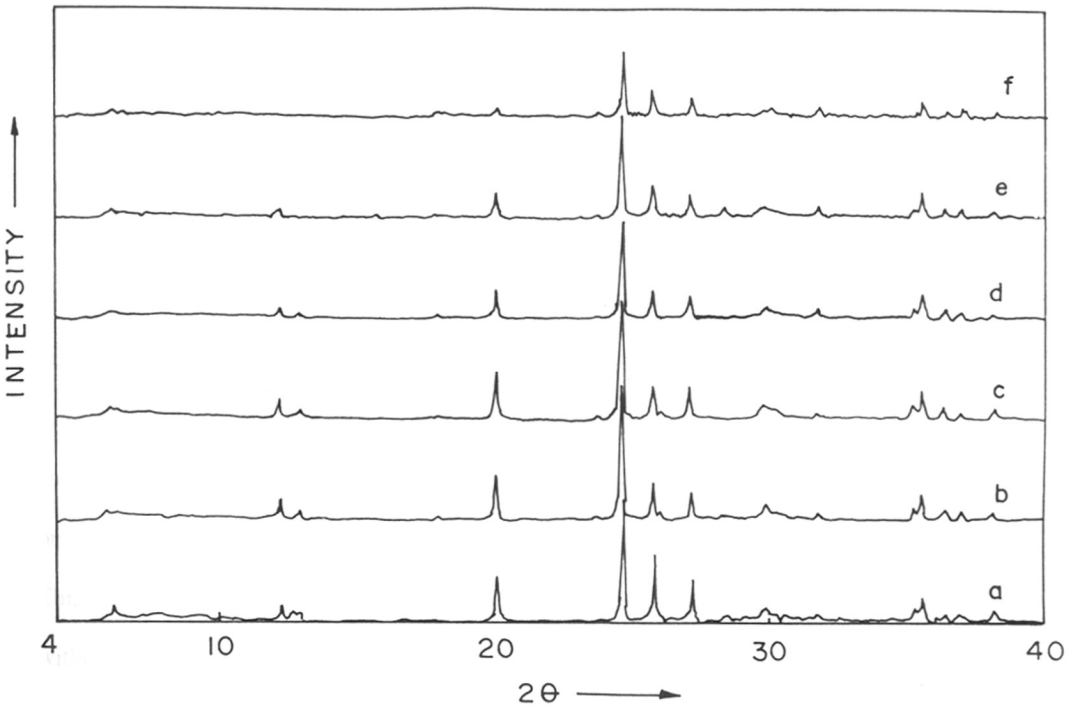

Fig. 3.5 : Powder XRD patterns of alkali metal exchanged ETS-10(E); (a) As-synthesized, (b) Li-ETS-10, (c) Na-ETS-10, (d) K-ETS-10, (e) Rb-ETS-10 and (f) Cs-ETS-10.

3.3.3 Infrared Spectroscopy

The IR spectra (in the region 450-1300 cm^{-1}) of ETS-4, ETS-10(B), ETS-10(A) (7.0% seed), ETS-10(A) (0.9% seed) and dried precursor gel are shown in Fig. 3.6 (curves A, B, C, D and E, respectively). ETS-4 shows a prominent band at 984 cm^{-1} corresponding to Si-O stretching vibration and weak absorptions at 916, 698, 654 and 542 cm^{-1} corresponding to Si-O stretching, Ti-O stretching, octahedral O-Ti-O and Ti-O-Ti bending, and O-Ti-O bending and Ti-O bond rocking, respectively *[11]*. The positions of the major absorption bands and shoulders corresponding to the different symmetric and asymmetric stretching vibrations *[12]* remain almost unchanged (±5 cm^{-1}) for all the titanosilicates prepared using seeds. However, the spectral bands for ETS-10(B) are not sharp, though the major bands occur at about the same positions as in ETS-10(A). The lack of sharpness may be due to contributions from amorphous material. No distinct sharp bands are observed in the IR spectrum of the precursor gel (amorphous material) except for a weak peak at 775 cm^{-1} (Fig. 3.6, curve E). This peak is also present as a very weak absorption in the spectrum of the sample prepared without seeds (Fig. 3.6, curve B).

The framework IR spectra (in the region 450-1300 cm^{-1}) of ETS-10(E) and calcined ETS-10(C) and ETS-1092 (D) are shown in Fig. 3.7. However, the spectral bands for ETS-10(C) (spectrum 1C) are not sharp, though the major bands occur at the same positions as those of ETS-10(E) and ETS-10(D) (spectrum 1E and 1D). A weak shoulder at ~985 cm^{-1} is also seen (Fig. 3.7, curves 1E, 1C and 1D, respectively) in the case of the calcined samples of these titanosilicates [Na and K forms of ETS-10(E), ETS-10(C) and ETS-10(D)]. The calcined samples were extracted with 0.5M H_2SO_4 solution (zeolite to acid solution ratio of 1:10) at ambient temperature overnight, filtered, washed and dried and their IR spectra were obtained. An IR absorption band appears at ~970 cm^{-1} (Fig. 3.7, curves 2C, 2D and 2E for

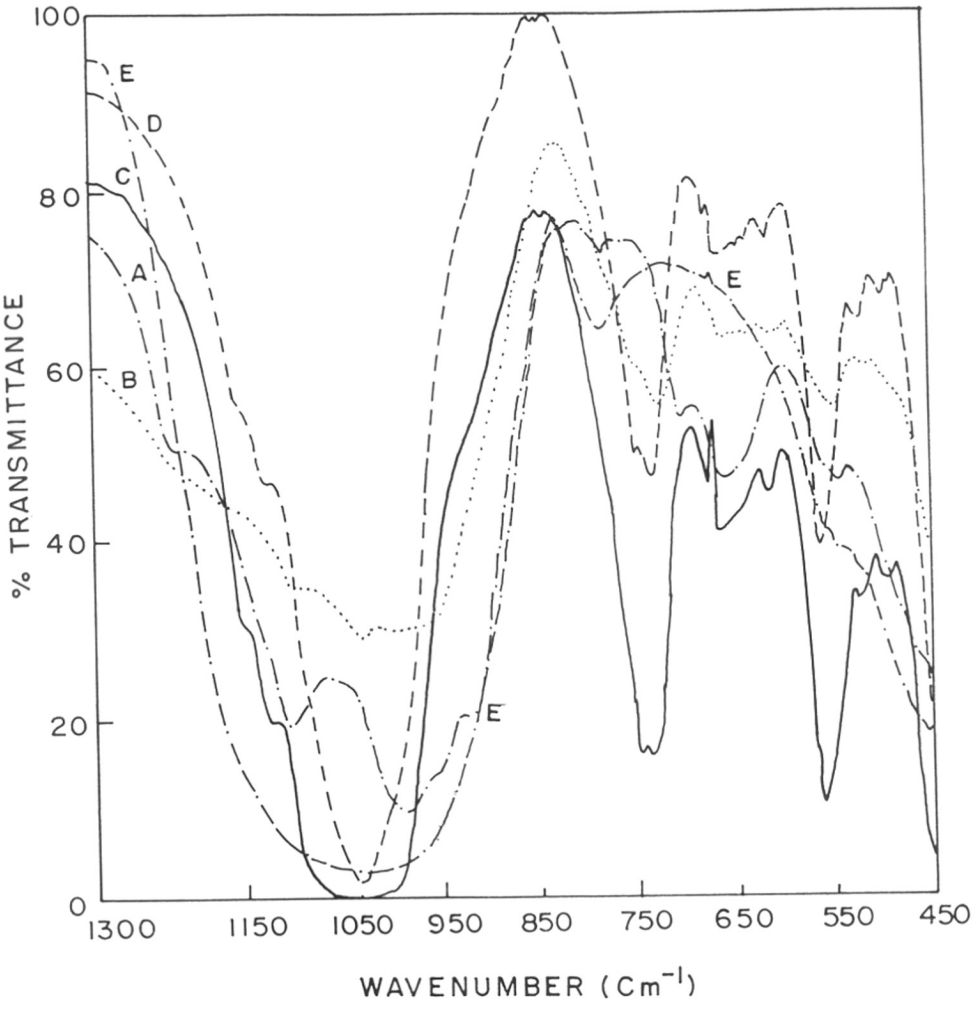

Fig. 3.6 : IR framework vibration spectra of the titanosilicates

A : ETS-4; B : ETS-10(B); C : ETS-10(A), 14.0% seed; D : ETS-10(A), 7.0% seed; E : precursor gel of ETS-10.

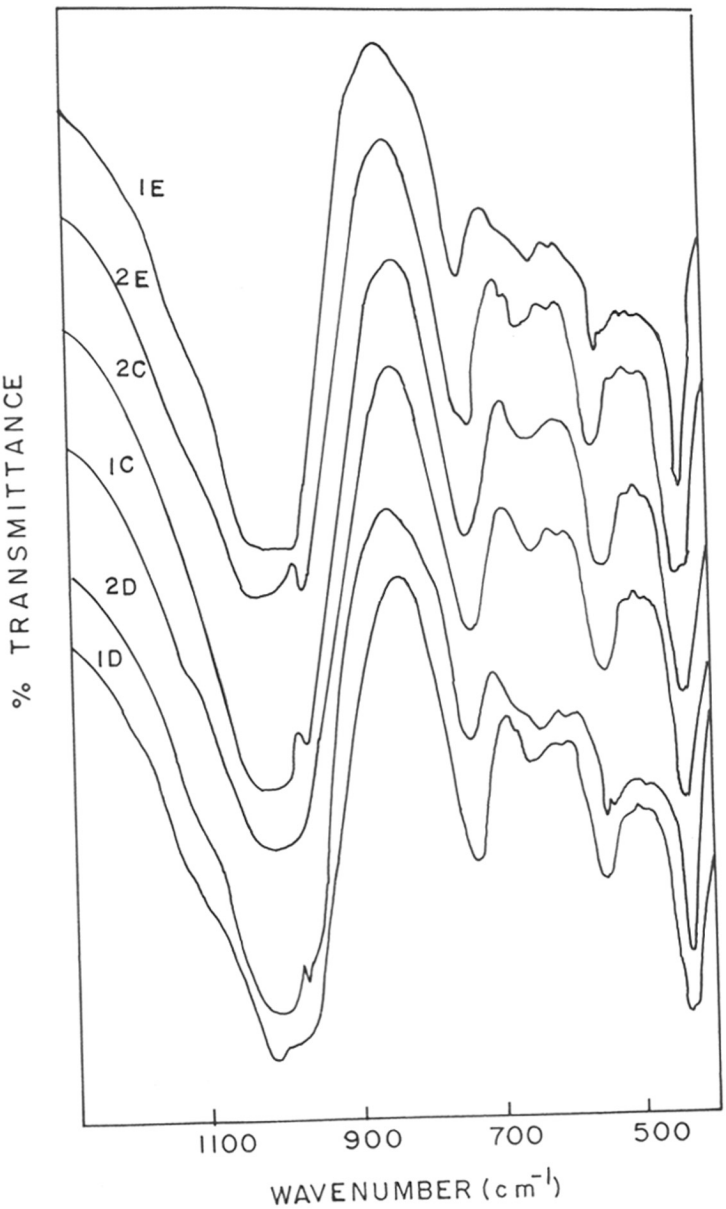

Fig. 3.7 : IR spectra of the titanosilicates. Curves 1C, 1D and 1E refer to the calcined samples of ETS-10(C), ETS-10(D) and ETS-10(E), respectively. Curves 2C, 2D and 2E refer to acid leached samples of ETS-10(C), ETS-10(D) and ETS-10(E), respectively.

ETS-10(C), ETS-10(D) and ETS-10(E), respectively) in the leached samples. A similar observation was made by Khouw and Davis *[13]* in the case of TS-1 samples synthesized in the presence of Na. Though the occurrence of this band in acid-washed samples is surprising, it could be due to -Si-O- vibrations as suggested by Camblor *et al.[14]* in the case of TS-1 and Ti-β.

The IR spectra in the pyridine (1575 - 1425 cm^{-1}) as well as hydroxyl stretching (400 - 3500 cm^{-1}) region are often used to investigate the nature of Brönsted and Lewis acid sites present in various zeolites and/or metal substituted molecular sieves *[15-17]*. The FTIR spectra of surface hydroxyl groups in dehydrated H-ETS-10(A) are shown in Fig. 3.8. The peak around 3735 cm^{-1} is due to isolated terminal silanol groups *[18]*. The sharp peak observed at 3700 cm^{-1} in H-ETS-10 is probably due to isolated Ti-OH groups. The broad band around 3200-3600 cm^{-1} is probably due to H-bonded surface hydroxyl groups of both Si and Ti.

The IR spectra (1750 - 1350 cm^{-1}) of pyridine adsorbed on H-ETS-10 is shown in Figure 3.9. The presence of Lewis and Brönsted acidity is usually determined by the presence of the 1445 and 1545 cm^{-1} bands, respectively. At 473K (Fig. 3.9b), the sample showed an intense band at 1544 cm^{-1} corresponding to Brönsted acidity and a less intense band at 1445 cm^{-1} corresponding to Lewis acidity. The other bands present at 1492, 1576, 1596, 1604 and 1638 cm^{-1} are also assigned to Brönsted and Lewis acid sites *[19]*.

3.3.4 UV-Visible Spectroscopy

The diffuse reflectance spectra in the UV-Visible region of ETS-10(A), ETS-4, ETS-10(B), ETS-10(D), ETS-10(E) and the dried precursor gel are presented in Fig. 3.10 (curves a, b, c, d, e and f, respectively). The broad absorption in the region 250-320 nm suggests the presence of Ti^{4+} in O_h coordination *[20]*.

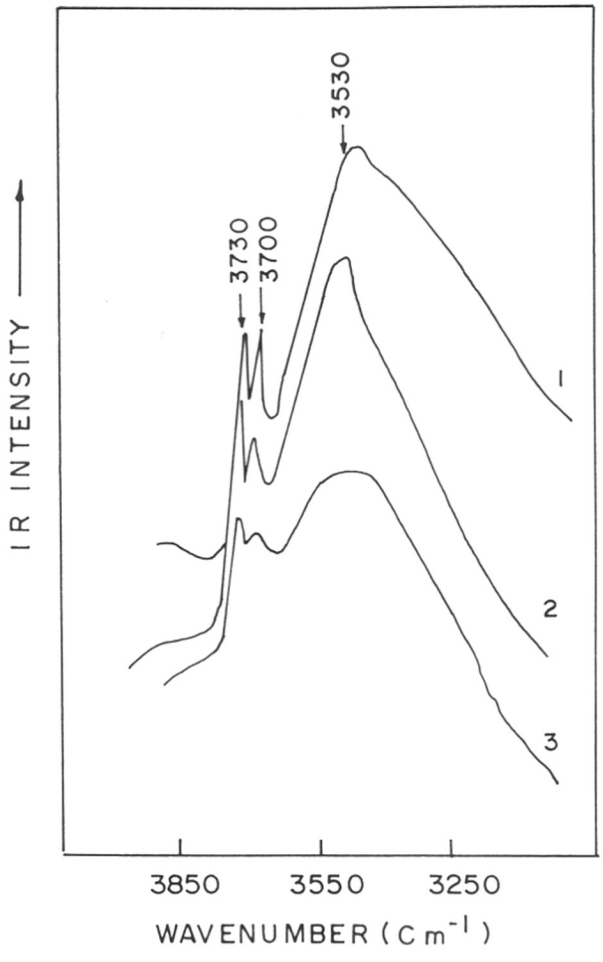

Fig. 3.8 : FTIR spectra of H-ETS-10(A) (seed = 7.0%) recorded at 313K, 373K and 473K (curves 1-3 respectively).

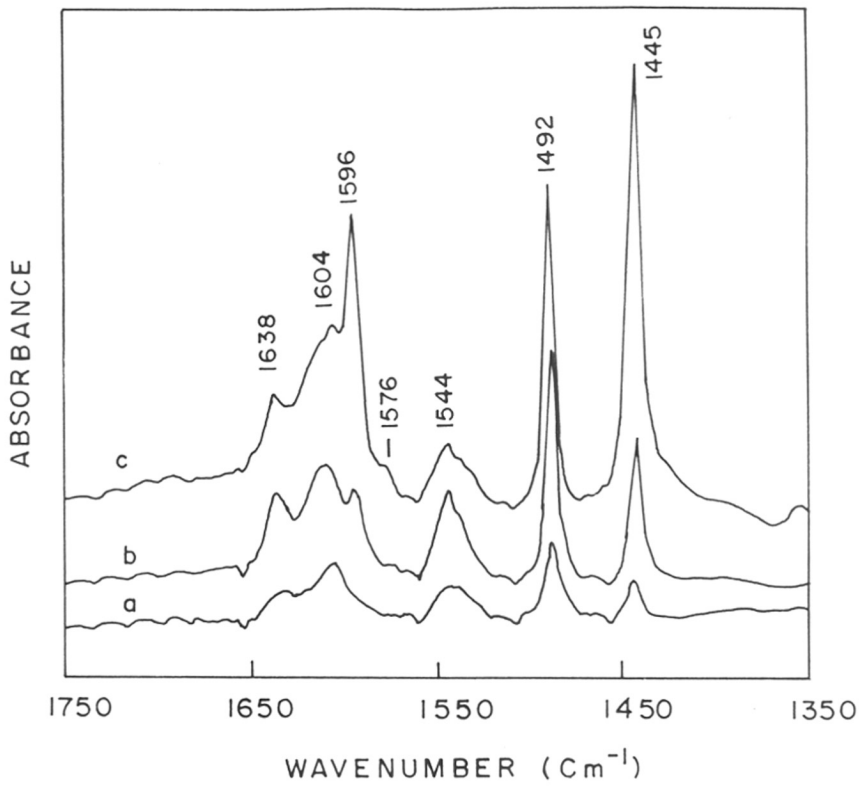

Fig. 3.9 : FTIR spectra of pyridine chemisorbed H-ETS-10(A) after evacuation at (a) 573K, (b) 473K and (c) 373K.

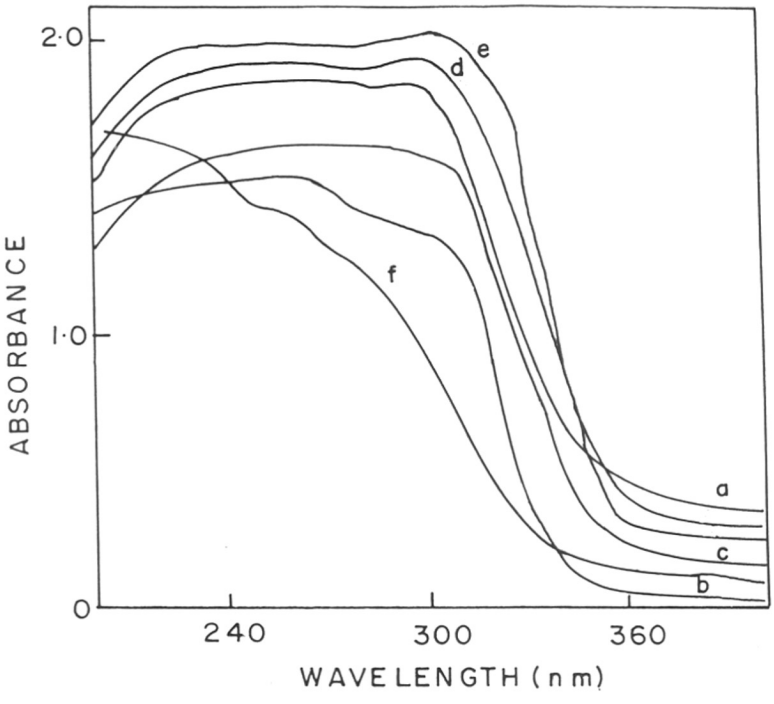

Fig. 3.10 : UV-Vis diffuse reflectance spectra of titanosilicate samples.

(A) : ETS-10(A) (seed = 7.0%); (b) ETS-4; (c) ETS-10(B); (d) ETS-10(D); (e) ETS-10(E) and (f) precursor gel of ETS-10(A) .

3.3.5 Thermal Analysis

The thermal behavior of ETS-4 and different as-synthesized ETS-10 samples are shown in Fig. 3.11A and 3.11B. All the samples exhibited an endotherm at ~393K due to physically sorbed or occluded water. The thermograms of ETS-10(C) and ETS-10(D) resemble the thermogram of the titanosilicate prepared by using TMACl *[21]*. The loss of water occurs up to 533K and is found to be 4.78 wt.% in the case of ETS-10(C), while it is 2.52 wt.% in the case of ETS-10(D). The oxidative decomposition of the templates in the range 533-843K results in a mass loss of 5.53% and 11.87%, respectively, for ETS-10(C) and ETS-10(D) (Fig. 3.11A, curves C and D). The sharp endotherm observed at 948K (Fig. 3.11B, curves C and D) for both ETS-10(C) and ETS-10(D) suggests the phase transformation of these materials.

The thermograms of different alkali metal exchanged ETS-10(E) and La-ETS-10(E) are shown in Figures 3.12A and 3.12B. As the atomic weight of the alkali metal increases from Li to Cs, the thermal stability of the ETS-10(E) samples increases (Fig. 3.12B, curves 2-6). It is noticed that the phase transformation of the Li-ETS-10(E) sample occurs about 923K (Fig. 3.12B, curve 2) whereas it occurs at about 1023K in the case of Cs-ETS-10(E) (Fig. 3.12B, curve 6). The La-ETS-10(E) shows a sharp exotherm at 1053K (Fig. 3.12B, curve 1) suggesting that it is more stable than the others.

3.3.6 Solid State MAS NMR Spectroscopy

The ^{29}Si NMR spectra of ETS-10(A) (Fig. 3.13A) reveal three sharp bands at δ = -94.4(1), -96.8(2) and -103.8(3) ppm, indicating the presence of at least three different Si environments in ETS-10. The weak band at δ = -90.74 ppm (marked by an arrow) is probably due to ETS-4 present as an impurity in the sample, as this band was prominent in the case of pure ETS-4 *[19]*. Further, this band disappeared after calcination at 623K. The

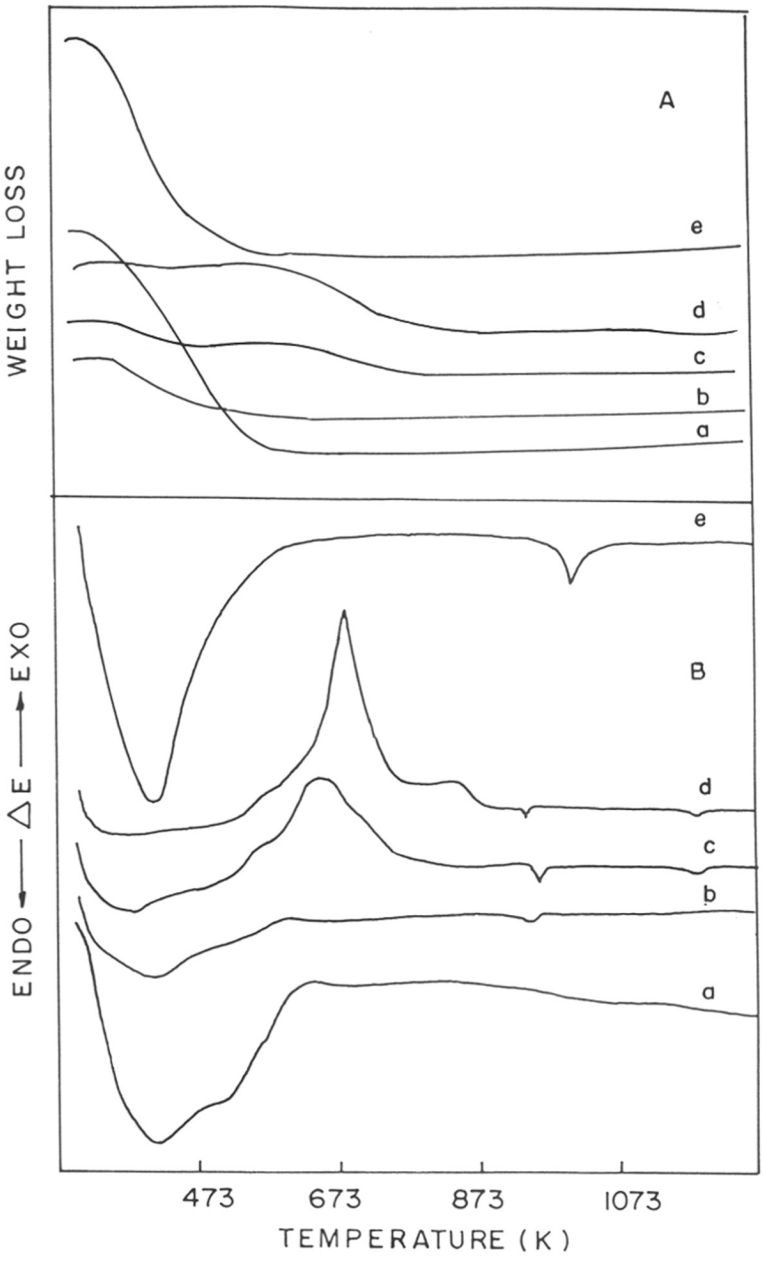

Fig. 3.11 : Thermoanalytical curves of the titanosilicates.

A : Curves a to e; TGA of ETS-4, ETS-10(A), ETS-10(C), ETS-10(D) and ETS-10(E), respectively.

B : Curves a to e; DTA of ETS-4, ETS-10(A), ETS-10(C), ETS-10(D) and ETS-10(E), respectively.

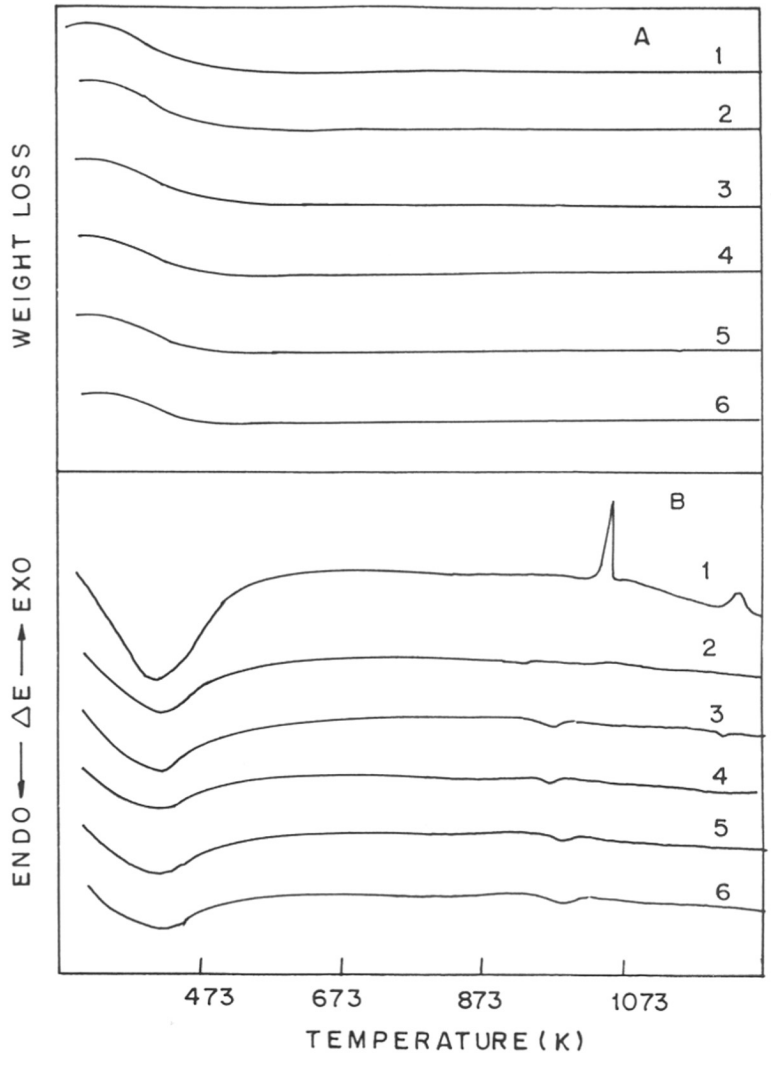

Fig. 3.12 : Thermoanalytical curves of the metal exchanged ETS-10(E) samples.

A : Curves 1 to 6; TGA of La-ETS-10, Li-ETS-10, Na-ETS-10, K-ETS-10, Rb-ETS-10 and Cs-ETS-10, respectively.

B : Curves 1 to 6; DTA of La-ETS-10, Li-ETS-10, Na-ETS-10, K-ETS-10, Rb-ETS-10 and Cs-ETS-10, respectively.

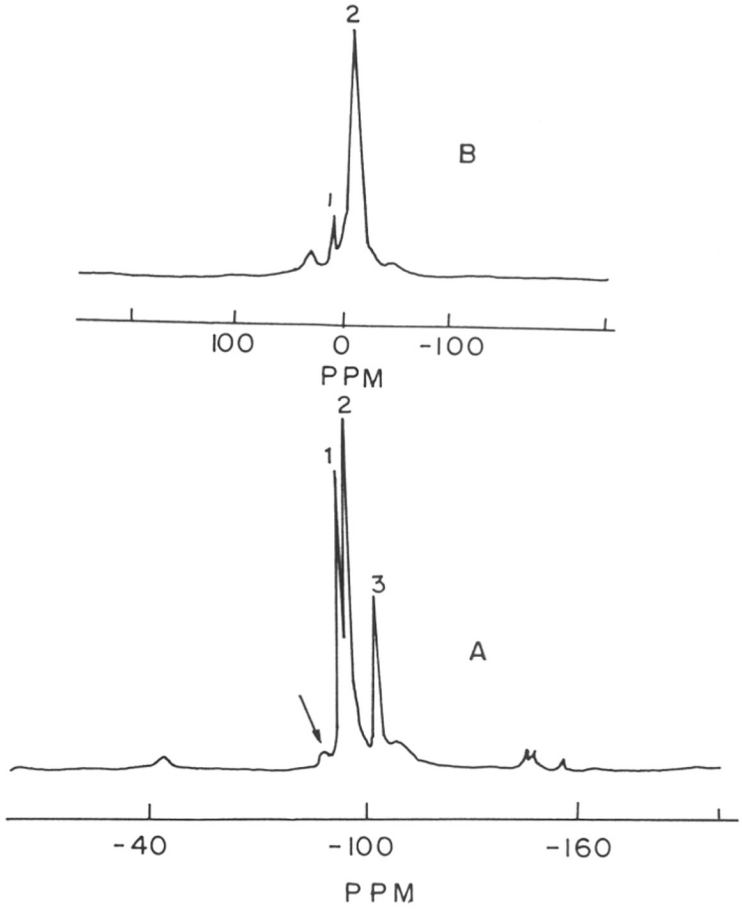

Fig. 3.13 : ^{29}Si and ^{23}Na MAS NMR (curves A and B, respectively) of ETS-10(A) (seed = 7.0%).

^{29}Si NMR spectra of ETS-10(C) and ETS-10(D) before and after calcination are shown in Fig. 3.14(A and B) and Fig. 3.14(C and D), respectively. Three sharp bands at δ = -95.01(1), -98.08(2) and -104.41(3) ppm are observed in the spectrum obtained using a 300 MHz instrument (Fig. 3.14A). These bands are slightly shifted to δ = -95.33(1), -97.50(2) and -104.99(3) ppm (Fig. 3.14B) when the titanosilicate sample is calcined at 723K to remove the organic template. Similarly three sharp bands at δ = -94.69(1), -97.73(2) and -104.01(3) ppm are also observed in ETS-10(D) (Fig. 3.14C). These bands are marginally shifted to δ = -95.06(1), -97.74(2) and -105.43(3) ppm on calcination (Fig. 3.14D). The nature of the spectrum is similar to that of ETS-10(A) *[1]* except for the absence of the weak band reported at δ = -90.74 ppm, which probably was due to ETS-4 impurities. Anderson *et al. [7,8]* have reported a four line spectrum for ETS-10 using an instrument with a higher resolution (400 MHz) and have assigned the lines observed by them at δ = -94.1, -95.8 and -96.5 ppm to Si(3Si, 1Ti) and the line at δ = -103.3 ppm to Si(4Si, 0Ti). Our lines at δ = -95.01 and -98.08 ppm are assigned to Si(3Si, 1Ti) while the line at δ = -104.41 ppm is assigned to Si(4Si, 0Ti).

^{23}Na NMR spectrum of ETS-10(A) (Fig. 3.13B) reveals two resonance bands at δ = 9.17(1) and -9.90(2) ppm corresponding to their presence in two different environments *[22,23]*.

3.3.6.1 ^{29}Si MAS NMR Spectra of ETS-10(E)

The high resolution ^{29}Si MAS NMR spectrum of ETS-10, referenced to tetramethyl silane is shown in Fig. 3.15a. There is a noticeable absence of the signal in the region around 90 ppm which confirms the absence of ETS-4 impurity and also the absence of silicon environment corresponding to Si($2Si_{Td}$, $2Ti_{Oh}$) or the defect sites. Thus, the NMR results also show that the synthesized material exhibits exceptional phase purity with the absence of defect sites.

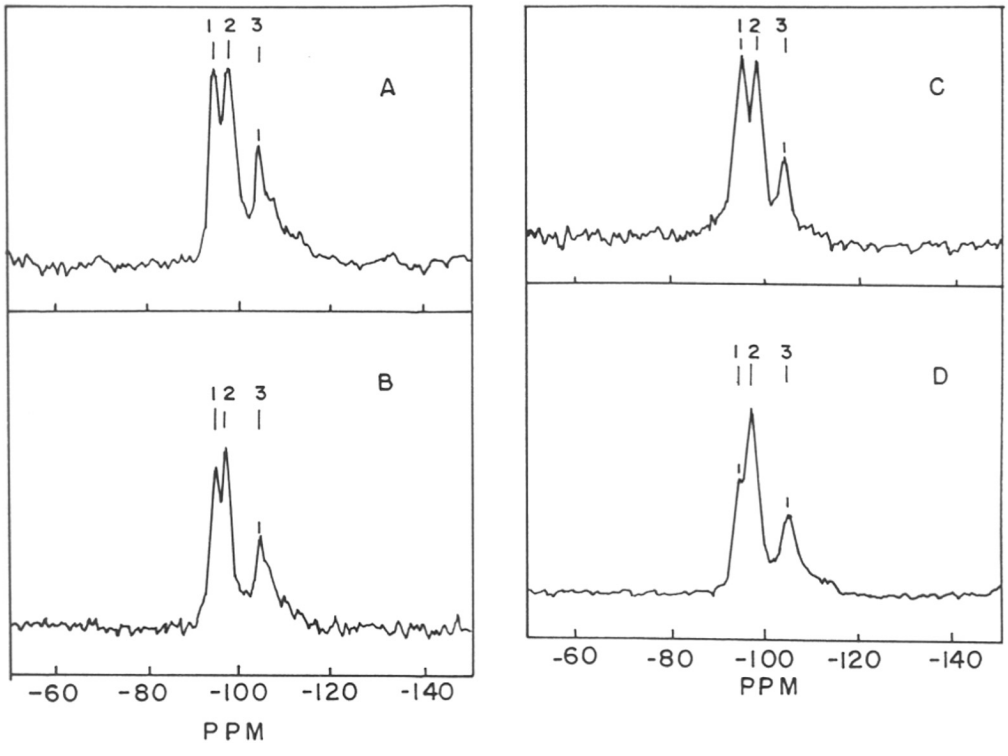

Fig. 3.14 : ^{29}Si MAS NMR spectra of ETS-10(C); A : Before calcination, B : After calcination and ETS-10(D); C : Before calcination, D : After calcination.

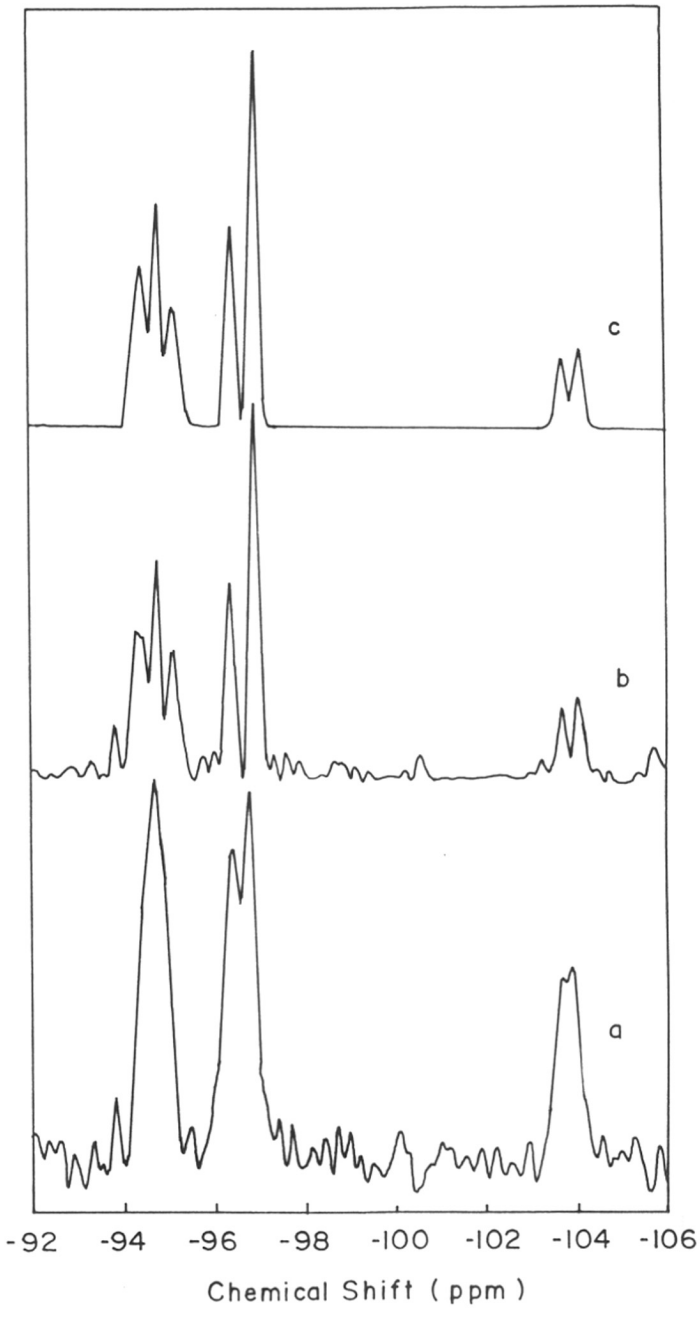

Fig. 3.15 : (a) ^{29}Si MAS NMR spectrum (reference TMS, external) of ETS-10 showing the three distinct resonances corresponding to Si(4Si,0Ti) and Si(3Si, 1Ti).

(b) Resolution enhanced spectrum of (a), exhibiting a seven line pattern.

(c) Simulated spectrum of (b) using Gaussian deconvolution.

As obtained, the spectrum in Fig 3.15a shows that there are three types of silicons. These three types of Si sites show a clear demarcation of the signals into three nonoverlapping regions centered in the range -94 to -95 (Type I), -96 to -97 (Type II) and -103 to -104 ppm (Type III), respectively. A resolution enhancement using a suitable window function was carried out by apodising the time domain NMR data with the UXNMR software package and the enhanced spectral resolution is depicted in Fig. 3.15b. This helps us to visually enhance the apparent spectral resolution and further deconvolute the spectrum into seven resonances as shown in Fig 3.15c, the chemical shifts and peak areas of which can be measured accurately for quantitative analysis. The results are given in Table 3.3. Still the resolution of the spectrum is insufficient to recognize all crystallographically non-equivalent Si-sites, which is attempted by molecular modeling methods (described in a later section).

The approximate ratio of the intensities of the three signals (Type I, II, III Si sites) is 4 : 4 : 2 which is in correspondence with the earlier reports *[7,8]*. There is a distinct correlation between M-O-M angle and chemical shifts *[24]*. The 'M' sites which have the lowest values show the highest chemical shift. The assignment of the lines and M-O-M bond angles and distances are presented in Table 3.1. The resonances in the region of δ = -94.12 to -94.73 ppm and the region of -96.08 to -96.60 ppm correspond to Type I and II silicons sites which are Si(3Si, 1Ti), whereas the signals in the region of -103.55 to -103.86 ppm correspond to Type III silicon sites which are Si(4Si, 0Ti). In ETS-10, among the 11 crystallographically distinct Si sites, Si_1, Si_{10} and Si_{11} are of the type III, namely Si(4Si, 0Ti). Si_1 and Si_{11} have half occupancy compared to the full occupancy of Si_{10}. Each of the two signals of equal intensity of type III Si sites can be assigned to Si_1 + Si_{11} and Si_{10} or vice-versa. This distinction within type III Si sites was not reported earlier presumably due to poor spectral resolution *[7]*. However, we could clearly distinguish two silicon resonances at -103.55 and -103.86 ppm (Fig. 3.15c) with almost 1 : 1 intensity. The exact assignment of

Table 3.3 : Results of the deconvoluted spectra.

Sample; spectrum	Property	Down field shifted Si	Type I			Type II		Type III	
ETS-10; ^{29}Si MAS NMR	Deconvoluted chemical shift value, δ (ppm)	-	-94.12	-94.45	-94.73	-96.08	-96.60	-103.55	-103.86
	Total intensity (%)	-	39.10			41.20		19.70	
	Integrated Area (%)	-	16.70	13.20	9.20	17.60	23.60	10.03	9.67
ETAS-10; Si/Al = 22.4; ^{29}Si MAS NMR	Deconvoluted chemical shift value, δ (ppm)	-89.64	-93.94			-96.19		-103.78	
	Integrated Area (%)	11.29	36.84			40.23		11.62	

these resonances to the silicon sites could be made from the results arising from modeling studies.

The signals due to type I and II Si sites have been classified into four distinct types, namely A, B, C and D by Anderson *et al. [7,8]*. This classification based on their location in a 12-ring or 7-ring becomes ambiguous, because all Si sites have locations common to 12- and 7-rings. From the CG analysis of the topography of these silicon sites, we observe that there are two types of silicons, with respect to their coordination to titanium; Si_2, Si_4, Si_6 and Si_8 are coordinated to Ti_3 whereas Si_3, Si_5, Si_7 and Si_9 silicons are coordinated either to Ti_1 or Ti_2. We believe that these two sets of Si sites are leading to Type I and II.

3.3.6.2 ^{27}Al, ^{29}Si MAS NMR of ETAS-10

The ^{27}Al MAS NMR spectrum of ETAS-10, synthesized with different Si/Al ratios [Si/Al = 62.5, 42.3 and 22.4] are shown in Fig. 3.16(a-c) . Complete tetrahedral framework incorporation of Al at low Al loadings is borne out in Fig. 3.16a by a single resonance at = 57.34 ppm, whereas at the higher Al loadings, the presence of a very small amount of octahedral Al is noticed by the appearance of a weak resonance at ~ 0 ppm (Figs. 3.16b and c). This low intensity signal can be assigned to occluded aluminum in the form of aluminum oxide inside the pores. The ^{27}Al MAS spectra clearly show that framework Al incorporation does occur during the synthesis of aluminium substituted ETS-10 (ETAS-10) and further evidence for the isomorphic substitution of Si by Al in the ETS-10 lattice is provided by ^{29}Si MAS NMR.

There are three distinct signals in the ^{29}Si MAS NMR spectra of ETAS-10 corresponding to three types of Si sites (as discussed for ETS-10) (Fig. 3.17). However, there is a loss in resolution and peak broadening of the silicon resonances shown in Fig. 3.17, compared to that in Fig. 3.15a, due to incorporation of Al in the framework. The increased broadening is attributable to second nearest neighbour effects through the dipolar interactions between the

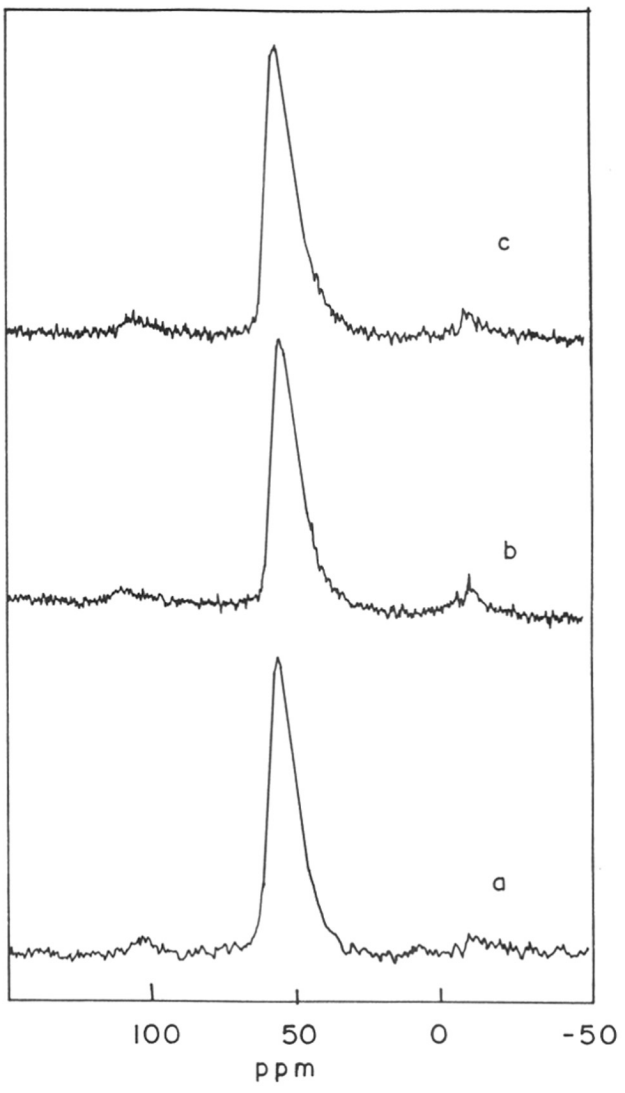

Fig. 3.16 : ^{27}Al MAS NMR spectrum (reference $[Al(H_2O)_6]^{3+}$, external) of ETAS-10 synthesized with different Si/Al (a : 62.5; b : 42.3; c : 22.4)

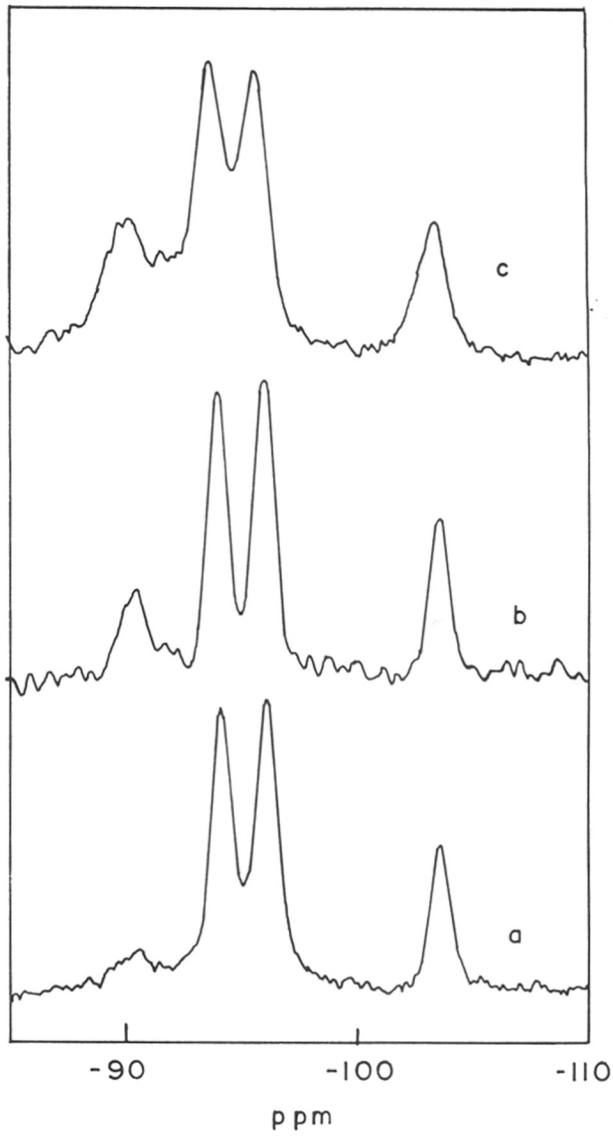

Fig. 3.17 : ^{29}Si MAS NMR spectrum (reference TMS, external) of ETAS-10, showing the additional peak at -89.64 ppm due to the Al substitution at type III silicon, with Si/Al ratio of (a : 62.5; b : 42.3; c : 22.4)

spin 1/2 ^{29}Si nucleus and the spin 5/2 ^{27}Al nucleus, not eliminated in MAS experiments due to non-vanishing electric field gradients at the aluminium sites. Resolution enhancement and deconvolution assuming a Gaussian type peak function were performed with UXNMR software package. The deconvoluted spectrum was simulated and the chemical shift values as well as the areas of these signals were calculated for quantitative analysis (Table 3.3). The overall pattern of the spectrum qualitatively matches with that of ETS-10 as mentioned earlier, except for an additional broad signal at δ = -89.64 ppm, the intensity of which increases with increase in Al. The broad signal occurs at a down field of 4.5 to 5.0 ppm with respect to the signal position of type I Si sites. It is known that Al substitution in various zeolite structures gives rise to a deshielding of ~ 4.0 ppm for Si substitution by one Al *[25]*. This would imply that the new resonance at ~ -89.64 ppm in ETAS-10 samples arises from lattice substitution corresponding to an environment where Si coordinates to titanium. Since this occurs in the neighborhood of a Si[3Si,1Ti] site, Al-Ti avoidance *[26]* and a preferential substitution of Al at the siliceous Si[4Si,0Ti] environments are indicated in these studies. In compliance to this, an increase in intensity of the signal at -89.64 ppm is found to occur at the expense of a decrease in intensity of signals due to type III and I Si sites (Table 3.3). The decrease in the intensity of signal of type III Si sites is due to depletion of these sites by Al incorporation at these sites and the decrease in the intensity of signal of type I is due to a down field shift arising from a coordination to Al.

3.3.7 Molecular Modeling Studies

MNDO (Modified Neglect of Differential Overlap) calculations were performed to compute the energies of substitution of a single aluminum atom in place of silicon in the ETS-10 framework leading to ETAS-10. The preferred site of aluminum substitution and its consequences on the acidic properties of ETAS-10 are also studied. The geometry of cluster

models representing all the 11 Si sites in ETS-10 is derived from (Fig. 3.18) the reported structure of polymorph B (Fig. 3.1). A cluster containing one tetrahedral group, namely $Si(OH)_4$ (denoted as monomer) is considered for studying the electronic properties. The terminal oxygen atoms of the SiO_4 group are bonded to hydrogen atoms to maintain the electrical neutrality of the cluster. The positions of these terminal hydrogen atoms were located at the nearest neighbour M-site (where M = Si or Ti) locations.

It has been shown in the literature *[27]* that there is a qualitative linear correlation between the NMR chemical shifts and the Si-site geometry, namely the average Si-O-Si angle. We derived the Si-O-Si angles for all the 11 sites from the structural report *[7,8]* and plotted them against the experimental chemical shifts. However, when more than one peak could not be deconvoluted, the average Si-O-Si angles were plotted against the chemical shifts as shown in Fig. 3.19. The total energy values for the $Si(OH)_4$ cluster models representing the 11 unique sites were very close. An attempt to correlate the net charge on the central silicon of the $Si(OH)_4$ cluster models for the 11 sites with chemical shift showed a poor correlation. The reason may be the approximate average Si-O bond lengths derived by the DLS refinement in the original structure reports or due to the small size of the cluster models.

A larger pentamer cluster model was generated to study the aluminum substitution process. The pentamer cluster model $\{SiO_4[Si(OH)_3]_4\}$ represents a SiO_4 group which shares a corner with four adjacent SiO_4 groups through bridging oxygen atoms. A typical cluster model representing the crystallographic site Si_{10} is shown in Fig. 3.18. Such pentameric cluster models were generated for the Si sites of type III, namely Si_1, Si_{10} and Si_{11}, since our MAS NMR studies have shown that these are the sites where Al substitution occurs. The process of substitution of aluminum in ETS-10 lattice is considered as follows :

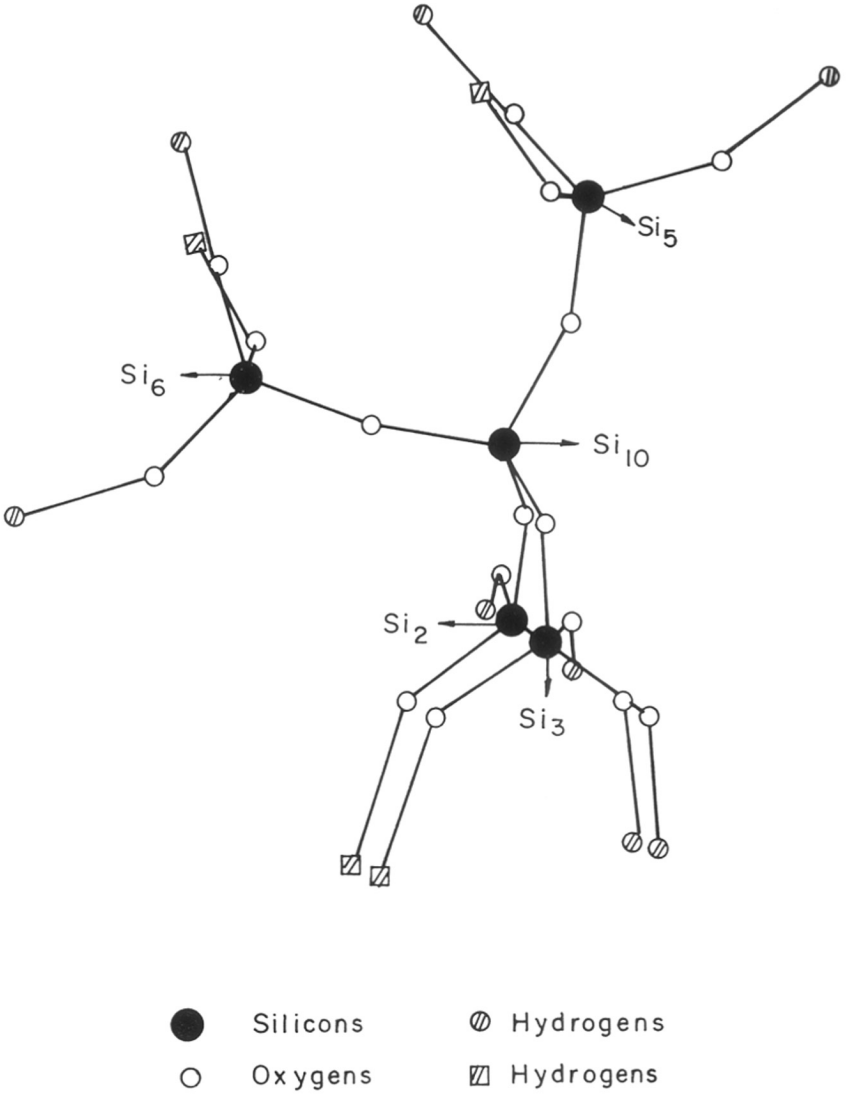

Fig. 3.18 : The local geometry of a typical Si site which is surrounded by 4 other SiO_4 groups.

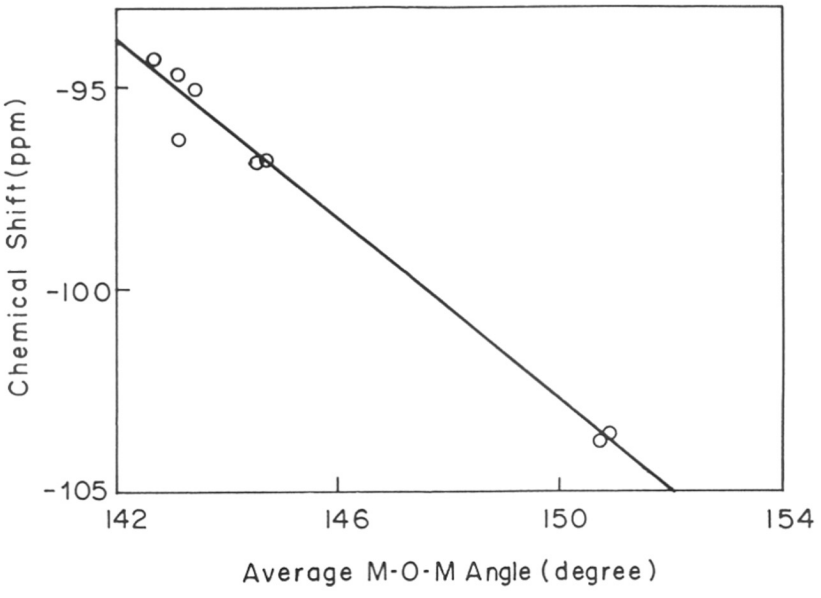

Fig. 3.19 : The correlation between the experimentally derived ^{29}Si MAS chemical shifts versus the M-O-M angles derived from X-ray structure of ETS-10.

$$SiO_4[Si(OH)_3]_4 + [Al(OH)_4]^- \rightarrow AlO_4[Si(OH)_3]^- + Si(OH)_4 \quad \text{---------- (1)}$$

The substitution energy (SE) of aluminum for silicon in the above process is calculated according to the equation :

$$S E = T E_{products} - T E_{reactants} \quad \text{---------- (2)}$$

The acidity is studied by compensating the negative charge in the $AlO_4[Si(OH)_3]_4^-$ cluster by adding a hydrogen to the bridging oxygen between Al and Si. Although there are 4 possible bridging oxygens, the hydrogen is attached to the bridging oxygen which is facing the large 12-member ring of the ETS-10 lattice. The binding energy of the proton (BE_H) is calculated by considering the following process :

$$AlO_4H[Si(OH)_3]_4 \rightarrow AlO_4[Si(OH)_3]_4^- + H^+ \quad \text{---------- (3)}$$

and the following relation :

$$BE_H = TE \text{ of } AlO_4H[Si(OH)_3]_4 - TE \text{ of } AlO_4[Si(OH)_3]_4^- \quad \text{---------- (4)}$$

The cluster site, the cluster model and total energy of the clusters are given in Table 3.4. The substitution energy evaluated according to equation (2) for the process (1) at the three possible sites are also given in Table 3.4. The substitution energy of aluminum at the Si_{10} site is the most favorable and hence preferential substitution at Si_{10} is expected. When Si_{10} is substituted by aluminum, the adjacent silicons to Si_{10}, which are Si_2, Si_3, Si_5 and Si_6 are expected to undergo a downfield shift by 4 ppm. Hence, the downfield shift of silicons of type I observed in Fig. 3.17 is understandable. Thus our calculations indicate that Al substitution occurs at Si_{10} site. It appears that the adjacent silicon sites of Si_{10}, could be assigned to type I silicons, namely Si_2, Si_3, Si_5 and Si_6 whose resonances are in the region -94.12 to -94.73 ppm. Therefore, the resonances of type II silicons could be assigned to Si_4,

Table 3.4 : Cluster site, cluster model, total energy, relative aluminum substitution energy and relative proton binding energy.

Cluster site	Cluster Model	Total energy (eV)	Relative aluminum substitution energy (eV)	Relative proton binding energy (eV)
1	$Si(OH)_4$	-3816.80	-	-
10	$Si(OH)_4$	-3815.22	-	-
11	$Si(OH)_4$	-3813.56	-	-
1	$[Al(OH)_4]^-$	-3562.40	-	-
10	$[Al(OH)_4]^-$	-3560.86	-	-
11	$[Al(OH)_4]^-$	-3559.23	-	-
1	$SiO_4[Si(OH)_3]_4$	-5724.73	-	-
10	$SiO_4[Si(OH)_3]_4$	-5724.45	-	-
11	$SiO_4[Si(OH)_3]_4$	5724.20	-	-
1	$AlO_4[Si(OH)_3]_4^-$	-5682.55	-0.15	-0.31
10	$AlO_4[Si(OH)_3]_4^-$	-5682.85	-0.69	0.00
11	$AlO_4[Si(OH)_3]_4^-$	-5681.94	0.00	-0.69

Si_7, Si_8 and Si_9 atoms. The assignment is further testified from the plot of chemical shift Vs M-O-M angle as shown in Fig. 3.19, which shows an almost linear variation. There are slight deviations as we have not considered the influence of other geometrical parameters such as M-O distances, O-M-O angles and O-M-O-M dihedral angles. These assignments of silicon sites based on quantum chemical calculations are qualitatively comparable with the empirical assignment derived from the M-O-M angles. However, it must be noted that the signals for the 8 silicons of type I and type II lie in a short interval between -94.12 to -96.60 ppm.

Proton compensating the anionic framework charge due to aluminum substitution impart Bronsted acidity. The binding strength of protons to the oxygen atoms bridging silicon and aluminum is an indication of the acid strength. We have evaluated the acidity of protons bonded to different oxygen sites, by calculating the proton binding energy according to equation 4. It is observed that the site where the most facile substitution of aluminum occurs, namely Si_{10} creates the stronger acidity. As predicted by the proton binding energy, the proton is weakly bound, when Al substitutes Si_{10} (Table 3.4).

3.3.8 Scanning Electron Microscopy

The SEM photographs of ETS-4, ETS-10(A) and ETS-10(B) were discussed in Chapter II (Figs. 2.5 and 2.6). SEM photographs of the titanosilicates [ETS-10(C) and ETS-10(D)] crystallized in the presence of choline chloride and hexaethyl diquat-5 are shown in Figures 3.20A and 3.20B, respectively. Agglomerates of cuboidal crystals (< 0.5 μm) with a few cuboidal growing clusters (2-4 μm) are seen in Fig. 3.20A [ETS-10(C)] and wheat shaped polycrystallites (2-4 μm) are seen in Fig. 3.20B [ETS-10(D)]. This shows that the nature of the organic template used during the crystallization of the titanosilicate has a

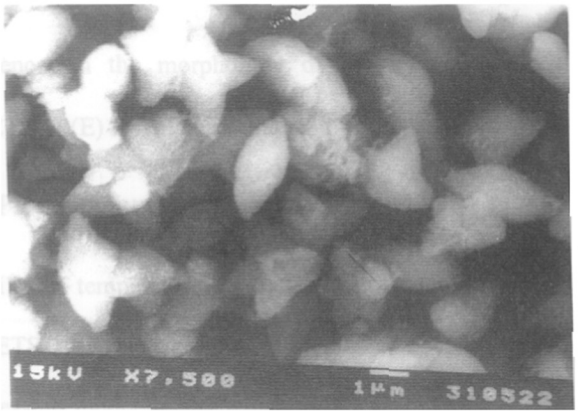

A

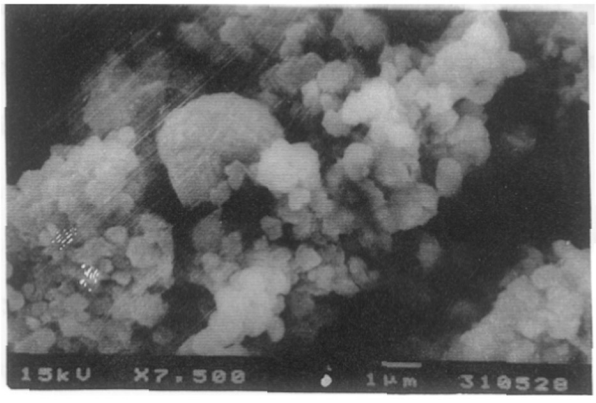

B

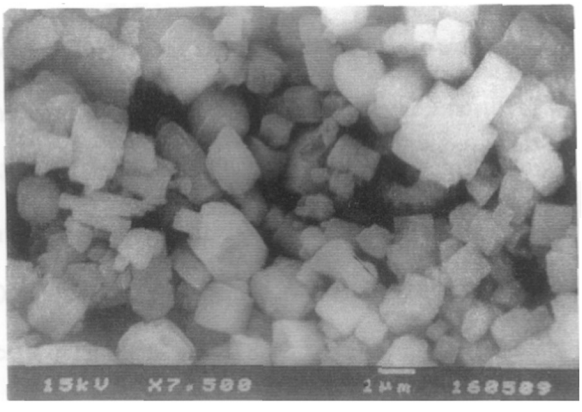

C

Fig. 3.20 : SEM photographs of different titanosilicates.

A : ETS-10(C), B : ETS-10(D) and C : ETS-10(E).

significant influence on the morphology of the ETS-10 crystals. Scanning electron micrographs of ETS-10(E) revealed an almost uniform particle size of ~1 μm (Fig. 3.20C).

3.3.9 NH_3-TPD Measurements

The profiles of temperature programmed desorption of NH_3 obtained over H-ETS-10(E) and Pt-H-ETS-10(E) are presented in Fig. 3.21. The profiles indicate that the acid sites are mostly of weak to moderate strength. Nearly all the NH_3 is desorbed below 623K, the peak maximum occurring around 400-420K. In comparison, strongly acidic zeolites such as H-ZSM-5 continue to desorb NH_3 beyond 733K with a distinct peak maximum for strong acid sites occurring around 670K *[28]*.

The NH_3-TPD spectra of the M-ETS-10 samples are presented in Fig. 3.22. The areas of the peaks (on constant weight basis) decrease in the order : Li-ETS-10 > Na-ETS-10 > Ba-ETS-10 > K-ETS-10 > Rb-ETS-10 > Cs-ETS-10. The decrease noticed is actually an artifact of the increasing atomic weight of the exchanged ions (Li to Cs) and the corresponding decrease in the actual molecular sieve component. As a result, when the areas are compared at constant unit cell content of the samples, all the values match within ± 2%. The desorption profiles of all the samples indicate that the acid sites are mostly of weak to moderate nature. Nearly all the NH_3 is found to desorb from the samples well below 600K, the peak maxima for the different samples being in the range 370-470K. Based on the peak maxima, the alkaline ETS-10 samples can be arranged in the following order of acid strengths : Li-ETS-10 $\simeq$ Na-ETS-10 > K-ETS-10 > Rb-ETS-10 > Cs-ETS-10. The above order is exactly as expected; the substitution by more alkaline (electro-positive) metal decreases the acidity to a larger extent.

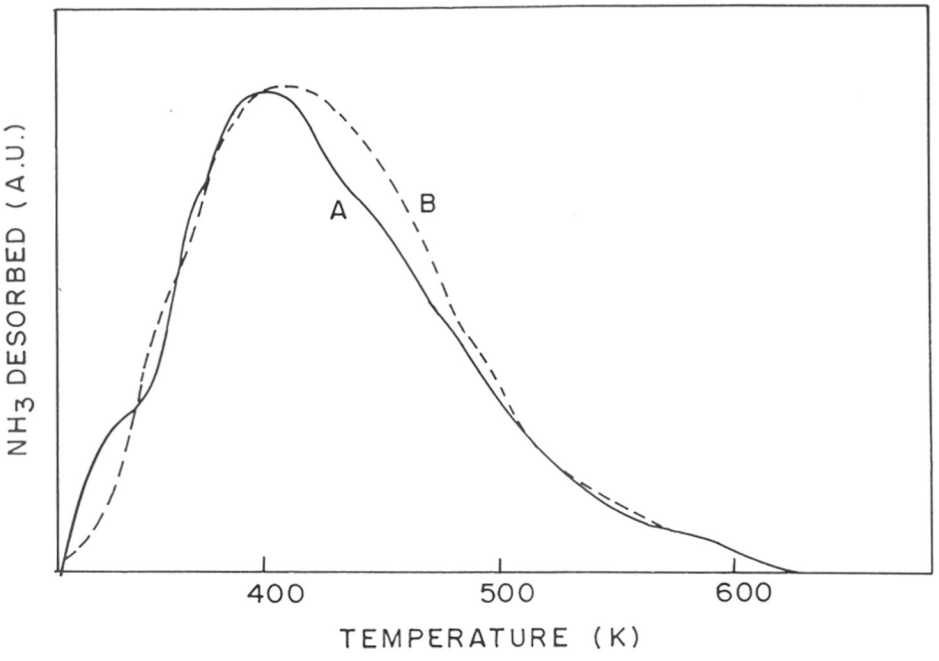

Fig. 3.21 : Temperature-programmed desorption of NH_3.

A : H-ETS-10(E), B : Pt(0.3%)-H-ETS-10(E).

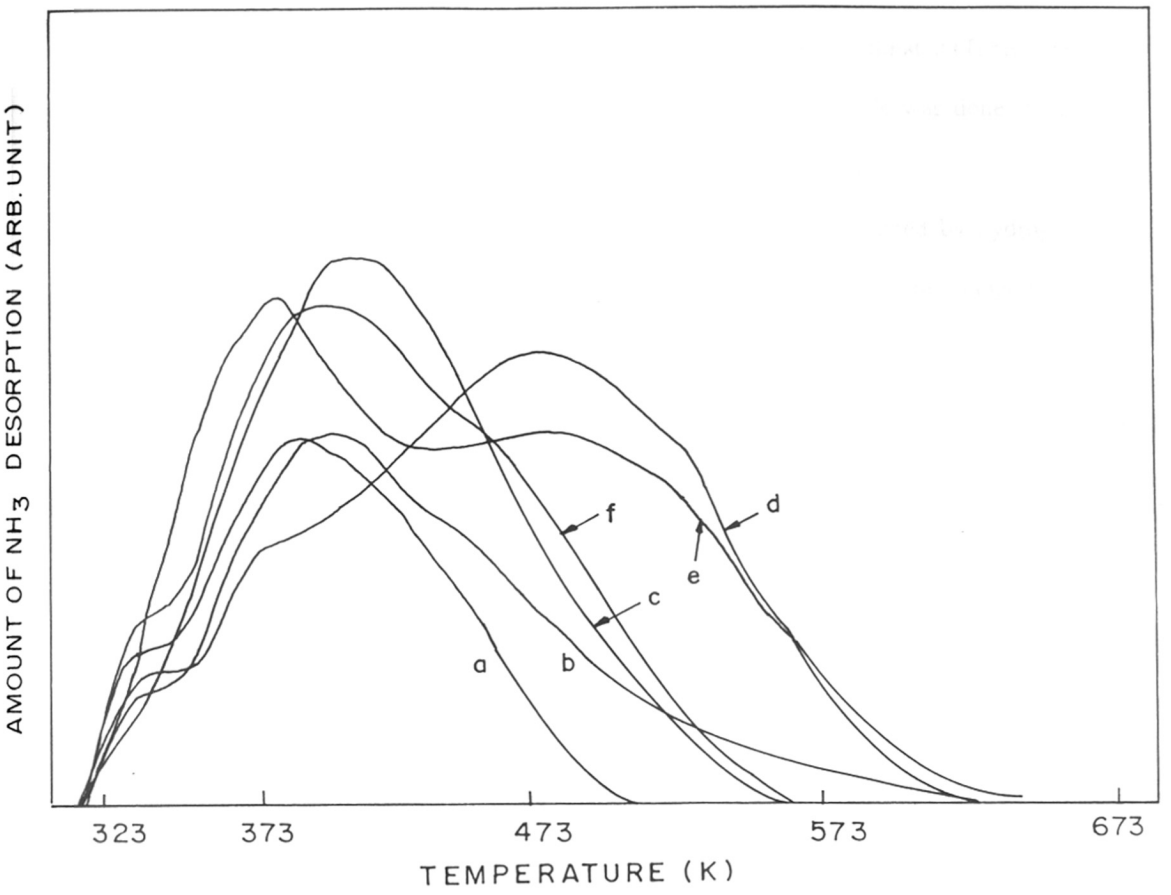

Fig. 3.22 : Temperature-programmed desorption of NH_3.

a : Cs-ETS-10(E), b : Rb-ETS-10(E), c : K-ETS-10(E), d : Na-ETS-10(E), e : Li-ETS-10(E) and f : Ba-ETS-10(E).

3.3.10 Pt-dispersion by H_2 Chemisorption

Pt-dispersion measurements were carried out on a 0.5 wt.% H-ETS-10(E) sample by H_2 adsorption at ambient temperature *[9]*. A Pt-dispersion of 72% was estimated (Table 3.5). The above value is probably low as the degassing of the reduced sample was done at the relatively low temperature of 598K to prevent structural damage to ETS-10.

The Pt dispersion values of different M-ETS-10 samples determined by hydrogen chemisorption are also presented Table 3.5. The dispersion values for the samples range from 45% to 85%, the values being higher for the more basic samples.

Table 3.5 Platinum dispersion of Pt-ETS-10 samples.

Sample	Dispersion D (H/Pt)[a]
Li-ETS-10(E)	0.45
Na-ETS-10(E)	0.52
K--ETS-10(E)	0.49
Rb-ETS-10(E)	0.62
Cs-ETS-10(E)	0.73
Ba-ETS-10(E)	0.85
H-ETS-10(E)	0.72

[a]Pt-content was 0.4 wt.% for Li, Na, K and Rb-ETS-10 and 0.5 wt.% for Cs-, Ba- and H-ETS-10 samples.

3.4 REFERENCES

1. Das, T.K., Chandwadkar, A.J., Budhkar, A.P., Belhekar, A.A., and Sivasanker, S., *Microporous Mater.*, **4**, 195 (1995).
2. Das, T.K., Chandwadkar, A.J., Budhkar, A.P., and Sivasanker, S., *Microporous Mater.*, **5**, 401 (1996).
3. Das, T.K., Chandwadkar, A.J., and Sivasanker, S., *Mater. Res. Bull.*, **17**, 1143 (1994).
4. Das, T.K., Chandwadkar, A.J., and Sivasanker, S., *J. Mol. Catal.*, **107**, 199 (1996).
5. Das, T.K., Chandwadkar, A.J., and Sivasanker, S., *J. Chem. Soc. Chem. Commun.*, 1105 (1996).
6. Vogel, A.I., "Text Book of Quantitative Inorganic Analysis including Elementary Instrumental Analysis" London, (1961).
7. Anderson, M.W., Terasaki, O., Ohsuna, T., Philippou, A., Mackay, S.P., Ferreira, A., Rocha, J., and Lidin, S., *Nature*, **367**, 347 (1994).
8. Anderson, M.W., Tarasaki, O., Ohuna, T., Malley, P.J.O., Philippou, A., Mackay, S.P., Ferreira, A., Rocha, J., and Lidin, S., *Philos. Mag. B*, **71**, 813 (1995).
9. Smirniotis, P.G., and Ruckenstein, E., *Appl. Catal.*, **123**, 59 (1995).
10. Valtchev, V., and Mintova, S., *Zeolites*, **14**, 697 (1994).
11. Mihailova, B., Valtchev, V., Mintova, S., and Konstantinov, L., *Zeolites*, **16**, 22 (1996).
12. Flaniger, E.M., and Katami, H., *Molecular Sieve Zeolites, I, Adv. Chem. Ser.*, **101**, 201 (1971).
13. Khouw, C.B., and Davis, M.E., *J. Catal.*, **151**, 77 (1995).
14. Camblor, M.A., Corma, A., and Perrez-Pariente, J., *J. Chem. Soc. Chem. Commun.*, 1557 (1993).
15. Jacobs, P.A., "Carboniogenic Activity of Zeolite" Elsevier, Amsterdam, p. 2 (1977).
16. Rabo, J.A., Zeolite Chemistry and Catalysis, Am. Chem. Soc., ACS Monograph, p. 171 (1979).
17. Dzwigaj, S., Briend, M., Shikholeslami, A., Peltre, M.J., and Barthomeauf, D., *Zeolites*,

10, 157 (1990).

18. Chandwadkar, A.J., Abdulla, R.A., Hegde, S.G., and Nagy, J.B., *Zeolites,* **13**, 470 (1993)

19. Deeba, M., Keweshan, C.F., Koermer, G.S., Kuznicki, S.M., and Madon, R.S., in M. Dekker (Ed.) "Catalysis of Organic Reactions", 383, (1994).

20. Jacobs, P.A., *DGMK Tagenbericht,* **171**, 9204 (1992).

21. Valtchev, V., *J. Chem. Soc. Chem. Commun.,* 261 (1994).

22. Yang, X., and Blosser, P.W., *Zeolites*, **17**, 237 (1996).

23. Sankar, G., Bell, P.G., Thomas, J.M., Anderson, M.W., Wright, P.A., and Rocha, J., *J. Phys. Chem.*, **100**, 449 (1996).

24. Fyfe, C.A., Grondey, H., Feng, Y., and Kokotailo, T., *J. Am. Chem. Soc.*, **112**, 8812 (1990).

25. Engelhardt, G., and Michel, D., "High Resolution Solid State NMR of Silicates and Zeolites", (John Wiley, New York) (1987).

26. Anderson, M.W.; Philippou, A.; Lin, Z.; Ferreira, A.; and Rocha, J., *Angew. Chem. Int. Ed. Engl.*, **34**, 1003 (1995).

27. Sivadinarayana, C., Ganapathy, S., and Choudhary, V.R., *Proceedings of Indian Academic of Science*, **106**, 1557 (1996).

28. Ratanasamy, P., Borade, R.B., Sivasanker, S., Shiralkar, V.P., and Hegde, S.G., *Acta Phys. Chem.*, **31**, 137 (1985).

CHAPTER IV

SORPTION PROPERTIES OF ETS-10

4.1 INTRODUCTION

The ability of molecular sieves to sorb molecules has been utilized extensively in characterizing them. From an examination of the adsorption properties, substantial structural information can be discerned about molecular sieve materials. The most fundamental characteristic is the pore volume of the individual molecular sieve. Several probe molecules such as oxygen, n-hexane and water have been routinely used to determine the pore volume.

The sorption of nitrogen or argon at liquid nitrogen temperature and fitting the results obtained into the BET equation yields the surface area of the zeolites. Sorption capacities for probe molecules such as water, n-hexane, xylenes and 1,3,5-trimethylbenzene yield information about the hydrophilicity/hydrophobicity, pore dimensions and pore volume of the zeolites. The application of various isotherm equations such as Langmuir, BET, Dubinin-Radushkevich and Sips equations to experimental isotherms could be combined with other statistical models to obtain information about the sorption characteristics of zeolites *[1-7]*. Study of the sorption properties of zeolites is not only scientifically interesting, it can also lead to innovative separation technologies. For example, the Parex process *[8]* used to separate p- and m-xylenes is based on Faujasite adsorbents. Other examples of the use of molecular sieves in separation technology are the separation of O_2 and N_2 in air and the separation of n-paraffins from the other components in kerosene.

The characterization of ETS-10 samples using various physico-chemical techniques *[9-13]* was discussed in Chapter III. In the present chapter, the sorption properties of ETS-10 are reported. Sorption of probe molecules such as water, n-hexane and 1,3,5-trimethylbenzene was carried out over ETS-10 samples. Surface areas of the samples were determined by nitrogen sorption at liquid nitrogen temperature. Sorption isotherms of water, m-xylene and p-xylene were obtained up to 7.0 Torr in the temperature range of 298K to

393K for water and 298K to 453K for xylenes. The results were fitted into different models and thermodynamic entities such as chemical affinity and isosteric heats of sorption were determined.

4.2 EXPERIMENTAL

4.2.1 Surface area Measurements

Nitrogen adsorption measurements were carried out using a commercial volumetric adsorption apparatus (Omnisorp 100CX, Coulter Corporation, USA) to determine the surface area. Approximately 200 mg of the calcined sample was degassed at 673K for 5 hours at 10^{-5} Torr prior to surface area measurements. The samples were then cooled to 77K using liquid nitrogen and the sorption of nitrogen was carried out. The results were fitted into the BET equation to obtain the surface areas. Anhydrous weights of the samples were used in the surface area calculations.

4.2.2 Adsorption Measurements

The adsorption measurements for water, n-hexane and 1,3,5 trimethylbenzene were carried out gravimetrically in a recording electrobalance (Cahn Instruments, USA) at p/p_o = 0.5 for 2 h at 298K. The titanosilicate sample (40 mg) was pressed into a small pellet and weighed into the aluminum bucket. The system was connected to high vacuum and the sample was activated in vacuum (10^{-5} Torr) at 673K for 4 hours. The sample was then cooled to the desired temperature under high vacuum. The sorbate vapours were admitted into the sample at a constant pressure and temperature and the weight gained was recorded continuously as a function of time. After completion of the experiment, the sample was evacuated and heated to 673K at 10^{-5} Torr and used for the next measurement.

4.2.3 Adsorption Isotherms

The sorption isotherms were obtained using an all-glass gravimetric apparatus, *viz.*, McBain-Baker type silica spring (sensitivity ≈ 70 cm/g) balance. About 40 mg of the sample was used in a pellet form. The spring was kept at a constant temperature (± 3K) by a jacket through which water at a constant temperature was circulated. Prior to the adsorption measurements, the titanosilicate sample was degassed at 673K. The temperature of the sample was raised at the rate of 2K min^{-1} with simultaneous evacuation at 10^{-5} Torr. After activation, the balance case containing the sample was maintained at an isothermal temperature for at least 2h before the commencement of the measurements. The sorption isotherms were obtained in the temperature range of 298K to 393K at ~30 degree intervals for water and in the range of 298K to 453K at ~50 degree intervals for m-xylene and p-xylene. The amount sorbed was measured from the change in weight of the sample after equilibration for 2h at each pressure.

4.3 RESULTS AND DISCUSSION

4.3.1 Surface area Measurements

N_2 -adsorption isotherms of all the samples were typically Type I curves. The surface areas and pore volumes of ETS-10 samples are presented in Table 4.1. ETS-10(E) possesses maximum surface area and pore volume suggesting the least pore blockage. X-ray powder diffraction shows the highest crystallinity for this sample. The surface areas of the alkali metal exchanged ETS-10 samples increased marginally from Li to K and then decreased from K to Cs. The increase in surface area from Li to K may be due to good charge compensation

Table 4.1 : Sorption of probe molecules and BET surface areas of ETS-10 samples.

Sample	[a]Sorption capacity (mass%)			[b]S_{BET} (m^2/g)	Pore volume (ml/g)
	Water	n-Hexane	1,3,5-TMB[c]		
ETS-4	11.1	0.6	Nil	#	#
ETS-10(A)	16.1	10.6	10.6	361	0.11
ETS-10(B)	13.1	7.3	6.2	340	0.10
ETS-10(C)	15.2	9.4	9.0	350	0.12
ETS-10(D)	16.2	11.8	10.4	365	0.14
ETS-10(E)	17.0	12.1	11.2	410	0.16
Li-ETS-10(E)	16.9	12.3	#	358	0.14
Na-ETS-10(E)	16.8	12.0	#	383	0.13
K-ETS-10(E)	16.9	11.9	#	395	0.13
Rb-ETS-10(E)	16.2	11.5	#	325	0.12
Cs-ETS-10(E)	16.0	11.3	#	270	0.10

[a]Sorption capacity measurements were carried out at 298K at $P/P_o = 0.5$

[b]S_{BET} = Sorption of nitrogen at liquid nitrogen temperature.

[c]TMB = 1,3,5-trimethylbenzene

= Not measured

by Na^+ and K^+. The decrease in surface area (per gram) from K to Cs is mainly due to the increase in cation mass. The pore volumes of all the ETS-10 samples are found to range from 0.1 to 0.16 ml/g. These values are similar to those reported by Kuznicki *[14]*.

4.3.2 Adsorption of Probe Molecules

The sorption capacity of ETS-10 samples was measured using H_2O (kinetic diameter 2.65 Å), n-hexane (4.3 Å) and 1,3,5-trimethylbenzene (8.1 Å). The quantity adsorbed as a function of time at 298K at $p/p_o = 0.5$ are presented in Figure 4.1 for all the probe molecules (Table 4.1). ETS-10(B) and ETS-10(C) had the lowest equilibrium sorption capacities for all the probe molecules. This is probably due to the presence of amorphous material and impurity phases (seen in XRD, $2\theta = 21.8°$ for ETS-10(C), discussed in Chapter II). ETS-10(E) has the highest sorption capacity for all the three probe molecules indicating it to be highly crystalline, without impurity and amorphous phases.

4.3.3 Adsorption Isotherms

The sorption capacities usually depend on the size of the probe molecules, the zeolitic void volume, the geometry of the cages and packing geometry/efficiency. Cation exchanged molecular sieves possess a wide distribution of sorption centers and hence offer a heterogeneous surface for sorption. The surface field depends upon the ionic radii, the ionic charge and the distribution of these ions. Simultaneously the polarity and polarizability of the adsorbate molecules constitute the counterpart of the adsorption system. The relevant cation radii *[15]* are tabulated below:

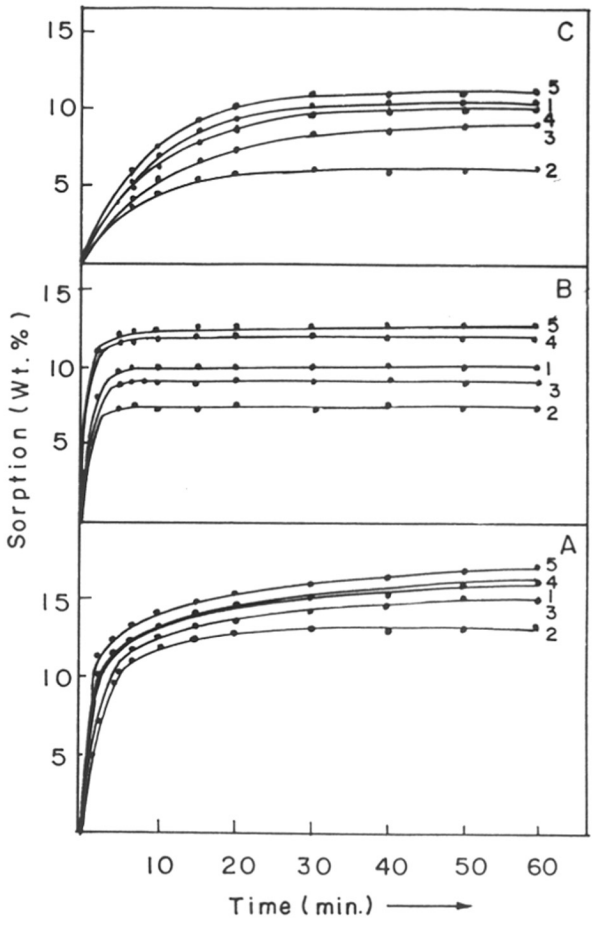

Fig. 4.1 : Sorption kinetics of probe molecules.

Curves 1-5 corresponding to ETS-10(A), ETS-10(B), ETS-10(C), ETS-10(D) and ETS-10(E), respectively.

A : water; B : n-hexane; C : 1,3,5-trimethylbenzene

Cation	Ionic radius (Å)
Li	0.60
Na	0.95
K	1.33
Rb	1.48
Cs	1.69

Polar water molecules, being sufficiently small in size (kinetic diameter 2.65 Å) penetrate almost all the cages in the zeolitic lattice and assume close packing in interaction with extra-framework cations. The equilibrium sorption capacity is usually regarded as an indication of the hydrophilic/hydrophobic character of the zeolitic (molecular sieve) framework.

Adsorption isotherms of water, m-xylene and p-xylene obtained at different temperatures over different alkali metal exchanged ETS-10(E) are presented in Figures 4.2 to 4.4. The shape of the isotherms in all the cases was found to be similar to Type 1 (Langmuir type) according to Kiselev's *[16]* classification. Obviously, the smallest probe molecule water (kinetic diameter 2.6 Å) is sorbed the most. The values obtained for m-xylene and p-xylene are almost equivalent in spite of the difference in their kinetic diameter (7.4 Å and 6.7 Å, respectively). It can be seen from the isotherms that ~80% of the total sorption takes place even at 0.2 Torr for m-xylene and p-xylene, and at 2 Torr for water. The equilibrium sorption capacities (molecules/U.C.) of water, m-xylene and p-xylene estimated from the adsorption isotherms decrease with an increase in the ionic radii of the exchanged ion.

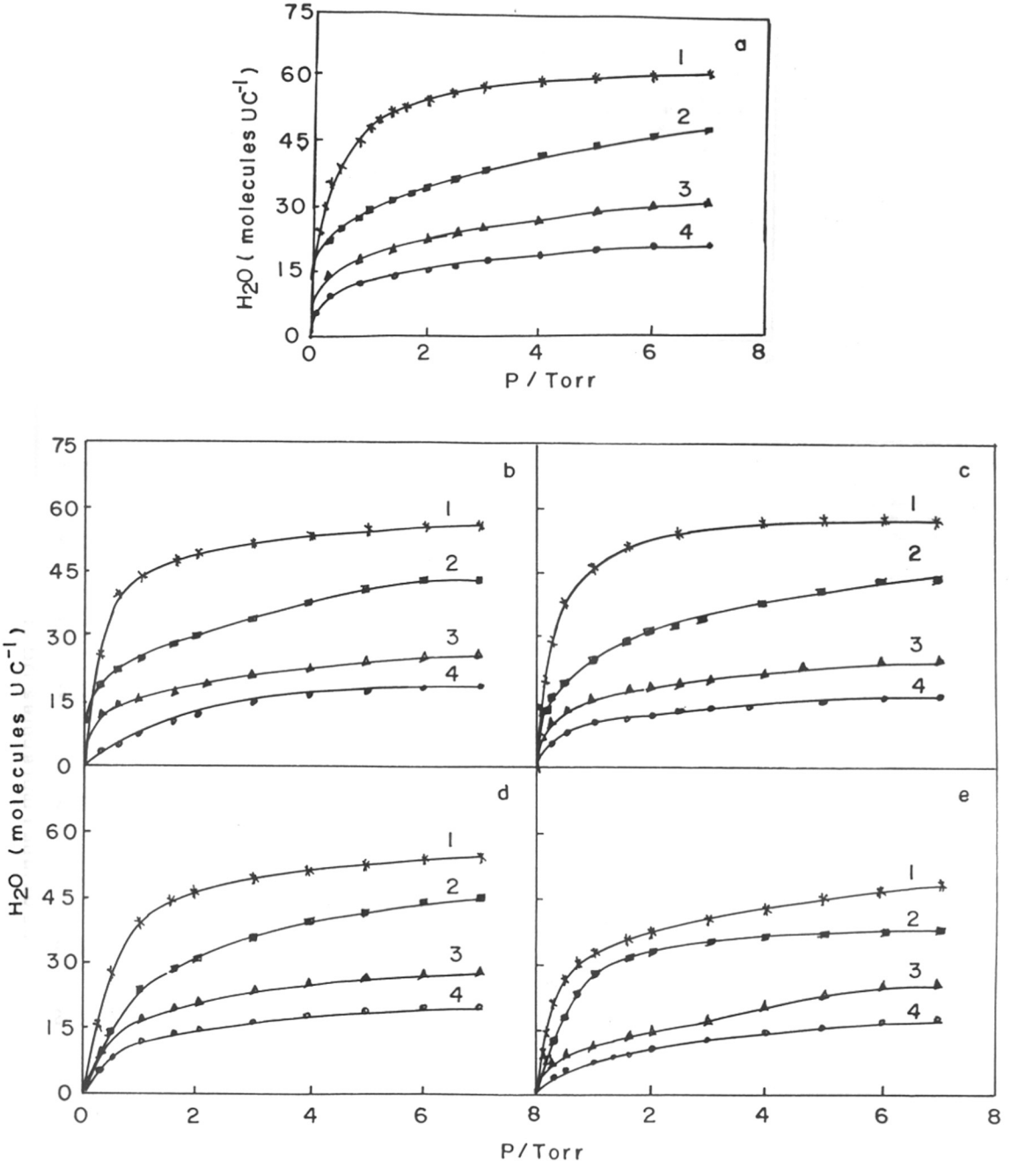

Fig. 4.2 : Water sorption isotherms in (a) Li-ETS-10(E), (b) Na-ETS-10(E), (c) K-ETS-10(E), (d) Rb-ETS-10(E) and (e) Cs-ETS-10(E) at (1) 298K, (2) 333K (3) 363K and (4) 393K.

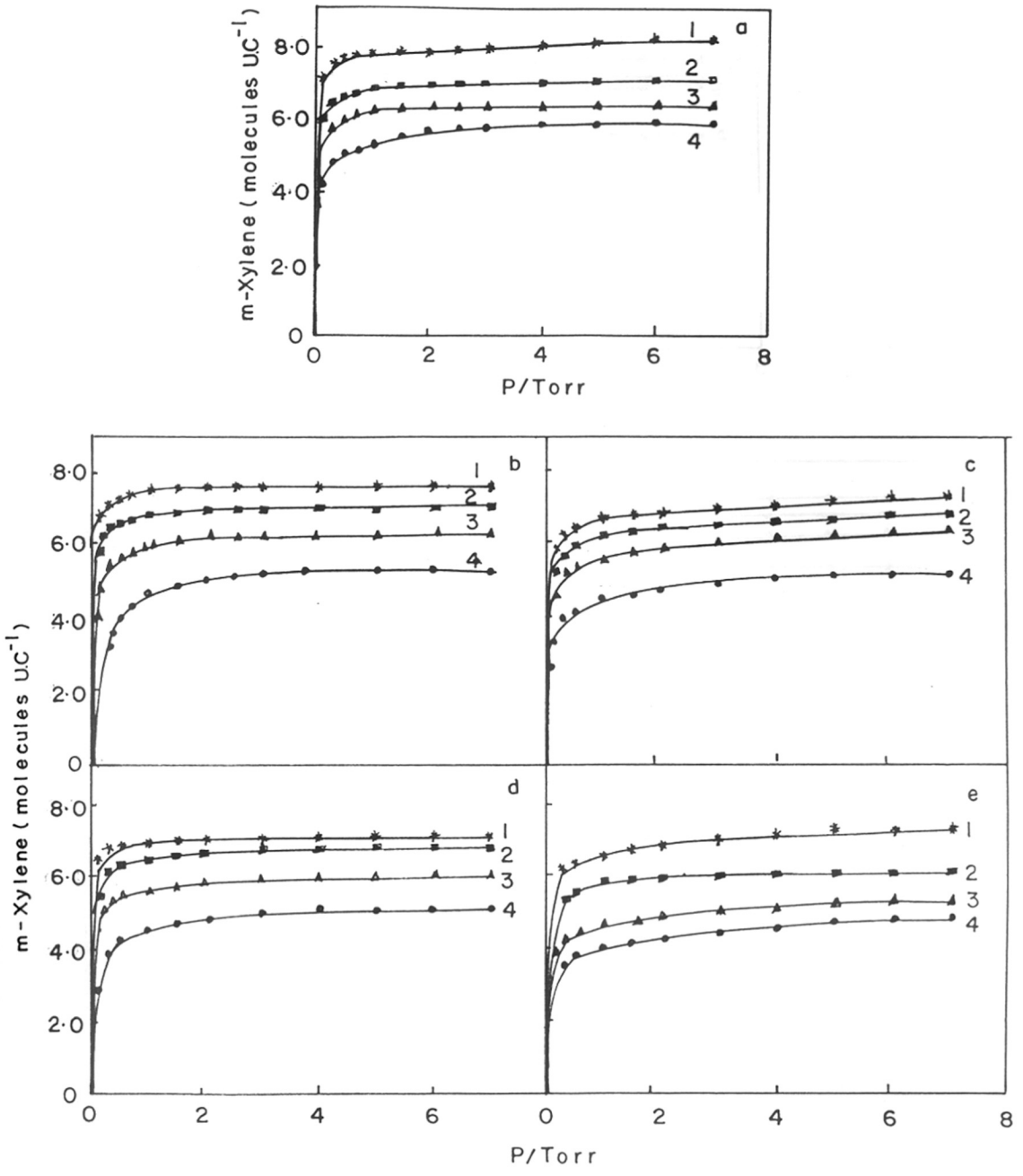

Fig. 4.3 : m-Xylene sorption isotherms in (a) Li-ETS-10(E), (b) Na-ETS-10(E), (c) K-ETS-10(E), (d) Rb-ETS-10(E) and (e) Cs-ETS-10(E) at (1) 298K, (2) 353K (3) 403K and (4) 453K.

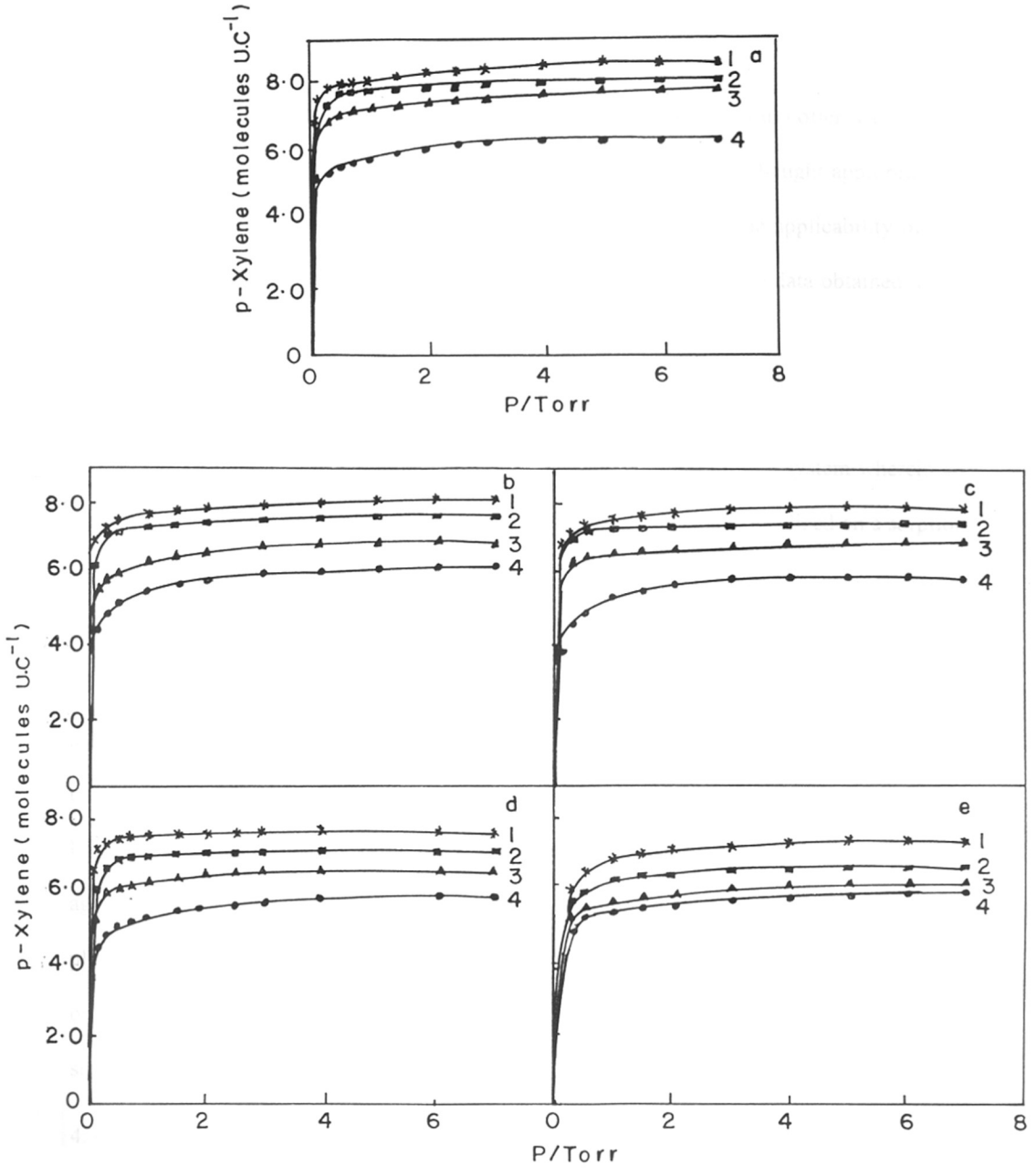

Fig. 4.4 : p-Xylene sorption isotherms in (a) Li-ETS-10(E), (b) Na-ETS-10(E), (c) K-ETS-10(E), (d) Rb-ETS-10(E) and (e) Cs-ETS-10(E) at (1) 298K, (2) 353K (3) 403K and (4) 453K.

4.3.4 Application of Isotherm Equations

Analysis of the sorption data using different isotherm models could often yield useful information about the nature of the sorption centers. It was therefore thought appropriate to investigate the influence of the nature of the framework cations on the applicability of two typical isotherm equations to the water, m-xylene and p-xylene sorption data obtained in the present study.

4.3.4.1 Langmuir Isotherm Equation

The Langmuir isotherm model describes sorption equilibrium in a system wherein all the sorption centers are of the same energy and the sorbate molecule is localized on a sorption center. Figures 4.5 to 4.7 show typical Langmuir plots for water, m-xylene and p-xylene, respectively, for different alkali metal exchanged ETS-10(E). It can be seen that all the ETS-10(E) samples exhibit excellent linear plots with different intercepts for water, m-xylene and p-xylene. Thus it is evident that the Langmuir sorption model is applicable to sorption in these samples. The monolayer capacities obtained from the reciprocals of the slopes of these linear plots are tabulated in Table 4.2. These values of saturation capacities are in good agreement with those obtained experimentally. Another salient feature of these Langmuir plots is the decrease in the value of the intercept with increasing temperature. The intercept on the y-axis is usually related to the strength of sorption, a smaller intercept implying stronger interactions.

4.3.4.2 Dubinin Isotherm Equation

An attempt is made here to apply Polanyi's potential theory modified by Dubinin and Radushkevich *[17-20]* for water, m-xylene and p-xylene sorption in alkali metal exchanged ETS-10(E) in the temperature range 298K to 393K for water and 298K to 453K for m-xylene and p-xylene. The Dubinin-Radushkevich equation is expressed as

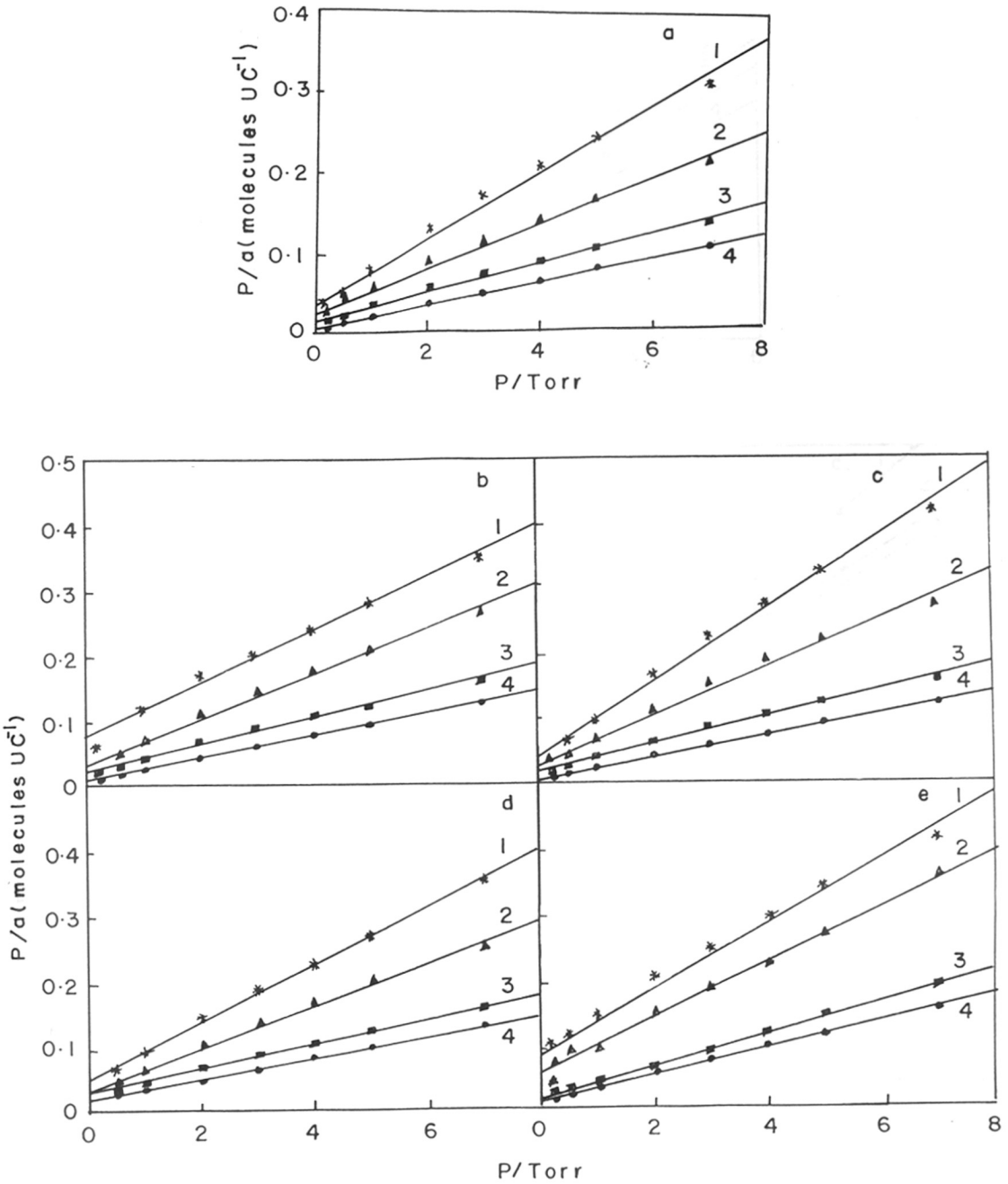

Fig. 4.5 : Langmuir plots for water sorption in (a) Li-ETS-10(E), (b) Na-ETS-10(E), (c) K-ETS-10(E), (d) Rb-ETS-10(E) and (e) Cs-ETS-10(E) at (1) 298K, (2) 333K (3) 363K and (4) 393K.

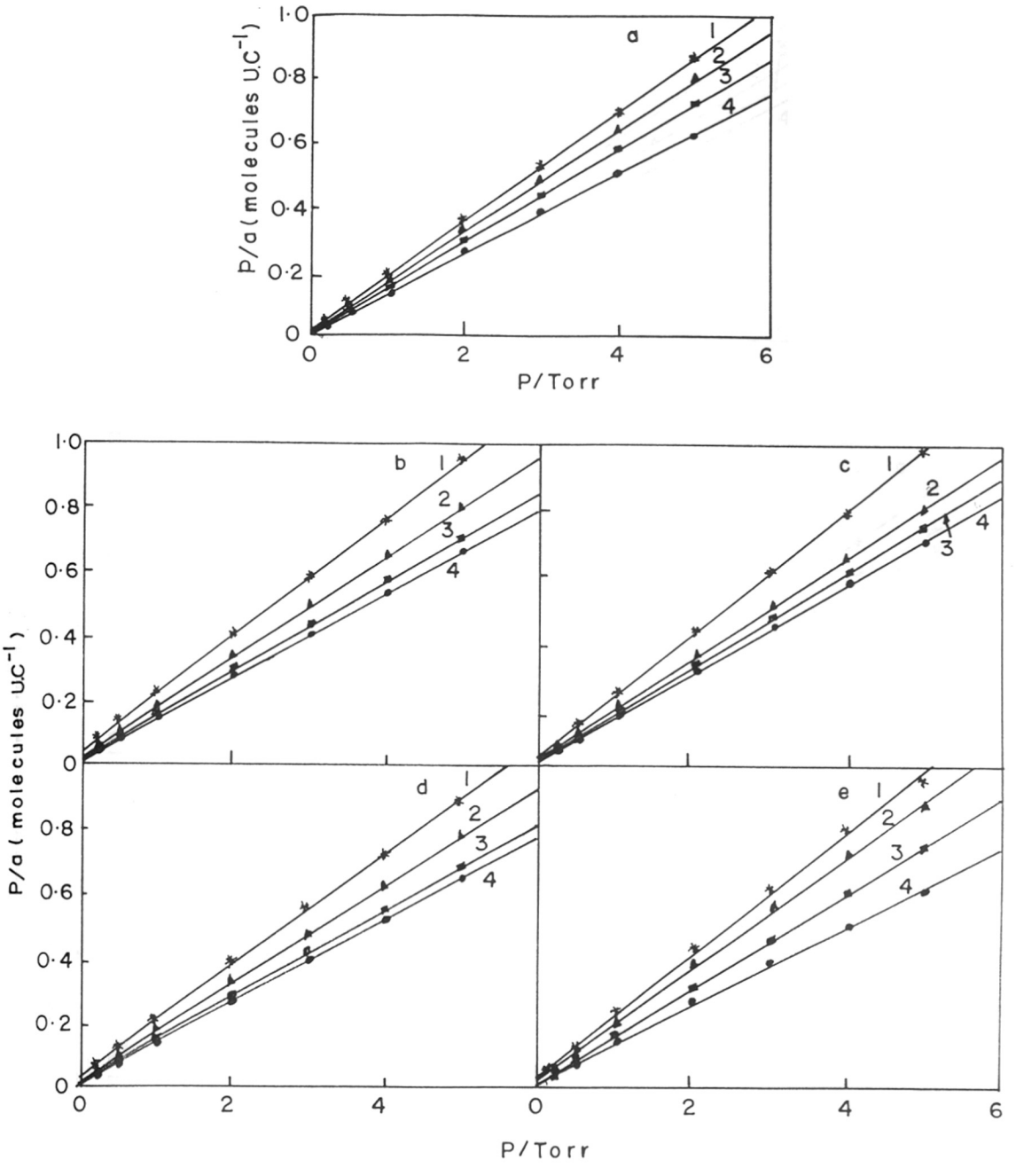

Fig. 4.6 : Langmuir plots for m-xylene sorption in (a) Li-ETS-10(E), (b) Na-ETS-10(E), (c) K-ETS-10(E), (d) Rb-ETS-10(E) and (e) Cs-ETS-10(E) at (1) 298K, (2) 353K (3) 403K and (4) 453K.

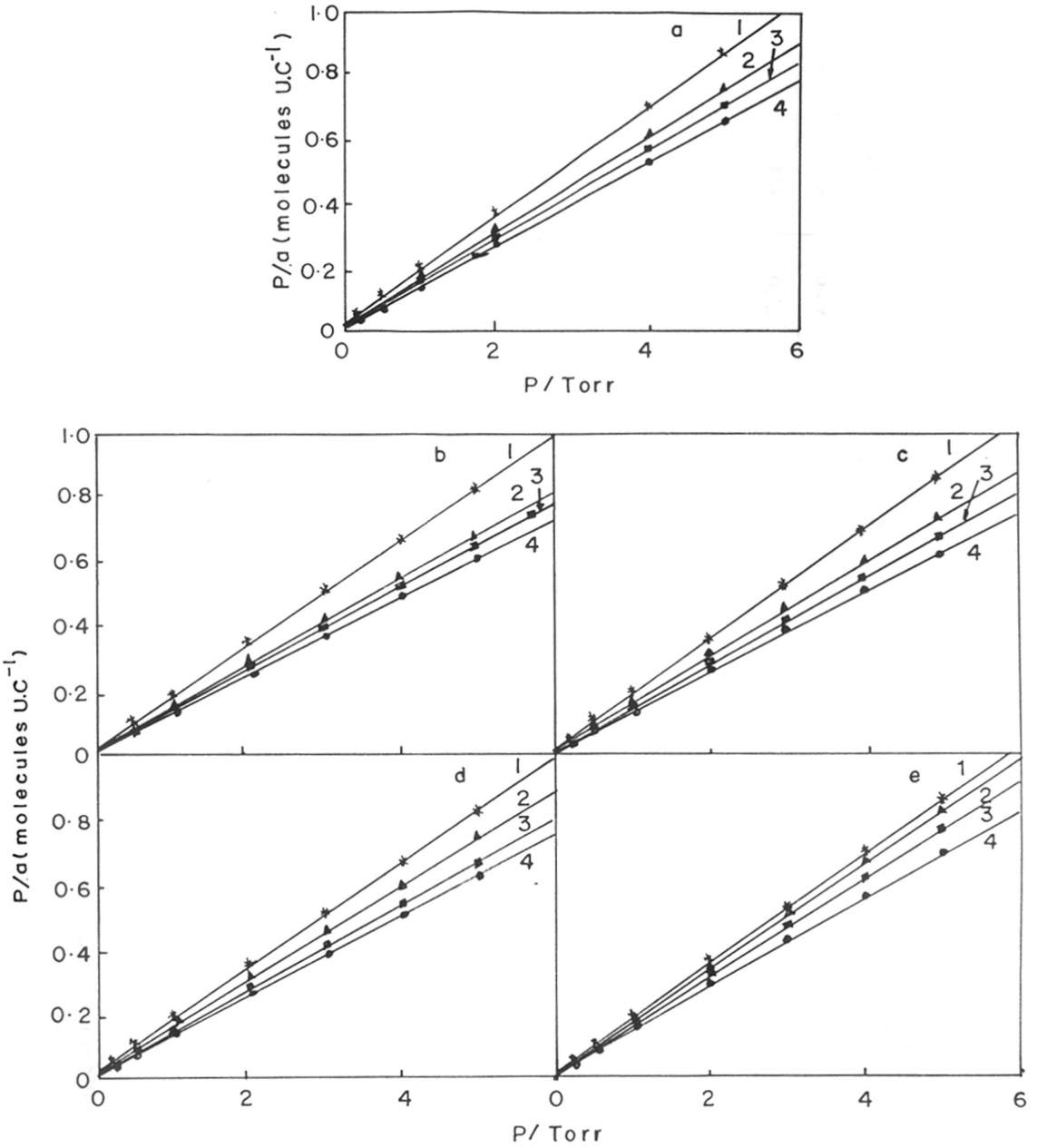

Fig. 4.7 : Langmuir plots for p-xylene sorption in (a) Li-ETS-10(E), (b) Na-ETS-10(E), (c) K-ETS-10(E), (d) Rb-ETS-10(E) and (e) Cs-ETS-10(E) at (1) 298K, (2) 353K (3) 403K and (4) 453K.

Table 4.2 : Saturation capacities of ETS-10(E) samples.

Sorbate	Temp.	Saturation capacities (molecules /U.C.)									
		Li-ETS-10		Na-ETS-10		K-ETS-10		Rb-ETS-10		Cs-ETS-10	
		[a]Expt	[b]Lang	[a]Expt	[b]Lang	[a]Expt	[b]Lang	[a]Expt	[b]Lang	[a]Expt	[b]Lang
Water	298K	62.71	62.10	57.88	57.64	56.24	56.10	53.46	52.28	47.78	47.52
	333K	49.26	49.56	45.56	45.12	44.12	44.24	42.12	42.56	37.94	37.84
	363K	33.58	32.98	30.57	29.98	28.84	28.62	25.00	24.89	23.28	22.89
	393K	23.34	23.20	19.78	19.52	17.62	16.98	15.34	14.58	13.03	13.10
m-xylene	298K	8.01	7.92	7.63	7.69	7.50	7.58	7.20	7.18	7.03	6.98
	353K	7.03	7.12	7.11	7.05	6.88	6.80	6.58	6.53	6.51	6.44
	403K	6.32	6.36	6.30	6.32	6.28	6.22	6.12	6.08	5.61	5.52
	453K	5.72	5.68	5.41	5.56	5.33	5.33	5.18	5.14	5.08	4.93
p-Xylene	298K	7.67	7.69	8.10	7.96	7.94	7.89	7.75	7.83	7.38	7.40
	353K	7.32	7.35	7.80	7.81	7.56	7.63	7.35	7.40	6.65	6.66
	403K	6.76	6.81	7.38	7.32	6.91	6.89	6.83	6.79	6.16	6.17
	453K	6.95	6.01	6.22	6.25	6.12	6.18	6.20	6.12	5.95	5.96

[a]Expt = Experimental (obtained from isotherms), [b]Lang = Langmuir.

$$\log(W) = \log W_o - B/2.303\beta^2 [T \log(P_o/P)]^2$$

where W is the amount sorbed at equilibrium pressure P, W_o is the total sorption capacity, B is a constant independent of temperature and characteristic of sorbent pore structure, and β is the affinity coefficient. The Dubinin plots so obtained were reasonably linear in all the cases at all temperatures. Typical Dubinin plots are shown in Figures 4.8 to 4.10 for water, m-xylene and p-xylene, respectively and these indicate that water, m-xylene and p-xylene sorption data in ETS-10 molecular sieve could be satisfactorily expressed by the Dubinin-Radushkevich equation. The slopes of these plots were found to decrease with increase in temperature. The values of saturation capacities and B/β^2 obtained from the intercepts on the y-axis and the slopes respectively are summarized in Table 4.3. These saturation capacities are in close agreement with those obtained experimentally (Table 4.2). From the values of B/β^2 , it is evident that the affinity coefficient β increases for water and decreases for m-xylene and p-xylene with increase in temperature for all the metal exchanged ETS-10(E) samples. The observation is difficult to explain and is apparently due to the differences in the nature of the adsorbate-adsorbent interactions for the different molecules.

4.3.4.3 Chemical affinity and the Selectivity of the Sorbate phase

A reversible and isothermal transformation of a gas, at a standard pressure P_o (760 Torr) into an infinite amount of sorbent-sorbate mixture under equilibrium pressure, P, decreases the chemical potential. The chemical affinity, when the non-ideality of the sorbate is neglected may be expressed *[21]* as :

$$\Delta\mu = RT \ln (P/P_o)$$

The value of Δμ may be taken as the quantitative measure of chemical affinity of sorbate for the sorbent. The plots of -Δμ against the amount sorbed also serve as useful criteria for the comparison of sorption affinities of probe molecules in the pores of various

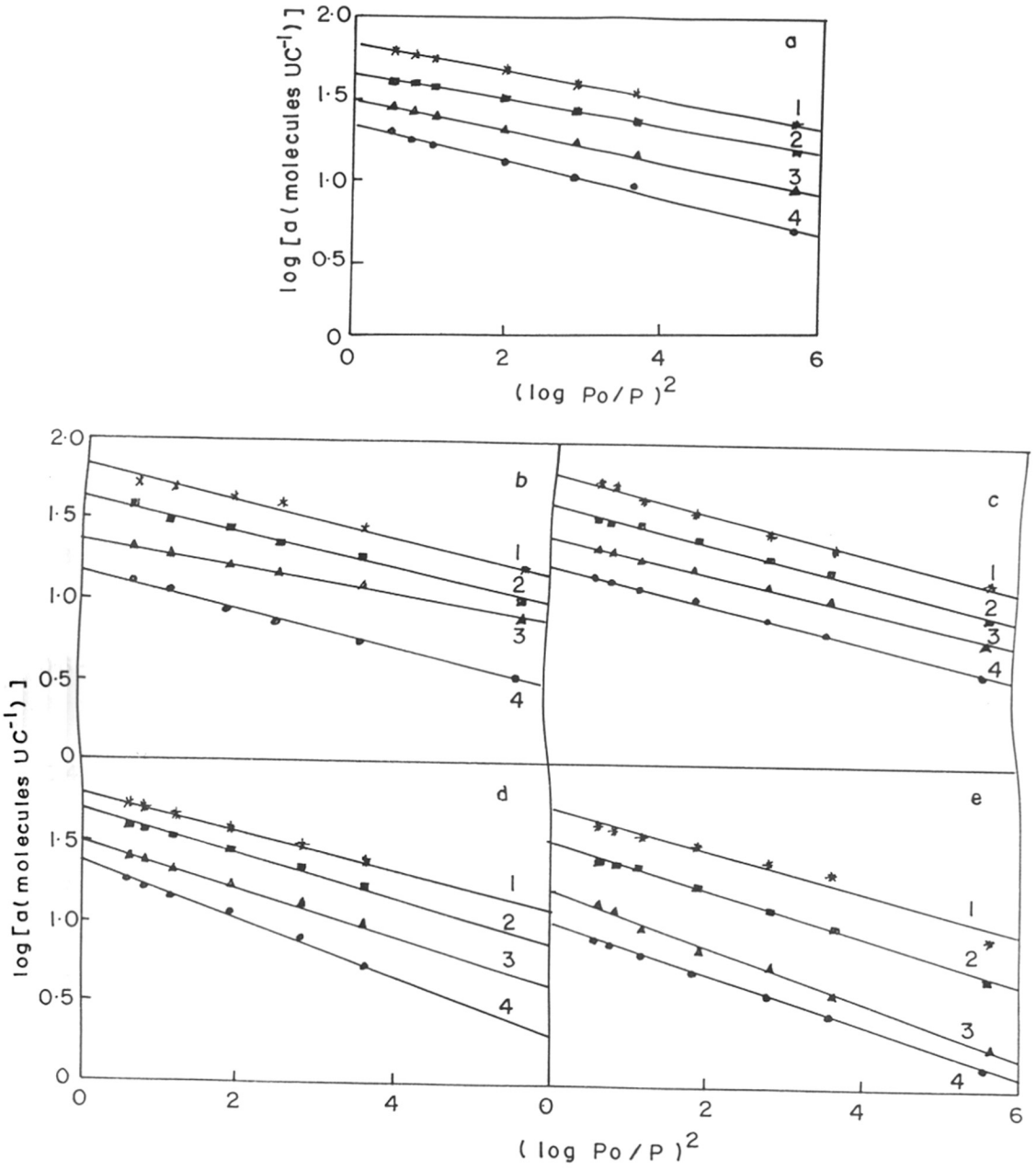

Fig. 4.8 : Dubinin plots for water sorption in (a) Li-ETS-10(E), (b) Na-ETS-10(E), (c) K-ETS-10(E), (d) Rb-ETS-10(E) and (e) Cs-ETS-10(E) at (1) 298K, (2) 333K (3) 363K and (4) 393K.

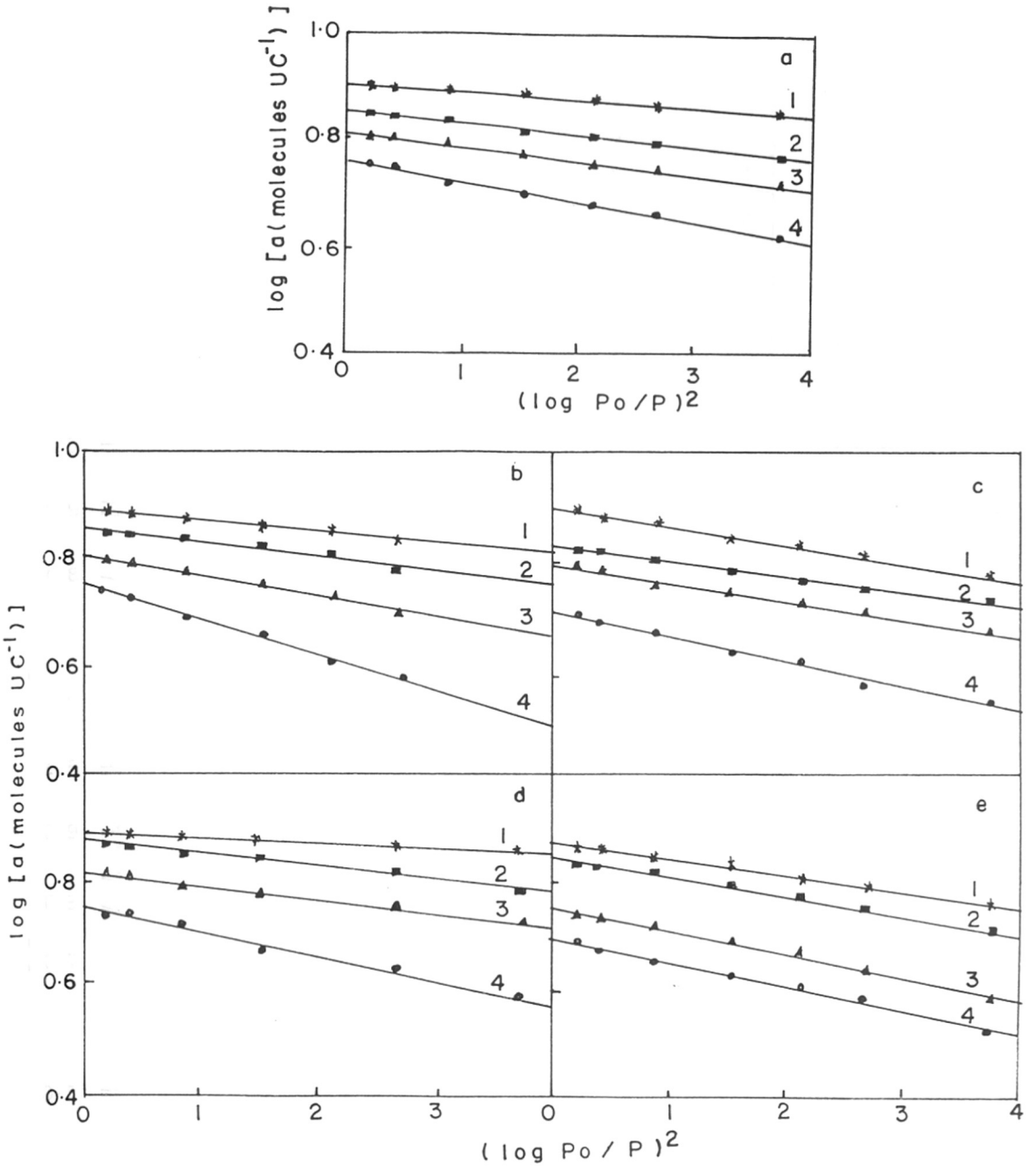

Fig. 4.9 : Dubinin plots for m-xylene sorption in (a) Li-ETS-10(E), (b) Na-ETS-10(E), (c) K-ETS-10(E), (d) Rb-ETS-10(E) and (e) Cs-ETS-10(E) at (1) 298K, (2) 353K (3) 403K and (4) 453K.

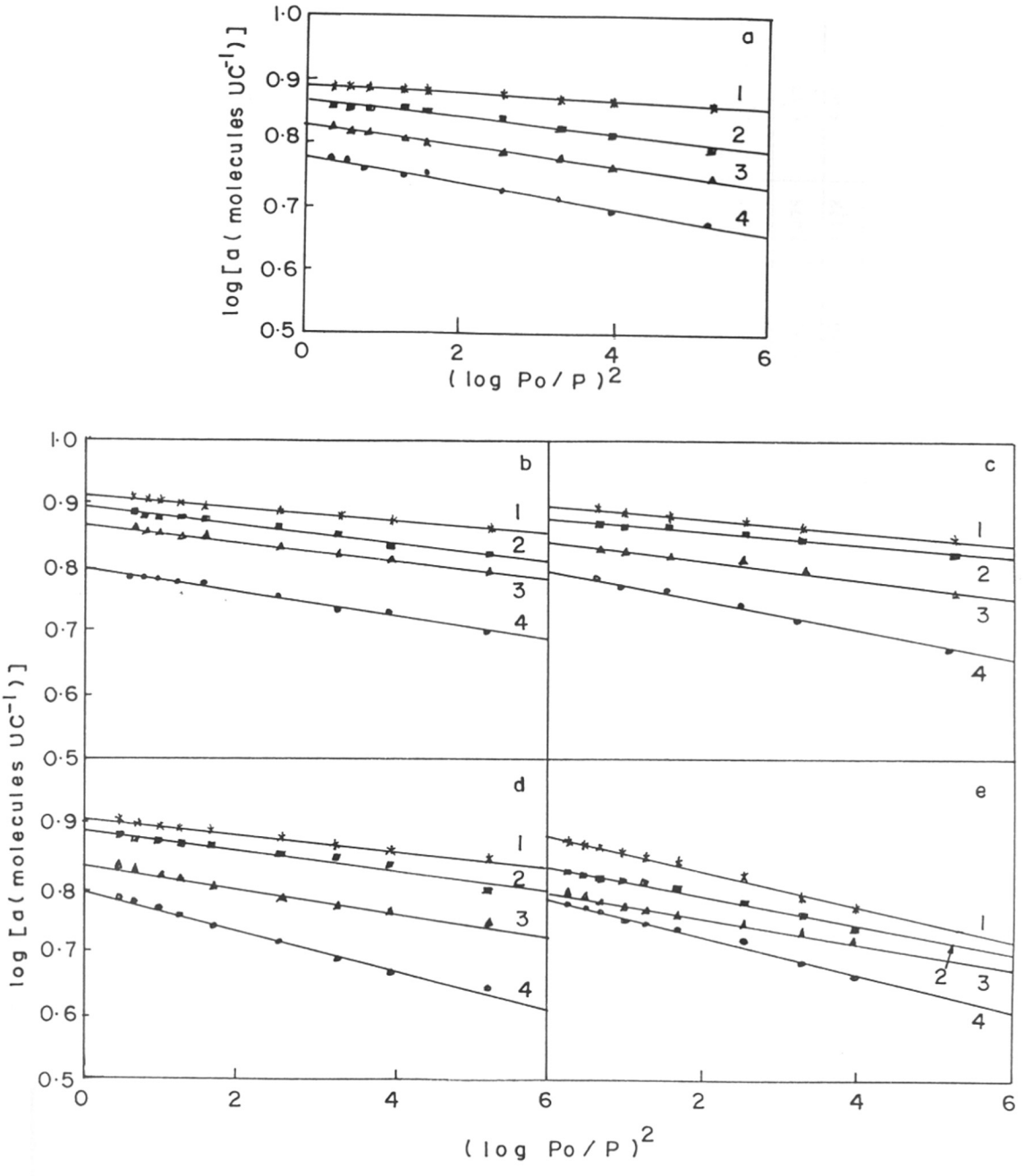

Fig. 4.10 : Dubinin plots for p-xylene sorption in (a) Li-ETS-10(E), (b) Na-ETS-10(E), (c) K-ETS-10(E), (d) Rb-ETS-10(E) and (e) Cs-ETS-10(E) at (1) 298K, (2) 353K (3) 403K and (4) 453K.

Table 4.3 : Saturation capacities and B/β^2 obtained from Dubinin plots for ETS-10(E) sample

Sorbate	Temp.	Li-ETS-10		Na-ETS-10		K-ETS-10		Rb-ETS-10		Cs-ETS-10	
		B/β^2 $x10^6$	Saturation capacity, molecules/U.C	B/β^2 $x10^6$	Saturation capacity, molecules/U.C	B/β^2 $x10^6$	Saturation capacity, molecules/U.C	B/β^2 $x10^6$	Saturation capacity, molecules/U.C	B/β^2 $x10^6$	Saturation capacity, molecules/U.C
Water	298K	1.99	65.06	2.95	62.18	3.03	61.12	3.10	55.65	3.32	49.48
	333K	1.41	46.68	2.22	43.65	2.47	43.73	2.82	40.97	3.17	35.70
	363K	1.48	32.84	1.98	28.90	1.90	27.12	2.57	24.22	2.41	21.89
	393K	1.52	22.42	1.70	18.45	1.73	16.59	2.65	14.24	2.53	13.10
m-Xylene	298K	0.313	7.88	0.482	7.72	0.492	7.66	0.440	7.21	0.639	7.05
	353K	0.362	7.16	0.486	7.01	0.530	6.85	0.443	6.55	0.671	6.42
	403K	0.368	6.39	0.527	6.34	0.592	6.25	0.468	6.11	0.684	5.57
	453K	0.395	5.65	0.561	5.62	0.622	5.35	0.614	5.12	0.690	4.87
p-Xylene	298K	0.225	7.71	0.249	7.92	0.234	7.87	0.281	7.85	0.413	7.56
	353K	0.231	7.29	0.258	7.63	0.245	7.53	0.290	7.42	0.417	6.77
	403K	0.219	6.98	0.260	7.24	0.255	6.91	0.293	6.70	0.475	6.13
	453K	0.245	6.11	0.261	6.29	0.265	6.25	0.325	6.10	0.428	5.92

cationic forms of zeolites. Typical chemical affinity plots for water, m-xylene and p-xylene sorption in alkali metal exchanged ETS-10(E) at 298K and 393K for water, and 298K and 453K for m-xylene and p-xylene are given in Figure 11. The chemical affinity sequence over the entire temperature range was Li-ETS-10(E) > Na-ETS-10(E) > K-ETS-10(E) > Rb-ETS-10(E) > Cs-ETS-10(E) for water, m-xylene and p-xylene. This is the expected direction as the smaller ions with greater charge/radius ratio are able to polarize the adsorbate molecules more strongly enabling stronger adsorbate-adsorbent interactions.

4.3.4.4 Isosteric Heats (Q_{st}) of Sorption

Vogt *et al.* have evaluated the thermodynamic parameters for the sorption of benzene, n-butylamine and ammonia on Ce-Na-Y and Cr-Na-Y *[22]*. Isosteric heats of sorption of ammonia, pyridine and n-butylamine have been evaluated from microcalorimetric studies on cation exchanged zeolites such as X, Y and mordenite *[1,23]*. The isosteric heat of sorption can also be derived from the sorption isosters by applying the Clausius-Clapeyron equation at constant sorbate loading using the equation :

$$Q_{st} = - \Delta H = R[T_2T_1 / (T_2-T_1)] \ln (P_2/P_1)$$

If Q_{st} is temperature independent, the plot of ln (P) against 1/T should be linear. The plots of ln (P) vs (1/T) yielded a straight line at constant coverage in all the cases. From the slope, isosteric heats were calculated by the following relation :

$$Q_{st} = (\text{Slope} \times 8.314)/1000 \text{ KJ mol}^{-1}$$

The isosteric heats calculated from the slope are presented in Table 4.4. At a constant coverage of 7.0 molecules/U.C of water sorption, the isosteric heat is between 25.3 KJ mol^{-1} to 18.5 KJ mol^{-1} for all the alkali metal exchanged ETS-10(E) samples. The isosteric heats of m-xylene and p-xylene at the coverage of 3.0 molecules/U.C are 56.3 KJ mol^{-1} to 68.0 KJ

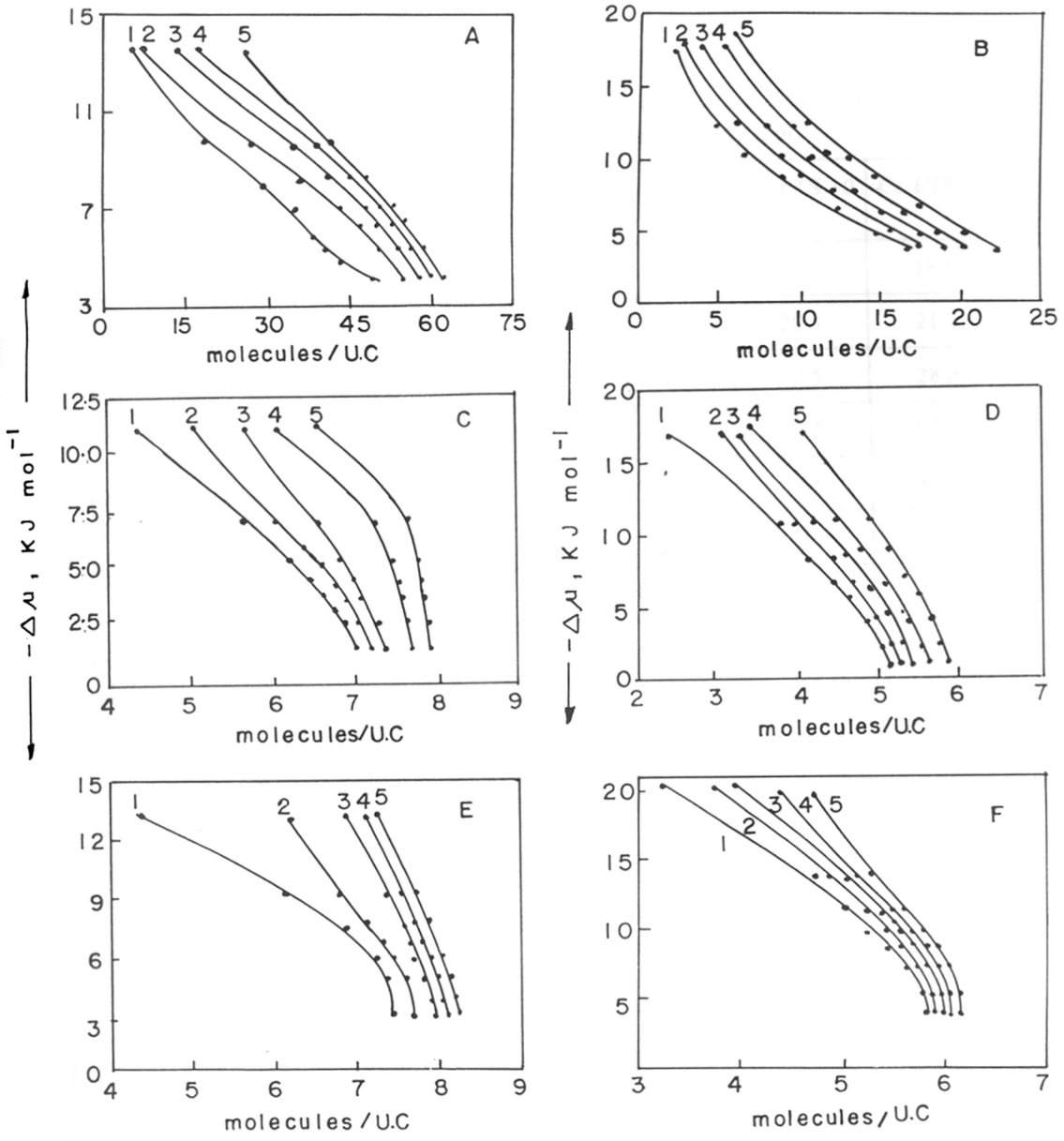

Fig. 4.11 : Chemical affinity curves for (A,B) water, (C,D) m-xylene and (E) p-xylene (A,C,E) : 298K, B : 393K and (D,F) : 453K.

Curves 1-5 correspond to Cs-ETS-10(E), Rb-ETS-10(E), K-ETS-10(E), Na-ETS-10(E) and Li-ETS-10(E).

Table 4.4 : Isosteric heats of adsorption over alkali metal exchanged ETS-10(E).

Sorbate	Coverage molecules/ U.C	Isosteric heats (Q_{st}), KJ mol^{-1}				
		Li-ETS-10	Na-ETS-10	K-ETS-10	Rb-ETS-10	Cs-ETS-10
Water	7.0	25.3	23.3	21.3	19.2	18.5
	12.0	29.8	24.9	29.1	28.5	21.2
	16.0	35.2	32.4	31.5	30.5	28.2
m-Xylene	3.0	70.6	72.3	75.4	78.2	82.5
	4.0	92.8	86.5	87.3	82.5	83.3
	5.0	98.2	81.3	78.9	79.7	73.5
p-Xylene	3.0	56.3	62.4	59.2	68.4	65.2
	4.0	59.9	64.4	65.2	78.8	67.7
	5.0	69.93	76.0	71.0	90.2	88.1

mol^{-1} and 70.6 KJ mol^{-1} to 82.5 KJ mol^{-1}, respectively for all the samples. There is in general a decrease in Q_{st} on increase of cation size (Li to Cs) in the case of water and an increase in the case of the xylenes. Eventhough the comparisons are made of different loadings of the molecules (per unit cell), the results appear to suggest that the sorbate-sorbent interactions are different for the polar and non-polar molecules. Besides, the Q_{st} values are in general found to increase with coverage for all the molecules. This suggests that as the coverage increases, intermolecular (sorbate-sorbent) interactions become predominant.

4.4 REFERENCES

1. Jacobs, P.A., VanCauwelaert, F.H., Vansant, E.F., and Utterhoeven, J.B., *J. Chem. Soc. Faraday Trans. I,* **69**, 1056 (1973).
2. Egertone, T.A., and Stone, F.S., *J. Colloid Interface Sci.,* **38**, 195 (1972).
3. Steinberg, K.H., Bremer, H., and Falke, P., *Z. Phys. Chem.* (Leipzig), **257**, 151 (1976).
4. Mirajkar, S.P., Thangaraj, A., and Shiralkar, V.P., *J. Phys. Chem.* **96**, 3073 (1992).
5. Joshi, P.N., and Shiralkar, V.P., *J. Phys. Chem.,* **97**, 619 (1993).
6. Joshi, P.N., Eapen, M.J., and Shiralkar, V.P., *J. Chem. Soc., Faraday Trans.,* **90(2)** 387 (1994).
7. Reddy, K.S.N., Eapen, M.J., Soni, H.S., and Shiralkar, V.P., *J. Phys. Chem.,* **96**, 7923 (1992).
8. Broughton, D.B., Neuzil, R.W., Pharis, J.M., and Brearly, C.S., *Chem. Eng. Prog.,* **66**(9), 70 (1970).
9. Das, T.K., Chandwadkar, A.J., and Sivasanker, S., *Mater. Res. Bull.,* **17**, 1143 (1994).
10. Das, T.K., Chandwadkar, A.J., Budhkar, A.P., Belhekar, A.A., and Sivasanker, S., *Microporous Mater.,* **4**, 195 (1995).
11. Das, T.K., Chandwadkar, A.J., Budhkar, A.P., and Sivasanker, S., *Microporous Mater.,* **5**, 401 (1996).
12. Das, T.K., Chandwadkar, A.J., and Sivasanker, S., *J. Mol. Catal.,* **107**, 199 (1996).
13. Das, T.K., Chandwadkar, A.J., and Sivasanker, S., *J. Chem. Soc. Chem. Commun.,* 1105 (1996).
14. Kuznicki, S.M., Thrush, K.A., Allen, F.M., Levine, S.M., Hamil, M.M., Hayhurst, D.T., and Mansour, M., *Synth. Microporous Mater.*, **1**, 427 (1992).
15. Pauling, L., *J. Am. Chem. Soc.*, **49**, 765 (1927).
16. Kiselev, A.V., *Discuss. Faraday Soc.,* **40**, 205 (1965).
17. Dubinin, M.M., Radushkevich, L.V., *Proc. Acad. Sci.,* USSR, **55**, 327 (1974).
18. Dubinin, M.M, *Chem Rev.,* **60**, 309 (1960)

19. Dubinin, M.M, *Pure Appl. Chem.,* **10**, 309 (1965).

20. Dubinin, M.M, and Astakhov, V.A., *Bull. Acad. Sci.,* USSR, **20**, 3 (1971).

21. Barrer, R.M., Coughlan, B., *Molecular sieves ;* Society of Chemical Industry, London, p. 141, 233 and 241 (1968).

22. Vogt, V.F., Wolf, H., Bremer, H., Rubinshtein, A.M., Klyacho, A.L., Brueva, J.B., and Mishin, I.V., *Z. Anorg. Allg. Chem.,* **439**, 153 (1978).

23. Coughlan, B., and McCann, W.A., *J. Chem. Soc. Faraday Trans. I,* **75**, 1769 (1979).

CHAPTER V

CATALYTIC PROPERTIES OF ETS-10

5.1 INTRODUCTION

The use of catalytic test reactions is a widely accepted method for estimating the effective pore dimensions of zeolites and molecular sieves with unknown structures *[1,2]*. The catalytic tests yield data obtained under realistic conditions, which include mass-transfer and intrinsic chemical effects *[3]*. The intrinsic chemical effects are not detectable by spectroscopic techniques and adsorption of probe molecules where no chemical transformation take place.

Apart from the typical catalytic test reactions such as, m-xylene and 1,3,5 trimethylbenzene isomerization and dehydration of alcohols, there are a number of industrially important reactions that are catalyzed by zeolites. Zeolites have found numerous applications in petroleum refining, petrochemical processing and in the synthesis of fine chemicals and drug intermediates.

ETS-10 has attracted much attention due to its unique pore structure and charge distribution *[4,5]*. It has already been tested as a catalyst in Fischer-Tropsch synthesis by Carli *et al. [6]*. The cation density in ETS-10 is approximately equivalent to that in a zeolite with Si/Al = 2.5 such as zeolite Y. This makes ETS-10 a potentially interesting material both for cation exchange and catalysis. Besides, the large cation exchange capacity imparts a basic character to the material when exchanged with alkali ions such as Na and K. On the other hand, acidic properties could be introduced by exchanging the alkali ions with H^+ and forming bridging hydroxyl groups such as Ti-(OH)-Si.

The present chapter [Chapter V] discusses the use of test reactions, *viz.*, the isomerization of m-xylene and 1,3,5-trimethylbenzene, and the dehydration of n-butanol over H-ETS-10 to characterize acidity and pore characteristics. Besides, it reports the use H-ETS-10 as an acid catalyst in the hydroisomerization of n-hexane over Pt-H-ETS-10. It also

reports the use alkali ion-exchanged ETS-10 as a basic support for platinum and the aromatization of n-hexane over Pt-(M)-ETS-10 into benzene.

5.2 EXPERIMENTAL

5.2.1 Preparation of Catalysts

The method of preparation of the ETS-10 samples and their modifications have been described in Chapter II. The ETS-10 catalysts used in all the reactions except the aromatization of n-hexane were in the protonic form (H^+). The powder catalysts were pressed into pellets and broken into -12 +18 mesh size particles before loading in the reactor.

5.2.2 Catalytic Reactions

The catalytic reactions were carried out in a fixed bed down flow tubular reactor at atmospheric pressure. The tubular reactor consisted of a fused silica tube, 1.5 cm in inner diameter and 35 cm length provided with a thermowell. The sieved catalyst material (2 g) was loaded in such a way that the tip of the thermocouple (kept inside the thermowell) was at the center of the catalyst bed. The catalyst was sandwiched by inert porcelain beads which provided a more uniform flow distribution. The top portion of the porcelain beads additionally served as a pre-heater zone and vaporizer. A condenser was attached to the outlet of the reactor which was cooled by water circulation from a cryostat maintained at approximately 277K. A sample receiver was connected to the bottom of the condenser. The outlet from the receiver was connected to a gas collection and measuring system.

The liquid and gas products were analyzed in a gas chromatography (HP 5880A), equipped with a capillary column coated with cross-linked methyl silicone gum (HP 1; 50 m × 0.5 mm) and a FID. Gas samples were also analyzed by a gas chromatographic refinery gas analyzer (RGA, Model 5880A, HP) with multiple columns and fitted with TCDs. In the case

of m-xylene isomerization, the products were analyzed using a gas chromatograph (Shimadzu GC R1A), equipped with 5% bentone + 5% diisodecyl phthalate column (2 m × 3 mm).

Prior to the reaction, the catalyst was activated in a flow of air at 673K for 6 h. The catalyst was then flushed with nitrogen and cooled to the reaction temperature. For hydroisomerization and aromatization of n-hexane, the catalyst was reduced in a flow of H_2 (100 ml min^{-1}) for 4 h at 573K prior to injection of the feed at the desired temperature. The reactant was fed into the reactor by a syringe pump (Sage Instruments, Model 352).

5.3 ISOMERIZATION OF m-XYLENE AND 1,3,5 TRIMETHYLBENZENE

5.3.1 Isomerization of m-xylene

The reaction of m-xylene on zeolites, besides its industrial importance, is abundantly described in the literature because it provides information on both the geometry of the zeolitic channels *[7]* and the acidic properties of solids. Evidence is provided in the literature that both isomerization and disproportionation of m-xylene are catalyzed by Brönsted acid sites *[8,9]* and that the disproportionation reaction requires stronger acid sites than isomerization *[10,11]*.

The H-ETS-10 catalysts are found to be active in the isomerization of m-xylene (Table 5.1), though the conversion levels are below the equilibrium value (equilibrium conversion ~46% at 573K *[12]*). The compositions of all H-ETS-10 samples are tabulated in Chapter III (Table 3.2). The activity of H-ETS-10 samples is in the following decreasing order : H-ETS-10(E) > H-ETS-10(D) > H-ETS-10(C) > H-ETS-10(A) > H-ETS-10(B). Disproportionation reactions generally accompany the isomerization of xylenes. These reactions are bimolecular in nature and involve bulky intermediates *[13]*. As a result, zeolites with high acid site densities enabling the adsorption of two xylene molecules at adjacent sites are more likely to catalyze the disproportionation reaction *[14]*. Again, zeolites with pore

Table 5.1 : Isomerization of m-Xylene over H-ETS-10 samples[a].

	ETS-10(A)	ETS-10(B)	ETS-10(C)	ETS-10(D)	ETS-10(E)	H-Y
Conv. (wt.%)	16.4	15.0	19.9	23.3	27.2	25.8
I/D[b]	0.48	0.5	0.5	0.5	0.52	0.66
Products (yield, wt.%)						
Benzene	1.9	1.8	2.1	2.5	2.6	0.04
Toluene	4.1	3.8	4.5	5.1	5.8	5.9
p-xylene	1.1	1.1	1.8	2.2	2.9	5.1
o-xylene	3.4	3.2	3.9	4.3	5.1	4.9
1,3,5-TMB[c]	1.3	1.1	2.1	2.4	3.0	2.6
1,2,4-TMB[c]	3.6	3.4	4.1	4.6	5.2	5.9
1,2,3-TMB[c]	0.4	0.2	0.6	0.9	1.1	0.6
TTMB[d]	0.2	0.1	0.3	0.6	1.4	0.4
Others	0.4	0.3	0.5	0.7	0.1	0.4

[a]Reaction conditions : Catalyst = 2g, Temp. = 573K, WHSV = 1 (h^{-1}), Gas : N_2 (5 ml/min.), Press. = 1 atm., TOS = 1 h.

[b]I/D = Based on no. of moles of isomerization and disproportionation products in the catalysate.

[c]Trimethylbenzene.

[d]Tetramethylbenzenes.

sizes large enough to accommodate the bulky transition states involved in disproportionation reactions tend to have higher disproportionation activities *[15]*. Hence, the isomerization/disproportionation (I/D) activity ratios during m-xylene conversion can be used as a measure of acid site density and/or pore dimensions in molecular sieves. The I/D activity ratios of all the ETS-10 catalysts are ~0.5. Earlier workers *[15]* have reported an I/D ratio of about 4 for H-β and 8 for H-mordenite at about 25% conversion. The very low I/D ratio obtained over ETS-10 is mainly due to the high acid-site density and a larger pore dimension (than Hβ and mordenite). The high acid-site density arises from the large number of Ti^{4+} (O_h) ions with two unbalanced (negative) charges on each ion *[4]*. Under identical conditions, the conversion over H-Y is 25.8% and the I/D activity ratio is 0.66.

5.3.2 Isomerization of 1,3,5-Trimethylbenzene

The conversion of 1,3,5-trimethylbenzene is 35.9% to 56.5% over all H-ETS-10 samples, compared to the expected equilibrium conversion of 71% at 573K (Table 5.2). The compositions of all H-ETS-10 samples are tabulated in Chapter III (Table 3.2). The activity of H-ETS-10 samples is in the following decreasing order : H-ETS-10(E) > H-ETS-10(D) > H-ETS-10(C) > H-ETS-10(A) > H-ETS-10(B). The I/D ratios (0.73 to 0.88; Table 5.2) are larger than those observed in the case of m-xylene isomerization as spatial requirements for the bimolecular disproportionation reactions involving two 1,3,5-trimethylbenzene molecules are more than for two m-xylene molecules. At the same reaction conditions, the conversion of 1,3,5-trimethylbenzene over a commercial H-Y sample (Linde, LZ-Y62, calcined at 773K for 6h) was 52.5%, the I/D ratio being 0.73. The performance of ETS-10 in the above reaction is similar to that of H-Y.

Table 5.2 : Isomerization of 1,3,5-trimethylbenzene over H-ETS-10 samples[a].

	ETS-10(A)	ETS-10(B)	ETS-10(C)	ETS-10(D)	ETS-10(E)	H-Y
Conv. (wt.%)	44.2	35.9	45.2	50.2	56.5	52.5
I/D[b]	0.79	0.88	0.78	0.75	0.73	0.73
Products (yield, wt.%)						
Benzene	0.01	0.01	0.01	0.01	0.01	-
Toluene	0.7	0.5	0.8	0.9	1.2	0.6
p-xylene	1.4	1.3	1.5	2.1	3.1	2.3
m-xylene	8.1	6.9	8.5	9.2	10.2	9.0
o-xylene	2.1	1.9	2.0	3.5	4.0	2.2
1,2,4-TMB[c]	17.3	15.6	17.5	18.5	20.3	19.2
1,2,3-TMB[c]	1.8	1.1	1.9	2.6	3.3	2.5
TTMB[d]	12.6	8.4	12.8	13.2	14.2	16.3
Others	0.2	0.2	0.2	0.2	0.2	0.4

[a]Reaction conditions : Catalyst = 2g, Temp. = 573K, WHSV = 1 (h^{-1}), Gas : N_2 (5 ml/min.), Press. = 1 atm., TOS = 1 h.

[b]I/D = Based on no. of moles of isomerization and disproportionation products in the catalysate.

[c]Trimethylbenzene.

[d]Tetramethylbenzenes.

5.4 DEHYDRATION OF n-BUTANOL

The results of the dehydration of n-butanol over the H-ETS-10 samples are presented in Table 5.3. The samples were quite active in the dehydration reaction, though much less than H-Y (Linde, LZ-Y62 calcined at 773K for 6 h). H-Y gave a conversion of 98.2% at 523K, while ETS-10(E) gave a conversion of 96.5% at 573K. The activities of the samples increases in the order H-ETS-10(B) < H-ETS-10(A) < H-ETS-10(C) < H-ETS-10(D) < H-ETS-10(E) which is the same order as the expected purity of the samples (Chapter II and III). The products, as expected, are mostly 1- and 2-butenes. Besides, small amounts (< 3%) of isobutene and other components (C_1-C_3 and C_4^+; < 5% in all) are also obtained. The 1-butene/2-butenes ratio in the products from the ETS-10 samples are 0.27 ± 0.02, compared to the thermodynamic equilibrium value of 0.20. The *trans*-butene-2/*cis*-butene-2 ratio in the products from all the samples is 1.28 ± 0.02. This value is only slightly smaller than the expected equilibrium value, 1.5. In the case of H-Y, the observed values are 0.2 and 1.6 compared to the expected equilibrium values of 0.14 and 1.6 (at 523K) for the 1-butene/2-butenes and *trans*-butene-2/*cis*-butene-2 ratios, respectively. These differences suggest that thermodynamic equilibrium is not fully obtained at the reaction conditions over H-ETS-10 samples. Besides, the product pattern could have also been affected by the formation of side products. The ratio of isobutene/(1-butene + 2-butenes) is very small (about 0.003 to 0.005) for all the H-ETS-10 samples and H-Y, being far below the equilibrium values of 1.4 (573K) and 1.5 (523K). All the above observations can be explained based on the minimum strength of acid sites required to catalyze the different reactions. The acidity requirement increases in the order *cis-trans* isomerization < double bond isomerization < skeletal isomerization. Apparently, the acid strength in H-ETS-10 and H-Y at that temperatures investigated are such that skeletal isomerization is not possible, while the cis-trans and double bond isomerizations and dehydration reactions take place to different extents. Besides, the water produced in the reaction might also poison/weaken the acid centers.

Table 5.3 : Dehydration of n-butanol over H-ETS-10 samples[a].

	ETS-10(A)	ETS-10(B)	ETS-10(C)	ETS-10(D)	ETS-10(E)	H-Y[b]
Conv. (wt.%)	88.0	82.1	88.4	93.8	96.5	98.2
1-Butene/2-butenes	0.27	0.25	0.27	0.29	0.29	0.20
Products (yield, wt.%)						
C_1	-	-	-	-	-	0.1
C_2	0.01	0.1	0.01	0.01	0.01	1.0
C_3	0.3	0.2	0.2	0.3	0.3	3.4
i-C_4	0.1	0.05	0.1	0.5	0.5	0.5
Butene	17.3	15.3	17.8	19.5	20.2	13.5
i-Butene	2.5	1.9	2.7	3.1	3.4	2.1
n-C_4	0.5	0.5	0.3	0.8	0.9	4.0
t-But-2-ene	36.8	34.6	37.2	37.5	38.2	41.7
c-But-2-ene	28.2	27.1	28.3	29.6	30.4	26.4
Others (C_5^+)	2.3	2.4	1.8	2.5	2.6	5.5

[a]Reaction conditions : Catalyst = 2 g, Temp. =573K, WHSV = 2.0 (h^{-1}), Gas : N_2 (5 ml/min.), Press. = atm., TOS = 1 h.

[b]Reaction temperature = 523K.

5.5 HYDROISOMERIZATION OF n-HEXANE

5.5.1 Introduction

Catalytic hydroisomerization of light naphtha (C_5-C_6 fraction) is practiced in many refineries to increase the gasoline pool octane *[16,17]*. The process essentially transforms the low octane components such as the n-paraffins into high octane branched chain components with minimal cracking. Highly acidic zeolites and silica alumina containing small amounts of a noble metal such as Pt have been reported to be suitable catalysts *[18]*. The hydroisomerization of model compounds such as n-hexane and n-heptane has been reported over large number of zeolites and aluminophosphate catalysts containing Pt *[19-21]*. The hydroisomerization of n-hexane over Pt-H-ETS-10 is now reported.

The profiles of temperature programmed desorption of NH_3 obtained over H-ETS-10(E) and Pt-H-ETS-10(E) were discussed in Chapter III (Fig. 3.21). The profiles indicate that the acid sites are mostly of weak to moderate strength. For example, nearly all the NH_3 is desorbed below 623K, the peak maximum occurring around 400-420K. In comparison, H-ZSM-5 desorbs NH_3 beyond 733K with a distinct peak maximum for strong acid sites occurring around 670K *[22]*. Pt-dispersion measurements were carried out on a 0.5 wt.% sample by H_2 adsorption at ambient temperature *[23]*. A Pt-dispersion of about 72% was estimated. The above value is probably low as the degassing of the reduced sample was done at the relatively low temperature of 598K to prevent structural damage to ETS-10.

5.5.2 Influence of Pt-content

The incorporation of Pt increases the activity of H-ETS-10(E) many fold, being about five fold at 523K and eight fold at 623K (Fig. 5.1). Fig. 5.1 also reveals that a decrease in n-hexane conversion occurs with duration of run, the decrease being generally more at higher

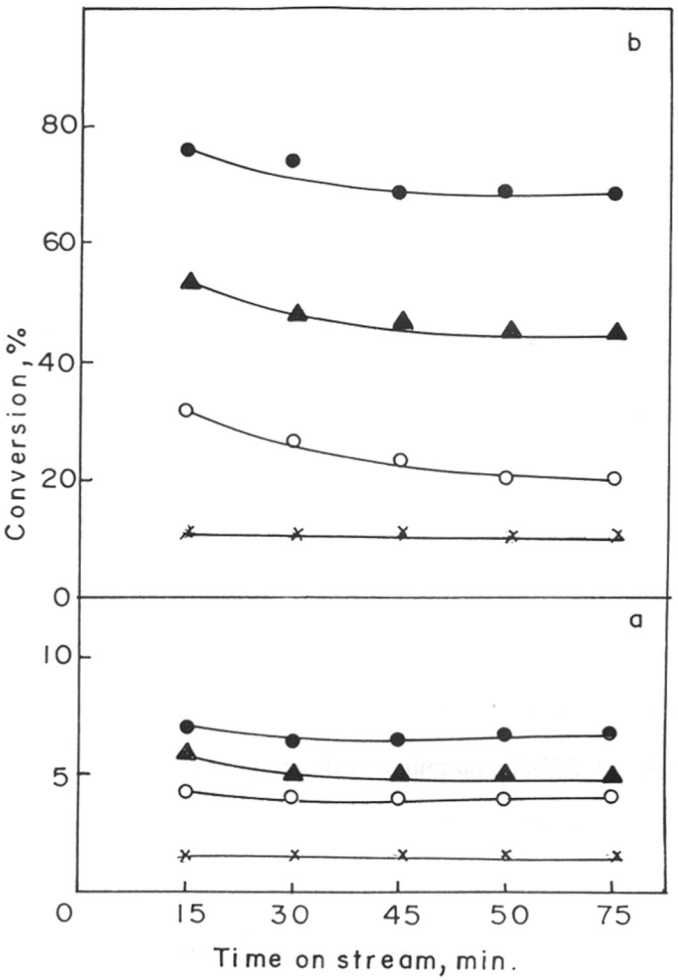

Fig. 5.1 : Effect of temperature and Pt-content on catalyst deactivation with duration of run (time on stream = TOS).

WHSV (h^{-1}) = 1.0; H_2/n-hexane (mole) = 4.5; (×) 523K; (o) 573K; (▲) 598K and (●) 623K.

a : H-ETS-10(E)

b : Pt-(0.3 %)-H-ETS-10(E).

temperatures than at lower temperatures. The decrease, however, is not noticeable beyond about 30 minutes. The data reported in the rest of the section were, hence, collected at a time on stream (TOS) of 45 mins.

The transformation of n-hexane was carried out at atmospheric pressure in the temperature range of 523 to 623K over Pt-ETS-10(E) samples containing different amounts of Pt (0.1 to 0.5 wt.%). The conversion increases with increasing Pt-content at all the temperatures studied (523 to 623K) and reaches a nearly a constant value beyond 0.3% Pt (Fig. 5.2a). The above observation is typical of bifunctional catalysis *[24-26]*. A similar constant conversion beyond 0.5 % Pt has also been reported by earlier workers *[27]* in the case of Pt-HY.

The influence of Pt-content on selectivity to isomerization expressed as the isomerization/cracking ratio (I/C) is depicted in Fig. 5.2b. The I/C ratio increases with Pt content and reaches a maximum at about 0.3 wt.% Pt. Alvarez *et al. [28]* have reported a similar maximum at 1.0 wt.% Pt during their studies on a Pt-H-Y (Si /Al = 9) catalyst. An examination of the distribution of the isohexanes in the product (at 598K; Fig. 5.2c) reveals that the distribution is altered by the addition of Pt. However, the distribution is similar when the Pt content is 0.3% or more. This is also evident from the ratio of the different hexane isomers (Fig. 5.2d). The 2-methyl pentane/3-methyl pentane ratio (2-MP/3-MP) is close to the equilibrium value of 1.57 *[26]* when the Pt content is 0.3% or more. When Pt is absent (H-ETS-10), the ratio is 1.27. Again, the 2,3-dimethyl butane/2,2-dimethyl butane ratio (2,3-DMB/2,2-DMB) is about 3.6 in Pt-ETS-10(E) samples and 6.8 in H-ETS-10(E), much farther from the equilibrium value of 0.86. The conclusions are that the incorporation of Pt greatly enhances the isomerization activity besides assisting the interconversions of the isomeric hexanes.

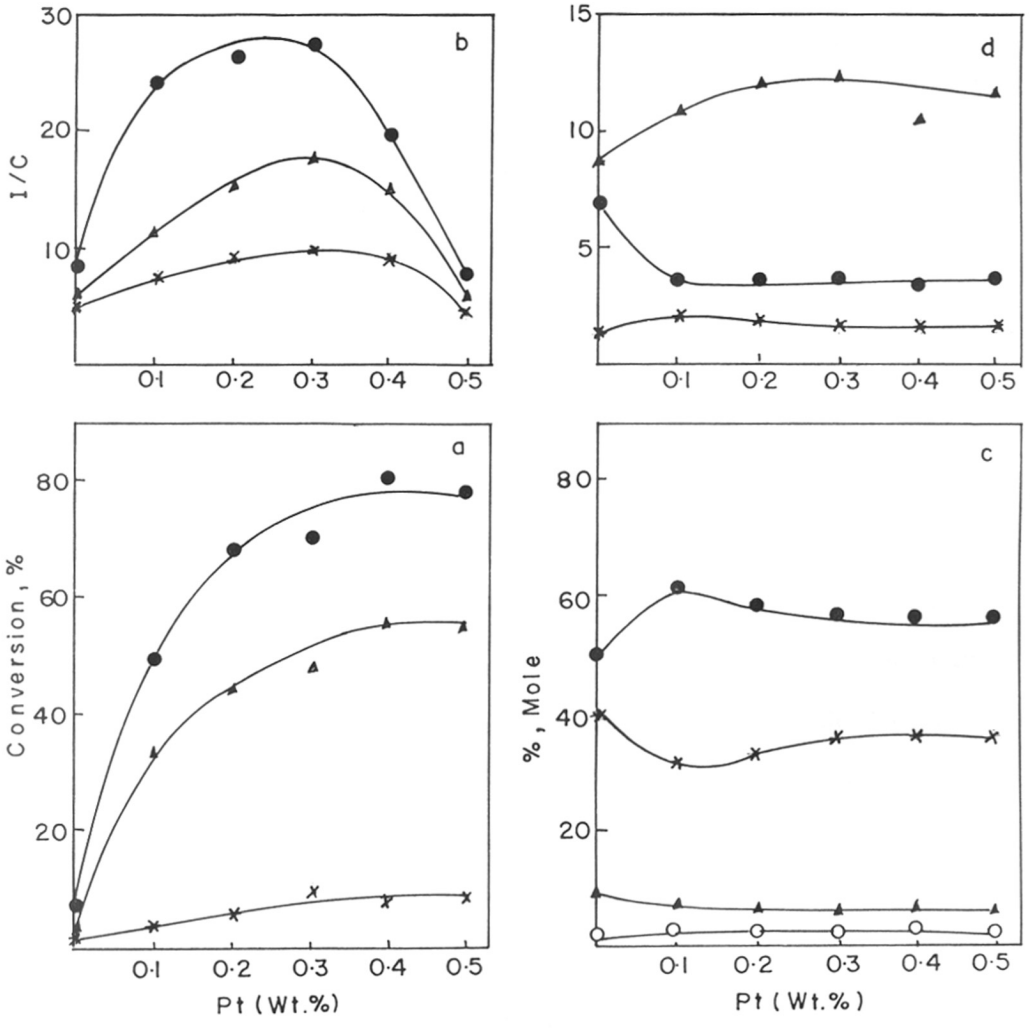

Fig. 5.2 : Influence of Pt-content on n-hexane isomerization.

Catalyst, Pt-(0.3 %)-H-ETS-10(E); WHSV (h^{-1}) = 1.0; H_2/n-hexane (mole) = 4.5; TOS = 45 min.

a : (×) 523K; (▲) 598K and (●) 623K

b : (×) 523K; (▲) 573K and (●) 598K

c : Temp. = 598K; (o) 2,2-DMB; (▲) 2,3-DMB; (×) 3-MP and (●) 2-MP

d : Temp. = 598K; (×) 2-MP/3-MP; (●) 2,3-DMB/2,2-DMB and (▲) MP/DMB.

5.5.3 Influence of Temperature

The influence of temperature on the reaction is presented in Fig. 5.3. n-Hexane conversion increases with temperature, the increase being more marked beyond 573K and at higher Pt contents (Fig. 5.3a). The I/C ratio on the other hand, interestingly, goes through a maximum for all the catalysts (with different Pt contents; Fig. 5.3b). Earlier workers have, however, reported a continuous decrease in the I/C ratio with temperature *[29]*. The reason for the maximum over the Pt-H-ETS-10(E) catalysts is not clear, though a possible explanation is that at moderate temperatures (598K), the desorption of the intermediate iso-olefin and its migration to the metal sites to undergo hydrogenation into stable isoparaffins is maximum. At the still higher temperature of 623K, hydrogenolysis activity by the metal sites becomes more, thereby lowering the I/C ratio. This is suggested by the lower I/C values for the 0.5% Pt catalyst than for the 0.3% Pt catalyst (Fig 5.3b). The concentration of 2-methyl pentane goes through a maximum at an intermediate temperature while those of the dibranched isomers increase (Fig. 5.3c). The decrease in the concentrations of the monobranched isomers is due to their undergoing isomerization into the dibranched isomers and cracking into C_1-C_5 products at higher temperatures. The 2-MP/3-MP ratios are close to the equilibrium value of 1.57 at all the temperatures (Fig. 5.3d). The 2,3-DMB/2,2-DMB ratio and mono/dibranched (M/D) ratios are, however, far from the equilibrium ratios, though there is a tendency for the ratios to approach the equilibrium values. Interestingly, the M/D ratios also go through a maximum at intermediate temperatures.

5.5.4 Influence of Space velocity

Increasing the contact time (1/WHSV) increases conversion and decreases the I/C ratios (Fig. 5.4a). The decrease in I/C ratios is probably mainly due to an increase in cracking, which being slower than the isomerization reactions are favoured at larger residence times. Besides, at these conditions, larger concentrations of the more easily cracked

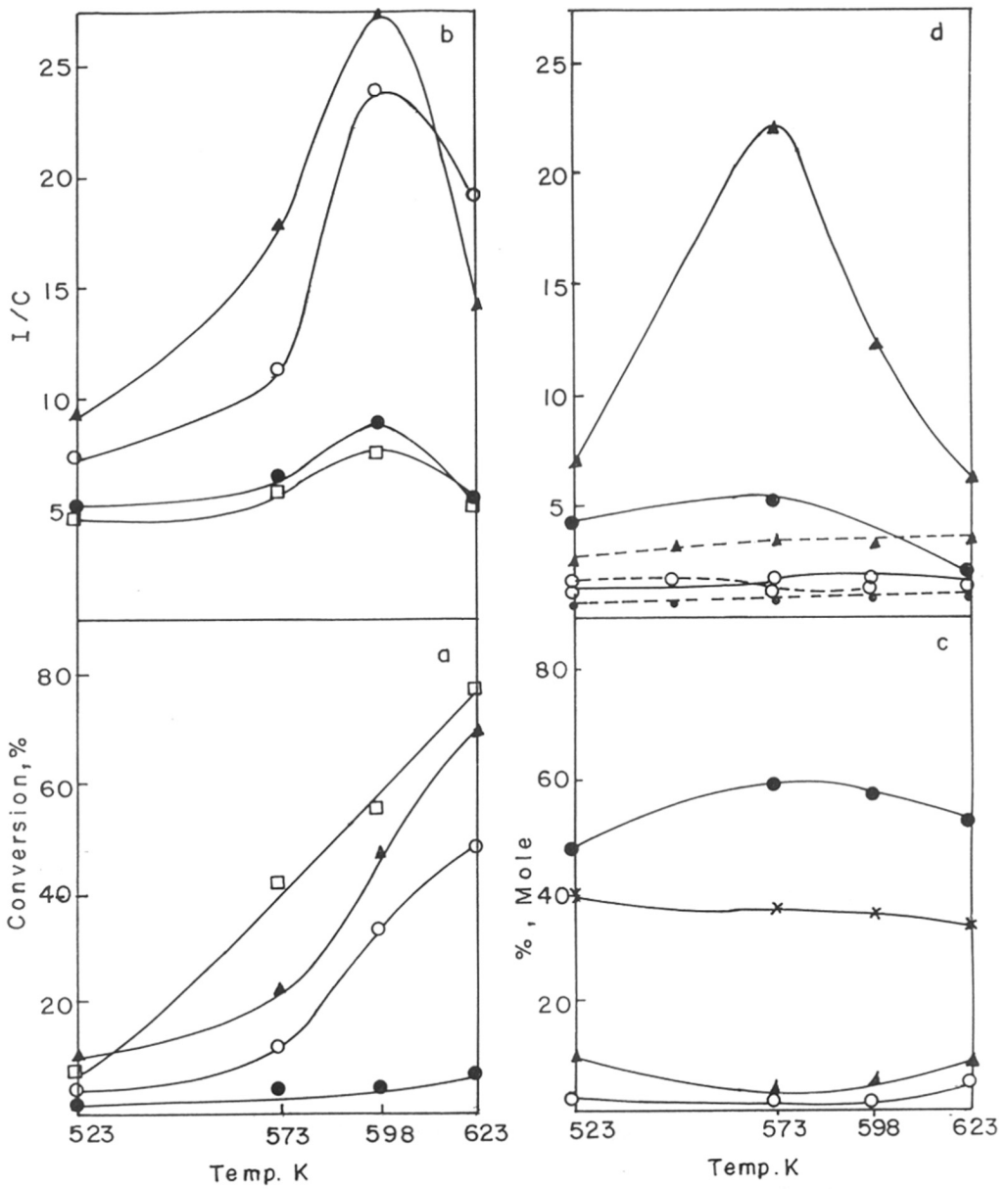

Fig. 5.3 : Influence of temperature on isomerization of n-hexane.

WHSV (h^{-1}) = 1.0; H_2/n-hexane (mole) = 4.5; TOS = 45 min.

a,b : (●) H-ETS-10(E); (o) Pt-(0.1 %)-H-ETS-10(E); (▲) Pt-(0.3 %)-H-ETS-10(E) and ( ) Pt-(0.5 %)-H-ETS-10(E).

c : Catalyst, Pt-(0.3 %)-H-ETS-10(E); (o) 2,2-DMB; (▲) 2,3-DMB; (×) 3-MP and (●) 2-MP

d : Catalyst, Pt-(0.3 %)-H-ETS-10; (●) 2,3-DMB/2,2-DMB; (o) 2-MP/3-MP and (▲) MP/DMB; (—) Experimental data and (---) Thermodynamic data.

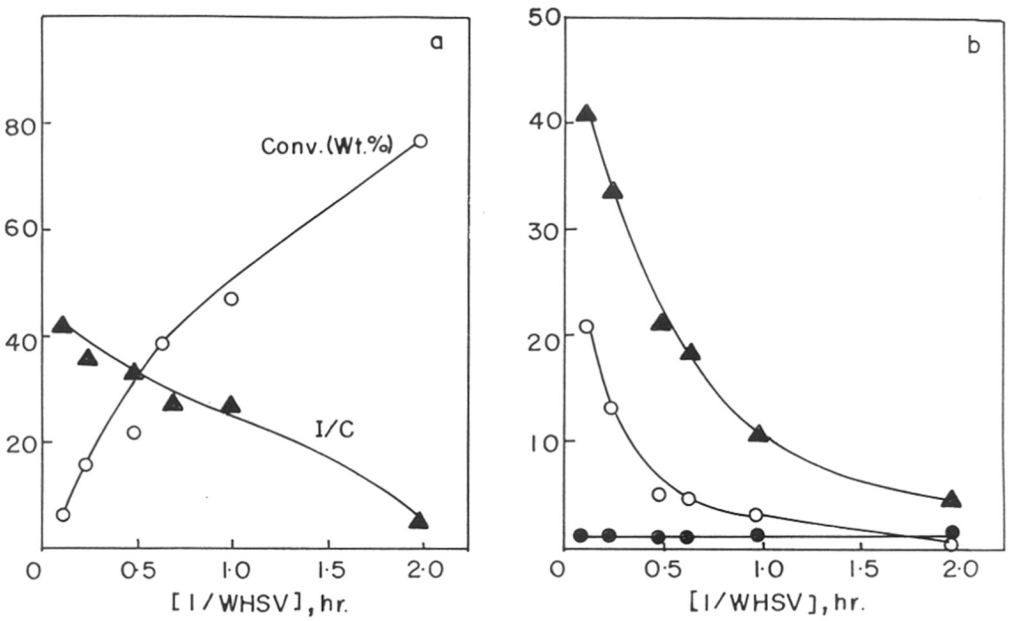

Fig. 5.4 : Influence of space velocity on n-hexane isomerization.

Catalyst, Pt-(0.3 %)-H-ETS-10(E); Temp. = 598K; H_2/n-hexane (mole) = 4.5; TOS = 45 min.

b : (●) 2-MP/3-MP; (o) 2,3-DMB/2,2-DMB and (▲) MP/DMB.

isomerized products (secondary and tertiary carbocations) are present. A 2-MP/3-MP ratio, of 1.62 ± 0.06 is observed in the WHSV range studied. This is close to the equilibrium value of 1.57 *[25]*. However, the 2,3-DMB/2,2-DMB and M/D ratios are farther away from the equilibrium ratios at low contact times and tend to approach the equilibrium values at higher contact times (Fig. 5.4b). These observations suggest that the sequence of n-hexane isomerization reactions is as shown :

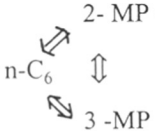

The above sequence has already been suggested by earlier workers *[24,25]*. The ratios of the different products also suggests that the isomerization of 2,3-DMB to 2,2-DMB is the most difficult step. McCaulay *[30]* has reported that it is indeed so; he has found that the relative rates of isomerization of the different hexane isomers over HF/BF_3 are as follows : 2-MP to 3-MP = 58 x 10^3; MP to DMB = 58; 2,3-DMB to 2,2-DMB = 8.6. The low yields of the dibranched isomers over the Pt-ETS-10 samples is probably due to the absence of strong acidity necessary to carry out the difficult mono- to di-branched isomer transformations.

5.5.5 Influence of H_2/n-hexane(mole) Ratio

The influence of $H_2/n\text{-}C_6$ mole ratio is presented in Table 5.4. Increasing the n-hexane mole ratio from 4.5 to 15 (at a constant feed rate of $n\text{-}C_6$) decreases the conversion. The decrease is probably due to an increase in total (H_2 + $n\text{-}C_6$) space velocity and due to a negative (or lower order) with respect to H_2. Earlier workers have reported reaction orders of 0 to 0.3 with respect to $n\text{-}C_6$ and 0.3 to - 0.6 with respect to H_2 for the hydroisomerization of $n\text{-}C_6$ over Pt-mordenite *[19]*. As the hydrogen partial pressure change was only ~ 13% (0.82 to 0.93), the larger change in conversion (~ 27%) from 47.4 to 34.5 suggests that the decrease in conversion is due to both the reasons mentioned above.

Table 5.4 : Influence of H_2/n-hexane (mole) ratio on the product distribution[a].

	H_2/n-hexane (mole) ratio		
	4.5	10.0	15.0
Conversion (%)	47.4	40.9	34.5
I/C[b] ratio	26.8	32.8	37.1
Products (yield, wt.%)			
C_1-C_5	1.7	1.2	0.9
2-MP	25.6	23.4	20.1
3-MP	15.9	13.1	10.2
2,3-DMB	2.6	1.9	2.1
2,2-DMB	0.8	0.6	0.6
Methylcyclopentane	0.7	0.4	0.4
C_6 + aliphatics	0.1	0.3	0.2
2-MP/3-MP	1.6	1.8	2.0
MP/DMB	12.2	14.6	11.2
2,3-DMB/2,2-DMB	3.3	3.2	3.5

[a]Reaction conditions : catalyst, Pt-(0.3 %)-H-ETS-10(E), Temp. = 598K; WHSV (h^{-1}) = 1.0; Pressure = 1 atm.; TOS = 45 min.

[b]I/C = Isomerization (including methylcyclopentane)/cracking; moles of n-C_6 isomerized / moles of n-C_6 cracked.

5.6 AROMATIZATION OF n-HEXANE

5.6.1 Introduction

Catalytic reforming is a major petroleum reforming process and owes its growth to the ever-increasing demand for high-octane gasoline and aromatics *[31]*. The conventional naphtha reforming catalysts such as platinum supported on chlorided Al_2O_3 promoted with one or more metals like Re, Ir, Sn and Ge have poor selectivities for the aromatization of the C_6 fraction *[32-35]*. Bernard *et al. [36,37]* have reported that Pt-containing alkaline L-zeolite is more active and selective than conventional catalysts for the aromatization of n-hexane at 733K and atmospheric pressure. Besoukhanova *et al.[38]* observed that the activity of L-zeolite in n-hexane dehydrocyclization increases with its basicity. The non-acidic, Pt-L reforming catalyst differs from conventional catalysts (Pt-Al_2O_3 *etc.*) in that it is monofunctional, only the metal function being active. Both electronic interactions between the metal and the support and structural parameters of the zeolite (steric effects) have been proposed to explain the spectacular aromatization activity of Pt-L.

ETS-10 consists of corner-sharing octahedral Ti^{4+} and tetrahedral Si^{4+} ions. As a result of the octahedral coordination of the Ti^{4+} ions, each Ti^{4+} is associated with two negative charges balanced by alkali ions (Na^+/K^+). Hence, ETS-10 has a high cation exchange capacity and is highly 'alkaline' in the Na^+/K^+-form. The aromatization of n-hexane over Pt supported on alkaline ETS-10(E) was studied. Comparison of the activities of the above catalysts at the same conditions with a commercial Pt-Al_2O_3 catalyst was also studied.

5.6.2 Effect of nature of the Exchanged Metal ion on the Aromatization of n-Hexane

The n-hexane adsorption capacities of M-ETS-10 (M = Li, Na, K, Rb, Cs, Mg, Ca, Ba, and La) samples have already been discussed in Chapter IV. The BET surface areas and

micropore volumes (discussed in Chapter IV) measured from N_2-adsorption (Omnisorp 100CX, Coulter Corporation, USA) are similar for the samples, a small decrease being noticed in the case of the Cs-ETS-10 presumably due to the large Cs ions occupying some pore volume.

The NH_3-TPD spectra of the M-ETS-10(E) samples have been presented in Chapter III (Fig. 3.22). The areas of the peaks (on constant weight basis) decrease in the order : Li-ETS-10(E) > Na-ETS-10(E) > Ba-ETS-10(E) > K-ETS-10(E) > Rb-ETS-10(E) > Cs-ETS-10(E). The decrease noticed is actually an artifact of the increasing weight of the exchanged ions (Li to Cs) and a corresponding decrease in the actual molecular sieve component. The desorption profiles of all the samples indicate that the acid sites are mostly of weak to moderate nature. Based on the peak maxima, the alkaline ETS-10 samples can be arranged in the following order of acid strengths : Li-ETS-10(E) $\simeq$ Na-ETS-10(E) > K-ETS-10(E) > Rb-ETS-10(E) > Cs-ETS-10(E). The above order is exactly as expected; the substitution by more alkaline (electro-positive) metal decreases the acidity to a larger extent.

The Pt dispersion values of different ETS-10(E) samples determined by hydrogen chemisorption have been presented in Chapter III (Table 3.5). The dispersion values for the samples range from 45% to 85%, the values being higher for the more basic samples.

The transformation of n-hexane was carried out at 723, 748 and 773K at atmospheric pressure over all the metal exchanged catalysts and two commercial Pt-Al_2O_3-Cl catalysts at identical conditions to compare their performances. The results for the different catalysts obtained at 723K and 773K are presented in Table 5.5. Both conversion of n-hexane and the yield of benzene increase in the order Li < Na < K < Rb < Cs. It is also observed that TON [turn over number; number of molecules converted (produced) per surface Pt atom per hour] for conversion and benzene yield also increase in the same order (Table 5.5). This removes any doubt that the above trend in activity was due to differences in Pt-dispersion. The

Table 5.5 : n-Hexane aromatization activity of Pt-alkali metal exchanged ETS-10(E)[a].

	Li-ETS-10		Na-ETS-10		K-ETS-10		Rb-ETS-10		Cs-ETS-10		$Pt-Al_2O_3$(0.6%)
	723K	773K	723K	773K	723K	773K	723K	773K	723K	773K	723K
Conv. (%)	11.7	29.9	17.2	42.3	27.2	52.4	47.0	69.5	84.8	98.1	33.0
Conv. (TON)[b]	2.94×10^2	7.53×10^2	3.75×10^2	9.22×10^2	6.29×10^2	1.21×10^3	8.59×10^2	1.27×10^3	1.32×10^3	1.52×10^3	4.67×10^2
Benz. Sel.(%)[c]	5.1	8.4	5.2	9.7	14.0	35.9	30.8	37.1	34.5	49.6	6.7
Benz. (TON)[b]	16.66	69.43	21.62	98.53	97.03	479.48	292.3	520.00	501.60	833.70	34.36
Products (yield, wt.%)											
C_1	0.2	1.5	0.4	2.3	0.8	1.9	2.1	6.3	7.0	15.7	1.2
C_2	0.5	2.6	1.0	4.8	1.3	1.3	1.6	1.7	1.8	4.4	1.1
C_3	0.6	2.9	1.4	6.9	1.8	1.2	1.4	1.8	1.8	5.1	2.2
C_4	0.4	1.7	0.5	3.1	1.2	1.4	1.7	4.6	4.7	9.1	4.1
C_5	0.1	0.1	0.1	0.5	0.7	3.3	3.0	13.4	16.4	9.1	1.3
i-C_6[d]	0.7	0.9	0.3	0.8	1.0	3.7	3.2	9.2	12.2	3.0	6.8
$McyC_5$[e]	0.1	0.4	0.4	0.4	0.7	1.8	1.5	3.5	5.4	0.4	1.0
Benz.	0.6	2.5	0.9	4.1	3.8	18.8	14.5	25.8	29.3	48.7	2.2
Others (C_6^+)	8.5	17.3	12.2	19.4	15.9	19.0	18.0	3.2	6.2	2.6	13.1

[a]Reaction Conditions : all ETS-10 catalysts contained 0.4 wt.% Pt; WHSV = 2 (h^{-1}); Press. = 1 atm.; TOS(Time on Stream) = 2h; H_2/n-C_6(mole) = 4.5.

[b]TON (turn over number) calculated as number of molecules of n-hexane converted or benzene formed per surface platinum atom per hour.

[c]Benz. Sel.(%) = (Benzene in product × 100) / n-Hexane conversion

[d]i-C_6 = 2,2-Dimethylbutane + 2,3-Dimethylbutane + 2-Methylpentane + 3-Methylpentane; [e]$McyC_5$ = Methyl cyclopentane.

performance of the Pt-Al_2O_3 is much inferior to those of the Pt-M-ETS-10(E) samples (except Pt-Li-ETS-10). Hence, the basicity of metal exchanged ETS-10(E) appears to be the most important factor responsible for the enhanced aromatization of n-hexane. In a way, the performance of the Pt-M-ETS-10(E) catalysts is similar to those of the Pt-M-L catalysts *[38]*. Besoukhanova *et al. [38]* have shown that in case of Pt-L zeolites also, the activity and benzene selectivity increase in the same order reported by us on exchange with different alkali ions. These authors have also shown by i.r. shifts of absorbed CO (on Pt) that the Pt is electron rich in these catalysts, the electron richness of the Pt-clusters arising from electron transfer from the basic O^{2-} ions in the zeolite lattice *[38]*. The extent of electron transfer from the lattice to the metal will depend on the net charge on the O^{2-} ion and the intermediate electronegativity (S_{int}) of the zeolite; S_{int} will be inversely related to the oxygen charge *[39]*. Barthomeuf *[39]* has reported an inverse relationship between the benzene yield (from the n-hexane) and S_{int} of a number of Pt-L zeolites exchanged with various cations. The relationship between benzene selectivity, S_{int} and oxygen charge in the case of Pt-alkali-exchanged ETS-10(E) samples is presented in Fig. 5.5. Values of S_{int} and oxygen charge were calculated following the method described by Mortier *[40]*. The similarity of the relationships in case of both the catalysts (Pt-M-ETS-10 and Pt-M-L) suggests that the reasons governing activity trends of the Pt-alkaline-L and Pt-alkaline-ETS-10 samples are similar.

A set of Arrhenius plots (Fig. 5.6) were constructed using the data obtained at 723, 748 and 773K and E_a and A were calculated. The Arrhenius plots (Fig. 5.6) intersected in a narrow range at about $1/T = (1.1625 \pm 0.005) \times 10^{-3}$ K^{-1} giving the T_i (isokinetic temperature) = 860 ± 5 K. The values of A and E_a decreased systematically with increase in basicity of the support leading to a compensation effect (Fig. 5.7).

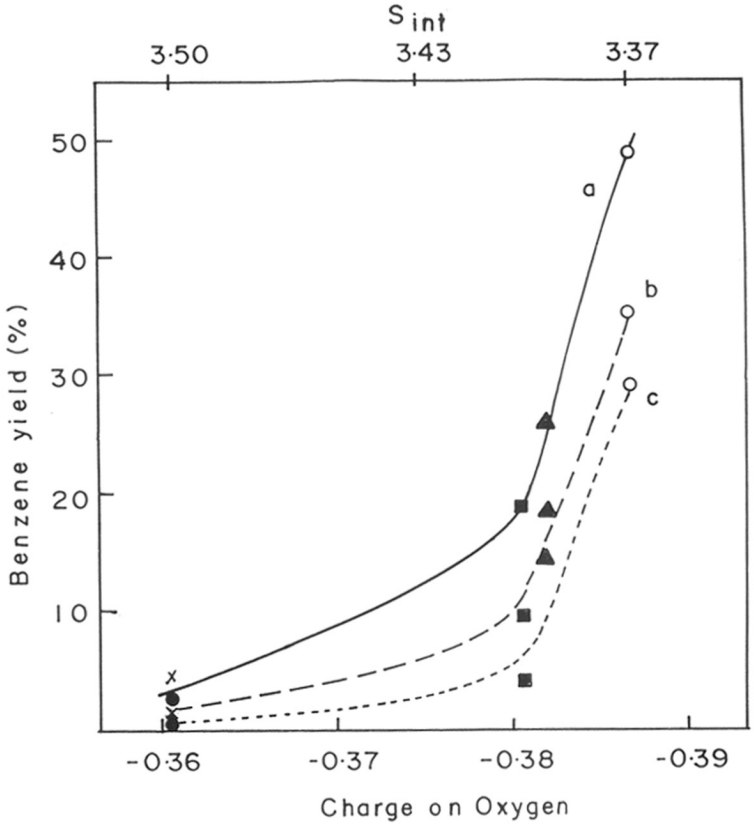

Fig. 5.5 : Benzene yield in n-hexane aromatization as a function of S_{int} and oxygen charge of Pt(0.4%)-ETS-10(E) samples exchanged with (•) Li-ETS-10, (×) Na-ETS-10, (■) K-ETS-10, (▲) Rb-ETS-10 and (o) Cs-ETS-10

a : 773K, b : 748K and c : 723K.

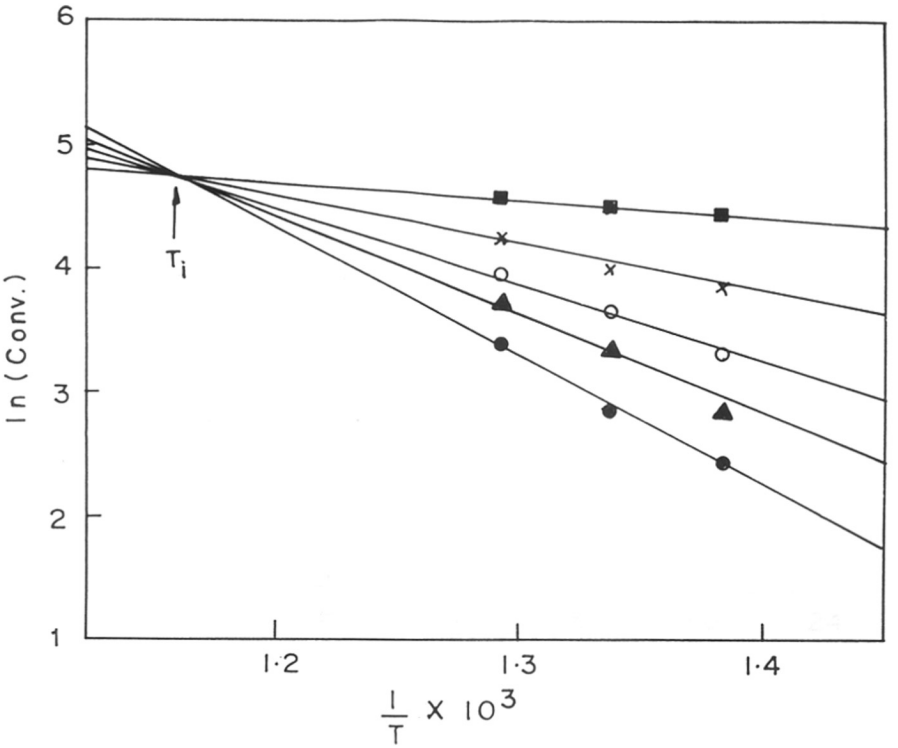

Fig. 5.6 : Arrhenius plots in n-hexane aromatization over a series of alkali metal exchanged ETS-10(E).

WHSV (h^{-1}) = 2.0, H_2/n-hexane(mole) = 4.5, TOS = 2h

(•) Li-ETS-10, (▲) Na-ETS-10, (o) K-ETS-10, (×) Rb-ETS-10 and (■) Cs-ETS-10.

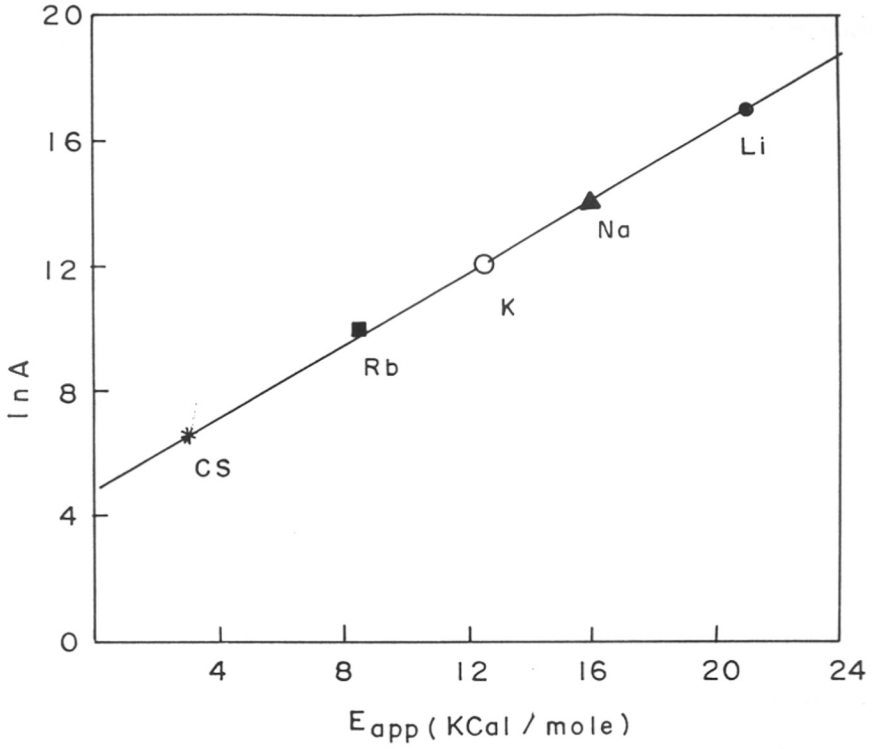

Fig. 5.7 : Compensation effect plot showing linear relationship between E_{app} and lnA_{app}.

The compensation effect describes a sympathetic variation of activation energy (E_{app}) with the logarithm of the pre-exponential factor A. It can be expressed as

$$\ln A = mE + c \quad \text{----------(1)}$$

where m and c are constants. The above effect is often observed when a given reaction is carried out on a series of different catalysts or when the same catalyst is used for a number different reactions *[41,42]*. The value of the isokinetic temperature T_i derived from the slope by the relation

$$T_i = (mR)^{-1} \quad \text{----------(2)}$$

where R is the gas constant, is 867K. This value is similar to the T_i value (860 ± 5 K) obtained directly from the intersection of the Arrhenius plots. The observation of the isokinetic temperature confirms the above compensation effect to be a true one.

The influence of exchange of ETS-10(E) with different alkaline earth metals (Mg^{2+}, Ca^{2+} and Ba^{2+}) and La^{3+} ions on catalytic activity is presented in Table 5.6. The activities and benzene selectivities increase again in the order of increasing basicity of the exchanged cations : Ba > Ca > Mg. Larsen and Halter *[43]* carried out competitive hydrogenation of toluene and benzene over a series of Pt-L catalysts containing Mg, Ca and Ba ions. They found that the ratio of adsorption constants for toluene and benzene ($K_{t/b}$) increased in the order Mg > Ca > Ba, which is also the order of decreasing basicity. In essence, the experiments suggested that electron transfer from lattice to the Pt-metal increased with increasing basicity of the exchanged cations.

5.6.3 Studies on Pt-Cs-ETS-10

Among the alkali metal exchanged catalysts, the Cs-exchanged catalyst had the highest conversion and aromatics selectivity (Table 5.5). This catalyst was investigated in greater detail.

Table 5.6 : n-Hexane aromatization activity of alkaline earth and La exchanged Pt-ETS-10(E)[a].

	Mg-ETS-10		Ca-ETS-10		Ba-ETS-10		La-ETS-10	
	723K	773K	723K	773K	723K	773K	723K	773K
Conversion (%)	35.9	41.2	16.1	72.9	59.6	88.9	31.6	51.9
Benzene Select. (%)[b]	2.8	8.7	28.0	35.4	28.7	47.3	8.2	16.4
Products (yield, wt.%)								
C_1	0.4	0.5	0.4	4.1	3.1	6.5	0.5	1.1
C_2	0.7	0.9	0.3	2.4	1.1	1.8	1.0	1.7
C_3	3.2	4.3	0.4	2.5	1.0	1.8	2.0	2.9
C_4	1.9	4.3	0.6	3.6	1.9	3.6	1.4	2.4
C_5	1.9	3.7	0.8	6.6	7.0	11.3	1.0	2.0
i-C_6[c]	7.5	5.6	2.7	7.5	11.7	7.5	7.4	8.9
$MCyC_5$[d]	0.5	2.0	2.0	4.8	7.0	2.6	1.2	2.5
Benzene	1.0	3.6	4.5	25.8	17.1	42.0	2.6	8.5
Others (C_6^+)	18.8	16.3	4.4	15.6	9.7	11.8	14.5	21.9

[a]Reaction Conditions : All catalysts contain 0.4 wt.% Pt; WHSV = 2 (h^{-1}); Press. = 1 atm.; TOS = 2h; H_2/n-C_6(mole) = 4.5.

[b]Benzene select. (%) = (Benzene in product × 100) / n-hexane conversion

[c]i-C_6 = 2,2-Dimethylbutane + 2,3-Dimethylbutane + 2-Methylpentane + 3-Methylpentane

[d]$McyC_5$ = Methyl cyclopentane

5.6.3.1 Influence of Pt-content

The influence of Pt-content on conversion and benzene yields at three different temperatures is presented in Fig. 5.8. Both conversion and benzene yields increase with Pt content and reach a steady value at about 0.4 wt.% (Fig 5.8a). The maximum conversion increases with temperature and is nearly 100% at 773K. Similarly, the benzene yields increase with increasing temperature (Fig. 5.8b). As the temperature increases, the C_5 and isohexanes increase.

5.6.3.2 Influence of Duration of Run

The influence of duration of run on conversion and benzene selectivity are presented in Fig. 5.9a. The catalyst (0.4 wt.% Pt-Cs-ETS-10) deactivates slightly with duration of run, the deactivation being slightly faster at higher temperatures. Similarly, benzene selectivity also decreases more rapidly at higher temperatures.

5.6.3.3 Influence of Temperature

The influence of temperature on conversion and benzene yield at different Pt-loadings has already been presented in Fig. 5.8. The detailed distribution of products at two temperatures for the Pt(0.4 wt.%)-Cs-ETS-10(E) catalyst has been presented in Table 5.5. The changes in the product patterns at the two temperatures indicate essentially increased hydrogenolysis due to the metal at higher temperatures; the C_1 and C_5 yields increase rapidly. Besides, the low i/n ratio of the C_4 hydrocarbon even at 773K (the equilibrium values at 800K is 0.56) suggests that the catalyst is highly non-acidic. At least, in the case of the C_6 fraction, the isomerization to the 2- and 3-methyl pentanes could have also taken place on the Pt sites through C_5 ring closure and opening reactions *[44]*. The presence of methylcyclopentane in the product suggests such a possibility.

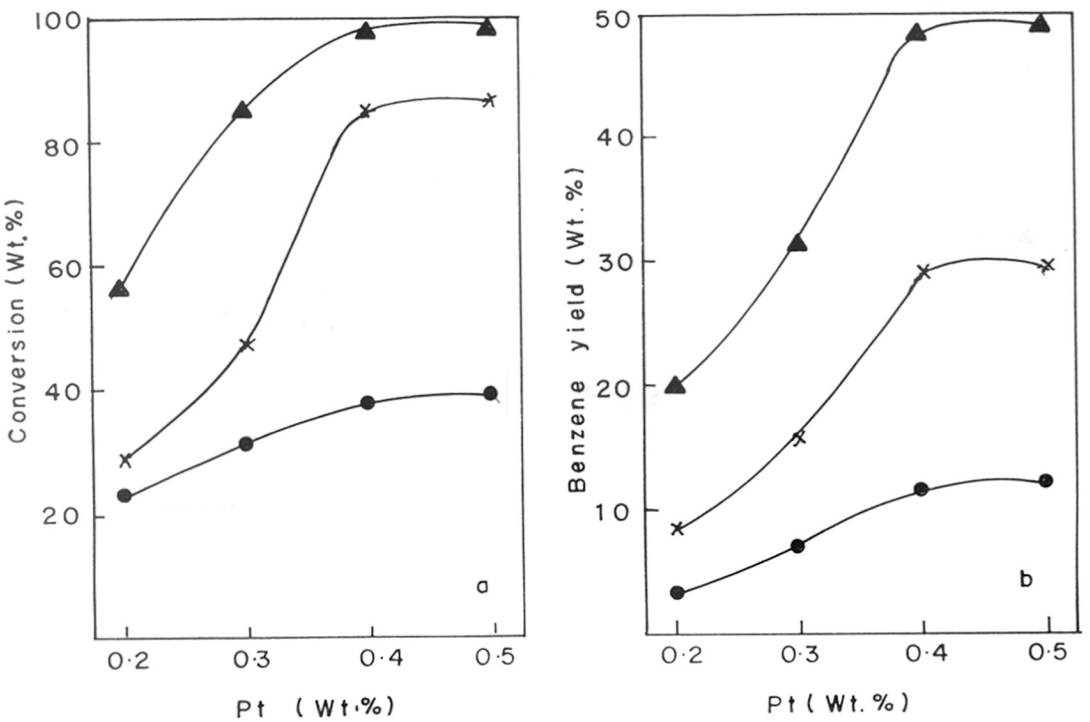

Fig. 5.8 : Influence of Pt-content on n-hexane aromatization.

Catalyst, Pt(0.4%)-Cs-ETS-10(E); WHSV (h^{-1}) = 2.0; H_2/n-hexane(mole) = 4.5;

TOS = 2h.

a,b : (•) 673K, (×) 723K and (▲) 773K.

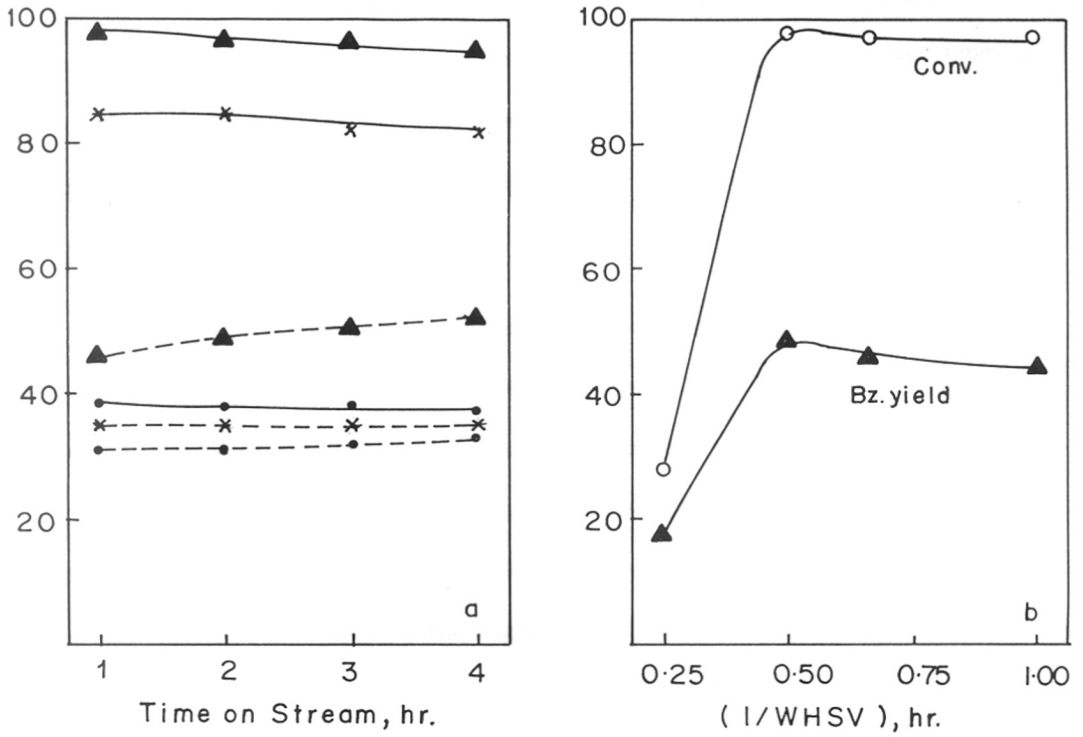

Fig. 5.9 : (a) Effect of temperature on catalyst deactivation and benzene selectivity with duration of run (time on stream = TOS).

Catalyst, Pt(0.4%)-Cs-ETS-10(E); WHSV (h^{-1}) = 2.0; H_2/n-hexane(mole) = 4.5

(–) Conversion (wt.%) and (---) Benzene selectivity (%)

(b) Influence of space velocity on n-hexane aromatization

Catalyst, Pt(0.4%)-Cs-ETS-10(E); Temp. = 773K; H_2/n-hexane(mole) = 4.5; TOS = 2h.

5.6.3.4 Influence of Space velocity

The influence of space velocity on conversion and benzene yield at 773K are presented in Fig. 5.9b. The conversion increases rapidly with contact time and reaches a maximum of about 98% at a contact time of about 0.5 h. At higher contact times, the conversion is nearly constant (~98%) though the benzene yield decreases marginally due to greater hydrogenolysis by Pt and increased formation of the C_1 to C_5 fraction (Table 5.7).

5.6.3.5 Comparison with Pt-Al_2O_3

The results of n-hexane aromatization over a commercial Pt-Al_2O_3 sample containing 0.3 and 0.6 wt.% Pt are presented in Table 5.8 and Fig. 5.10. It is immediately apparent that Pt-ETS-10(E) catalysts produce many times more benzene, the benzene selectivity over Pt-Cs-ETS-10(E) being 34.5% when compared to 6.7% over the Pt(0.6%)-Al_2O_3 catalyst. In this respect, the monometallic Pt-ETS-10 catalysts appear to be very similar to the Pt-K-L zeolites reported earlier *[36,37]*. The deactivation rate (Fig. 5.10a) is less over Pt-Cs-ETS-10 while it is much more rapid in the case of the Pt-Al_2O_3 catalyst.

Table 5.7 : n-Hexane aromatization activity : influence of space velocity.

	WHSV (h^{-1})			
	1.0	1.5	2.0	4.0
Conversion (%)	97.6	97.2	98.1	28.8
Benzene Select. (%)[b]	45.1	47.1	49.6	64.6
Products (yield, wt.%)				
C_1	5.8	12.0	15.7	0.5
C_2	1.8	3.7	4.4	1.6
C_3	1.7	4.0	5.1	1.5
C_4	2.8	7.3	9.1	1.1
C_5	10.1	12.1	9.1	0.4
i-C_6[c]	7.9	5.1	3.0	1.0
$MCyC_5$[d]	4.8	1.2	0.4	0.8
Benzene	44.0	45.8	48.7	18.6
Others (C_6^+)	18.7	6.0	2.6	3.3

[a]Reaction Conditions : Catalyst, Pt(0.4%)-Cs-ETS-10(E); Temp. = 773K; Press. = 1 atm.; TOS = 2h; H_2/n-C_6(mole) = 4.5

[b]Benzene select. (%) = (Benzene in product × 100) / n-hexane conversion

[c]i-C_6 = 2,2-Dimethylbutane + 2,3-Dimethylbutane + 2-Methylpentane + 3-Methylpentane

[d]$McyC_5$ = Methyl cyclopentane.

Table 5.8 : Comparison of n-hexane aromatization activity of Cs-ETS-10(E) and Al_2O_3[a]

	Cs-ETS-10 (0.4 wt.% Pt)	Pt-Al_2O_3 (0.3 wt.% Pt)	Pt-Al_2O_3(0.6 wt.% Pt)
Conversion (%)	84.8	26.9	33.0
Benzene Select. (%)[b]	34.5	5.2	6.7
Products (yield, wt.%)			
C_1	7.0	0.7	1.2
C_2	1.8	1.5	1.1
C_3	1.8	3.2	2.2
C_4	4.7	4.4	4.1
C_5	16.4	0.8	1.3
i-C_6[c]	12.2	3.7	6.8
$MCyC_5$[d]	5.4	0.9	1.0
Benzene	29.3	1.4	2.2
Others (C_6^+)	6.2	10.3	13.1

[a]Reaction Conditions : Temp. = 723K; WHSV = 2 (h^{-1}); Press. = 1 atm.; TOS = 2h; H_2/n-C_6(mole) = 4.5.

[b]Benzene select. (%) = (Benzene in product × 100) / n-hexane conversion

[c]i-C_6 = 2,2-Dimethylbutane + 2,3-Dimethylbutane + 2-Methylpentane + 3-Methylpentane

[d]$McyC_5$ = Methyl cyclopentane.

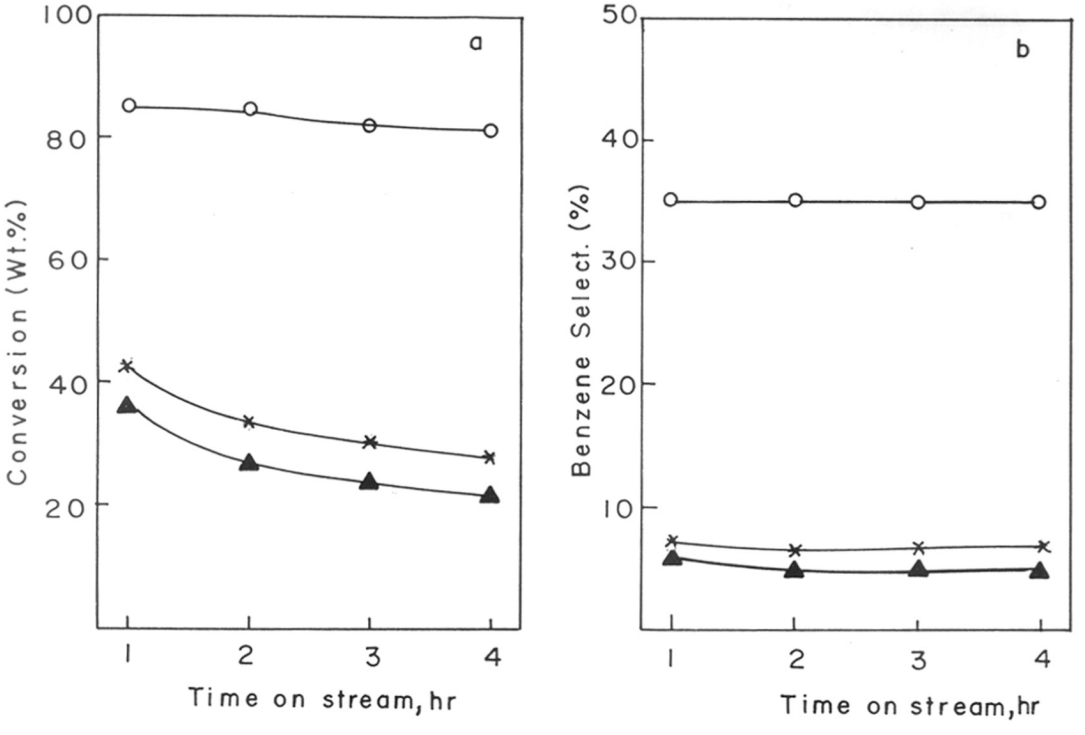

Fig. 5.10 : Aromatization of n-hexane : comparison of Pt-Cs-ETS-10(E) and Pt-Al_2O_3

Temp. = 723K, WHSV (h^{-1}) = 2.0, H_2/n-hexane(mole) = 4.5.

(o) Pt(0.4%)-Cs-ETS-10(E), (×) Pt(0.6%)- Al_2O_3 and (▲) Pt(0.3%)-Al_2O_3.

5.7 REFERENCES

1. Jacobs, P.A., and Martens, J.A., *Stud. Surf. Sci. Catal.*, **28**, 23 (1988).
2. Weitkamp, J., and Ernst, S., *Stud. Surf. Sci. Catal.*, **38**, 367 (1988).
3. Csicsery, S.M., *Zeolites*, **4**, 202 (1984).
4. Anderson, M.W., Terasaki, O., Ohsuna, T., Philippou, A., Mackay, S.P., Ferreira, A., Rocha, J., and Lidin, S., *Nature,* **367**, 347 (1994).
5. Anderson, M.W., Tarasaki, O., Ohuna, T., Malley, P.J.O., Philippou, A., Mackay, S.P., Ferreira, A., Rocha, J., and Lidin, S., *Philos. Mag. B,* **71**, 813 (1995).
6. Carli, R., Bianchi, C.L., and Ragaini, V., *Catal. Lett.*, **33**, 49 (1995).
7. Jacobs, P.A., and Martens, J.A., Proceedings 7th International Zeolite Conference, Tokyo, August 17-22, p. 23 (1986).
8. Jacobs, P.A., Leeman, H.E., and Uytterhoeven, J.B., *J. Catal.*, **33**, 31 (1974).
9. Karge, H.G., Ladebeck, J., Sarbak, Z., and Hataba, K., *Zeolites*, **2**, 94 (1982).
10. Ratnasamy, P., Sivasanker, S., and Vishnoi, S., *J. Catal.*, **69**, 428 (1981).
11. Giordano, N., Vitarelli, P., Cavallaro, S., Ottana, R., and Lembo, R., Proceedings 6th International Zeolite Conference, Butterworths, London, p. 331 (1984).
12. Stull, D.R., Westrum, E.F. Jr., and Sinke, G.C., The Chemical Thermodynamics of Organic Compounds, John Wiley and Sons, New York, (1969).
13. Martens, J.A., Perez-Pariente, J., Sastre, E., Corma, A., and Jacobs, P.A., *Appl. Catal.*, **45**, 85 (1988).
14. Van Broekhoven, E., and Wijngaards, H., Proceedings of the AKZO Catalysts Symposium, Scheveningen, CIP Data Koninklijke Bibliotheek, Den Haag, p. F-8 (1988).
15. Kumar, R., and Reddy, K.R., *Microporous Mater.*, **3**, 195 (1994).
16. Cusher, N.A., Greenouch, P., Rolfe, J.R.K., and Weiszmann, J.A., in R.A. Meyers (Editor), *Handbook of Petroleum Refining Process,* McGraw-Hill, New York, ch. 5, p. 51 (1986).

17. Kouwenhoven, H.W., in W.M. Mier and J.B. Uytterhoeven (Editors), *Molecular sieves, Adv. Chem. Ser.*, American Chemical Society, Washington, **121**, 529 (1973).

18. La Pierre, R.B., and Partridge, R.D., Eur. Pat. Appl., 94827 (1983).

19. Guisnet, M., Fouche, V., Belloum, M., Bournonville, J.P., and Travers, C., *Appl. Catal.*, **71**, 295 (1991).

20. Leu, L.J., Hou, L.Y., Kang, B.C., Li, C., Wu, S-T, and Wu, J.C., *Appl. Catal.*, **69**, 49 (1991).

21. Campelo, J.M., Lafont, F., and Marinas, J.M., *Zeolites,* **15**, 97 (1995).

22. Ratnasamy, P., Borade, R.B., Sivasanker, S., Shiralkar, V.P., and Hegde, S.G., *Acta Phys. Chem.*, **31**, 137 (1985).

23. Smirniotis, P.G., Ruckenstein, E., *Appl. Catal.*, **123**, 59 (1995).

24. Weisz, P.B., *Adv. Catal.*, **13**, 137 (1962).

25. Jacobs, P.A., Uytterhoeven, J.B., Steijns, M., Froment, G., and Weitkamp, J., in L.V.C. Rees (Ed.), Proceedings of the Fifth International Conference on Zeolites, Naples, Heyden and Sons, London, p. 607 (1980).

26. Chen, J-K, Martin, A.M., Kim, Y.G., and John, V.T., *Ind. Eng. Res.*, **27**, 401 (1988).

27. Giannetto, G.E., Perot, G.R., and Guisnet, M.R., *Ind. Eng. Chem. Prod. Res. Dev.*, **25**, 481 (1986).

28. Alvarez, F., Giannetto, G., Guisnet, M., and Perot, G., *Appl. Catal.*, **34**, 353 (1987).

29. Ravishankar, R., and Sivasanker, S., *Appl. Catal.*, **142**, 47 (1996).

30. McCaulay, D.A., *J. Am. Chem. Soc.*, **84**, 6437 (1959).

31. Sinfelt, J.H., in Anderson, J.R., and Boudart, M., (Editors), *Catalysis, Science and Technology*, Spring, New York, Vol. **1**, 257 (1981).

32. Kluksdahl, H.E., US Pat. 3415737 (1968).

33. Carter, J.L., Mc Viker, G.C., Weisshan, M., Kmak, W.S., and Sinfelt, J.H., *Appl. Catal.* **3**, 327 (1982).

34. Burch, R., and Mitchell, A.J., *Appl. Catal.*, **6**, 121 (1983).

35. Beltramini, J.N., and Trimm, D.L., Proc. 9th International Congress on Catalysis,

Calgary, Canada, p. 1268 (1990).

36. Bernard, J.R., and Nury, J., US Pat. 4,104,320 to Elf France (1978).

37. Bernard, J.R., in L.V.C. Rees (Editor), Proceedings 5th Int. Conf. Zeolites, Heyden, London, 1980, 686.

38. Besoukhanova, C., Guidot, J., and Barthomeuf, D., *J. Chem. Soc. Faraday Trans. I*, **77**, 1595 (1981).

39. Barthomeuf, D., *Stud. Surf. Sci. Catal.*, **65**, 157 (1991).

40. Mortier, W.J., *J. Catal.*, **55**, 138 (1978).

41. Bond, G.C., "Catalysis by Metals" Chap. 7, Academic Press, New York, (1962).

42. Louis Raj, S., and Srinivasan, V., *J. Catal.*, **65**, 121 (1980).

43. Larsen, G., and Haller, G.L., *Catal. Lett.*, **3**, 1003 (1989).

44. Derouane, E.G., and Vanderveken, D.J., *Appl. Catal.*, **45**, L15 (1988).

CHAPTER VI

SUMMARY AND CONCLUSIONS

6.1 SYNTHESIS AND KINETICS OF CRYSTALLIZATION

ETS-10 could be synthesized by three different synthesis procedures *viz.*, in the absence of templates, in the presence of templates and by a rapid method using $TiCl_4$.

6.1.1 Synthesis in Absence of Templates

ETS-10 could be synthesized both in the presence and absence of ETS-4 seeds. It was found that ETS-10 synthesized in absence of seeds of ETS-4, was not pure and contained amorphous materials. The presence of ETS-10 seeds yielded good crystalline materials. From the kinetics of crystallization it was found that the amount of seed used influenced the crystallite size of ETS-10. On decreasing the seed content from 14.0 wt.% to 0.9 wt.% (based on SiO_2 input) individual cuboids tended to form clusters of increasing size. Similarly, the H_2O/SiO_2 ratio of the synthesis gel influenced the nature of the product.

6.1.2 Synthesis in the Presence of Templates

ETS-10 could be synthesized in the presence of the organic templates, choline chloride and the bromide salt of hexaethyl diquat-5 without using ETS-4 seeds. The templates reduced the synthesis time required for obtaining well crystallized samples. The size and morphology of the crystals were altered by the templates. The use of hexaethyl diquat-5 led to a purer material than choline chloride.

6.1.3 A rapid Method of Synthesis using $TiCl_4$

While $TiCl_3$ was used as the source of Ti in the above procedures which required synthesis time of many days, the use of $TiCl_4$ reduced the time to 16 hrs. The use of $TiCl_4$ significantly altered the crystallization process, the morphology and the purity of ETS-10. Kinetic analysis of the crystallization curves revealed that the synthesis of ETS-10 using $TiCl_4$ as the titanium source was energetically more favourable and the use of $TiCl_4$ reduced

the nucleation time and accelerated the crystal growth. Besides, ETS-10 synthesized using $TiCl_4$ was highly crystalline and pure.

6.2 CHARACTERIZATION

X-ray powder diffraction analysis of the samples suggested that ETS-10 synthesized by using the $TiCl_4$ as the titanium source was highly crystalline and pure. The stability of the samples were also checked by XRD after calcining at different temperatures and the studies revealed that the sample synthesized using $TiCl_4$ was more stable than those synthesized using $TiCl_3$.

UV-Vis(DRS) studies showed that the Ti^{4+} ions are in an octahedral symmetry in ETS-10. IR studies revealed the presence of a band at 970 cm^{-1}, attributed by Khouw and Davis to Si-O-Ti or Si-O$^-$ vibrations in TS-1, in acid washed ETS-10 samples. Thermal analysis of ETS-10 samples indicated that ETS-10 synthesized using $TiCl_4$ was more stable. The stability of the sample could be improved by exchanging with ions like La^{3+}. Scanning electron micrographs revealed that the particle sizes of the ETS-10 samples were between 1-4 μm. The size and morphology of the crystals were altered by the template and water content. ETS-10 synthesized rapidly using $TiCl_4$ was made up of nearly uniform cuboids of < 1 μm.

Detailed MAS NMR (^{29}Si and ^{27}Al) studies were carried out over ETS-10 and ETAS-10 synthesized using $TiCl_4$. The ^{29}Si spectra of the samples were well-resolved and the assignments of individual crystallographic sites were possible. Three types of silicon sites could be recognised from the ^{29}Si MAS NMR signals and the silicon sites corresponding to different signals could be rationalized based on their geometry as well as their coordination to different Ti sites. In the case of ETAS-10, ^{27}Al MAS NMR recorded for 3 samples with different Si/Al ratios revealed that the amount of occluded Al in the samples increased with increasing Al content, though in the case of the samples with Si/Al = 62.5, all the Al was in

Td position. The variation of the intensity in the ^{29}Si signals and the appearance of a downfield shifted new ^{29}Si signal were used to assign the location of Al in ETAS-10. The connectivity and coordination of Ti to Si has been well established and the location of the Al ions has been identified as Si_{10} positions. The assignment made by NMR studies further has been confirmed by aluminium substitution energy calculations by the semi-empirical cluster model approach.

Molecular modeling studies carried out with the aid of computer graphics and semi-empirical quantum chemical methods have helped in understanding the connectivity of M-sites and further confirming the assignment of the Si sites to experimentally observed chemical shifts. The Brönsted acidity resulting from the presence of protons to compensate the anionic charge of the aluminum substituted framework was also predicted.

6.3 SORPTION PROPERTIES

N_2-adsorption isotherms at liquid nitrogen temperature revealed that the BET surface areas and pore volumes were between 360 to 410 m^2/g and 0.11 to 0.16 ml/g, respectively for all the ETS-10 samples. Adsorption studies indicated that the molecular sieves were hydrophilic and had pores of diameter of at least 8 Å. Sorption of probe molecules and surface area measurements revealed that the ETS-10 sample synthesized using $TiCl_4$ was the most crystalline and pure. The sorption isotherm of alkali metal exchanged ETS-10 were obtained. The adsorption was found to be of the Langmuir type, with a rapid uptake at low adsorbate pressures and complete void filling as pressures approached saturation. Affinity coefficients were calculated from the Dubinin equation and monolayer capacities were calculated from Dubinin and Langmuir equations. Isosteric heats of adsorption and chemical affinities of water, m-xylene and p-xylene were calculated for the various samples.

6.4 CATALYTIC PROPERTIES OF ETS-10

6.4.1 Isomerization of m-Xylene and 1,3,5-Trimethylbenzene

Partially exchanged H-form of ETS-10 was active in the reactions normally catalyzed by acid catalysts. Disproportionation reactions occurred to a considerable extent during the isomerization of m-xylene and 1,3,5 trimethylbenzene. The activity of ETS-10 in these reactions was more or less similar to that of HY. The I/D ratio of 0.5 for m-xylene and 0.73 to 0.88 for 1,3,5 trimethylbenzene conversions suggested that ETS-10 behaved as a wide pore molecular sieve with a pore dimension of about 8 Å.

6.4.2 n-Butanol Dehydration

The H-ETS-10 samples were highly active in the dehydration of n-butanol. HY gave a conversion of 98.2% at 523K, while ETS-10 samples gave a conversion between 82.1 to 96.5% at 573K. The main products formed in this reaction were *trans*-but-2-ene, *cis*-but-2-ene and 1-butene. The studies revealed that H-ETS-10 is less acidic than HY.

6.4.3 Hydroisomerization of n-hexane

The hydroisomerization of n-hexane occurred over Pt-H-ETS-10 with high selectivities due to the moderate acidity of the material. The isomerization selectivity was maximum at around 0.3 wt.% Pt in the catalyst and at around 600K. Though the yields of methyl pentanes were in near equilibrium amounts, the di-methyl isomers were produced in low yields.

6.4.4 Aromatization of n-hexane

Pt-Cs-ETS-10 showed the highest aromatization selectivity among the alkali metal exchanged ETS-10 samples. The large basicity of the Cs^+ cations is believed to be responsible for the large aromatization activity. The aromatization selectivity was maximum with 0.4 wt.% Pt in the catalyst. The Pt-Cs-ETS-10 was many times more active than the commercial Pt-Al_2O_3 in the aromatization of n-hexane.

LIST OF PUBLICATIONS

1. Studies on the synthesis of ETS-10 : Part I, Influence of synthesis parameters and seed content.

   Tapan Kr. Das, A.J. Chandwadkar, A.P. Budhkar, A.A. Belhekar and S. Sivasanker, ***Microporous Mater.,*** **4** (1995) 195.

2. Studies on the synthesis of ETS-10 : Part II, Use of organic templates.

   Tapan Kr. Das, A.J. Chandwadkar, A.P. Budhkar and S. Sivasanker, ***Microporous Mater.,*** **5** (1996) 401.

3. Studies on the synthesis, characterization and catalytic properties of large pore titanosilicate, ETS-10.

   Tapan Kr. Das, A.J. Chandwadkar and S. Sivasanker, ***J. Mol. Catal.***, **107** (1996) 199.

4. A rapid method of synthesizing the titanosilicate, ETS-10.

   Tapan Kr. Das, A.J. Chandwadkar and S. Sivasanker, ***J. Chem. Soc. Chem. Commun.***, (1996) 1105.

5. Preparation, characterization and catalytic properties of the microporous titanosilicate, ETS-10.

   Tapan Kr. Das, A.J. Chandwadkar and S. Sivasanker, ***Bull. Mater. Sci.,*** 17 (1994) 1143.

6. Synthesis and catalytic properties of mesoporous Tin Silicate molecular Sieves.

   Tapan Kr. Das, Karuna Chaudhari, A.J. Chandwadkar and S. Sivasanker, ***J. Chem. Soc. Chem. Commun.*** (1995) 2495.

7. Synthesis, Characterization and Catalytic properties of Vanadium containing VPI-5

   Karuna Chaudhari, **Tapan Kr. Das**, A.J. Chandwadkar, J.G. Chandwadkar and S. Sivasanker, ***Stud. Surf. Sci. Catal.,*** **105,** 253 (1997).

8. Comparison of the catalytic properties of the titanosilicates, TS-1 and ETS-10 in acid catalyzed reactions.

   Tapan Kr. Das, A.J. Chandwadkar and S. Sivasanker, ***Catalysis, Modern Trends*** (Eds. N.M. Gupta and D.K. Chakraborthy), Narosa Publishing House, New Delhi, (1995) p. 227.

9. Hydroisomerization of n-hexane over Pt-H-ETS-10.

   Tapan Kr. Das, A.J. Chandwadkar, H.S. Soni and S. Sivasanker, ***Catal. Lett.,*** in press.

10. n-Hexane aromatization over platinum ETS-10.

    Tapan Kr. Das, A.J. Chandwadkar and S. Sivasanker, ***J. Catal.,*** Communicated.

11. Synthesis of titanosilicate ETS-10 : The influence of $TiCl_3$ and $TiCl_4$ on the crystallization kinetics.

    Tapan Kr. Das, A.J. Chandwadkar and S. Sivasanker, ***National workshop on Catalysis,*** Bhavnagar, India, December, 20-22, (1995) p. 78.

12. Aromatization of n-hexane over platinum alkaline ETS-10 molecular sieves.

    Tapan Kr. Das, A.J. Chandwadkar and S. Sivasanker, ***13th National symposium on Catalysis,*** IIP, Dehradun, India, (1997), accepted.

13. N-DBA-VPI-5 : Synthesis and characterization.

    Karuna Chaudhari, **Tapan Kr. Das**, H.S. Soni, P. Rajmohanan and A.J. Chandwadkar, ***13th National symposium on Catalysis,*** IIP, Dehradun, India, (1997), accepted.

14. Synthesis, characterization and catalytic properties of titanium containing mordenite.

    A. A. Belhekar, **Tapan Kr. Das**, K. Chaudhari, S.G. Hegde and A.J. Chandwadkar, ***13th National symposium on Catalysis,*** IIP, Dehradun, India, (1997), accepted.

15. Anisotropic chemical shielding, T-site ordering and acidity in ETS-10 molecular sieves studies through MAS NMR and molecular modeling.

    S. Ganapathy, **Tapan Kr. Das**, R. Vetrivel, S. Roy, Tapas Sen and S. Sivasanker, (manuscript in preparation).

PATENTS

1. An improve process for the preparation of a crystalline titanosilicate molecular sieve.

   Tapan Kr. Das, A.J. Chandwadkar, A.P Budhkar and S. Sivasanker, ***Indian Patent,*** No. 432/DEL/95.

2. An improved process for the rapid synthesis of crystalline titanosilicate molecular sieve.

   Tapan Kr. Das, A.J. Chandwadkar and S. Sivasanker, ***Indian Patent,*** No. NF-94/96.

3. A process for the preparation of tin containing mesoporous molecular sieve.

   Tapan Kr. Das, Karuna Chaudhari, A.J. Chandwadkar and S. Sivasanker, ***Indian Patent***, No. NF-140/96.

4. An improved process for the preparation of vanadium containing molecular sieve.

   Karuna Chaudhari, **Tapan Kr. Das**, A.J. Chandwadkar and S. Sivasanker, ***Indian Patent***, No. 1086/DEL/96.